Glasgow Theses Service
http://theses.gla.ac.uk/
theses@gla.ac.uk

An investigation into the transport and modulation of synaptophysin positive vesicles

Paul Turko

A thesis submitted in fulfilment of the requirements

for the Degree of Doctor of Philosophy

Institute of Neuroscience and Psychology

College of Medical, Veterinary & Life Sciences

University of Glasgow

April, 2013

Dedication

This thesis is dedicated to my mum

Julie May Turko

The one person who has always believed in me

Abstract

Neuronal function, survival and architecture all critically depend on the precise transport of intracellular proteins to a vast array of synaptic connections. Disrupted intracellular transport leads to deficits in synaptic transmission, irregular cell morphology, misallocated organelles and cell death. In addition, axonal transport deficits have been noted in the early stages of several debilitating neurological conditions, thus, axonal transport deficits may contribute to disease progression. This makes it important that we understand the contribution of axonal transport to both physiological and pathophysiological cellular processes and to the transport of essential organelles.

As such the aims of this project were as follows: to investigate the long-term transport properties of visualised synaptic vesicles, to investigate whether vesicle transport could be modulated by changes in neuronal activity, to examine whether vesicle transport deficits exist in certain disease models and to develop novel assays for focusing the study of vesicle transport to specific neuronal cell types.

To investigate the transport properties of visualised synaptic vesicles we exploited a lentiviral vector to express a fluorescently tagged version of an abundant synaptic vesicle transmembrane protein, synaptophysin. Using synaptophysin-GFP (syp-GFP) as a synaptic vesicle marker we then tracked the movements of synaptic vesicles in the axons of dissociated hippocampal neurons. Synaptophysin-GFP expression revealed two fluorescent vesicle populations, one population that moved in a rapid and bi-directional manner and one population that accumulated into clusters of stationary vesicles at putative presynaptic sites. Each vesicle population was analysed independently. Moving vesicles were termed motile particles, whilst vesicle accumulations were termed vesicle clusters. To investigate potential activity-dependent changes in vesicle transport and vesicle cluster localisation we used acute or co-culture application of the GABA$_A$ receptor antagonists bicuculline (bic) (20µM) or Gabazine (gbz) (20µM), which can generate increased neuronal activity or epileptiform-like activity *in vitro*. As a result of bic treatment we observed a significant decrease in the size of stationary

presynaptic vesicle clusters. Under control conditions the average size of vesicle clusters was 14.7±1.67μm^2, reducing to 12.1±1.41μm^2 following 10 hours of increased neuronal activity (p=0.0042, Wilcoxon-matched pairs test, n=80, 8 experiments). In addition, increased neuronal activity also led to a significant increase in vesicle cluster turnover, which increased from 28±6.89% under control conditions to 44±8.46% as a result of increased neuronal activity (p=0.0261, unpaired student t-test, n=25, 11 experiments). However, these changes were not accompanied by any alteration in vesicle transport, with the speed, the density and the proportion of motile particles remaining unaffected by increased neuronal activity (table 3.1). This suggests that each vesicle population may therefore be differentially modulated by increased neuronal activity.

To probe deeper for potential activity-dependent vesicle transport changes we restricted our study of vesicle transport to a specific axonal subtype, the hippocampal mossy fiber. To visualise mossy fiber vesicle transport, lentivirus expressing syp-GFP was pressure injected directly into the cell body layer of the dentate gyrus (DG) in hippocampal organotypic slice cultures. This revealed syp-GFP positive vesicles occupying both small (2-15μm^3) and large (>15μm^3) mossy fiber synaptic terminals, which were found in and along the stratum lucidum. By examining the distribution of vesicle clusters at different time points following gbz or bic treatment (0hrs, 4hrs, 12hrs, 24hrs and 48hrs) we were able to show that epileptiform activity caused a delayed (>12 hours) but significant decrease in the proportion of large vesicle clusters. By 24 and 48 hours there was a significant decrease in the proportion of large vesicle clusters following bic treatment, decreasing from 9.4±1.21% under control conditions (n=11, 5 experiments) to 4.84%±0.72% after 24hrs (n=10, 4 experiments) and to 3.3±0.73% after 48hrs (n=12, 5 experiments), P<0.001, one-way ANOVA. This decrease in the proportion of large vesicle clusters may represent an important pathophysiological change triggered by epileptiform activity. Importantly, we also observed the same decrease in the proportion of large vesicle clusters in a mouse model of Rett syndrome, which models a severe neurodevelopmental disorder caused by a mutation in the gene coding MeCP2. As a consequence of bic treatment we observed a significant decrease in the proportion of large vesicle clusters from 7.2% ±1.78% in control cultures (n=6, 2 experiments), down to 0.9% ±0.6% in 48hr

bic treated cultures (n=8, 3 experiments) and recovering to 6.9%±1.5% following bic wash out (n=11, 3 experiments); p<0.0001, one way ANOVA. Interestingly, *Mecp2$^{Stop/y}$* hippocampal organotypic slices showed a greater decrease in the proportion of large vesicle clusters following 48hrs of bic treatment. The proportion of large vesicle clusters in 48hr bic treated WT slices was 3.3%±0.73%, whilst in 48rs bic treated Mecp2$^{Stop/y}$ slices it was 0.9%±0.6%, p=0.01, two-way ANOVA. These observations suggest that Mecp2$^{Stop/y}$ hippocampal organotypic slices are more sensitive to epileptiform activity than WT slices and may possess deficits in the vesicle transport system.

Primary dissociated hippocampal cell cultures benefit from being both optically and experimentally accessible but lack a defined cellular arrangement. This hampers both the identification and study of specific cell types and specific synaptic connections. To overcome this limitation we developed a modified dissociated cell culture assay for defining the arrangement of dissociated hippocampal neurons. We cultured purified DG and CA3 cell populations in close opposition using a magnetic barrier, but transduced only DG granule cells with lenti-synaptophysin-GFP in order to visualise vesicle transport specifically in mossy fibers. Immunocytochemistry and vital dyes were used to confirm that specific cell populations could be cultured in close proximity, to confirm that lentiviral transduction was highly selective to DG granule cells and to post-hoc identify that vesicle trafficking was occurring specifically in mossy fibers. Using this method it was possible to image vesicle transport specifically in mossy fibers and to investigate vesicle cluster dynamics at putative MF-CA3 synapses. We conclude that this method is a significant improvement to previous techniques because dissociated cells can be arranged to form physiologically relevant synaptic connections, whilst remaining highly accessible to both live imaging and experimental manipulation.

Acknowledgements

Firstly, I would like to say a kind thank you to my supervisor Dr. Stuart Cobb, for all of his help, time, support and patience over the last 4 years and for making my PhD so enjoyable. I am privileged to have worked with him. I appreciate not only his thoughtful contributions to my project, but also to my development as a scientist. He gave me the freedom to explore new ideas and to make mistakes and for this I will be forever grateful.

I would like to say a big thank you to all the students and researchers that I had the pleasure of meeting during my PhD and who were such an important part of my PhD experience, in particular: Faye Mcleod, Kamal Gadalla, Shih-Ming Weng, Jake Griffen, Loud-Stuart, David Houston, Paul Ross, Rosie Spike, Manuel Denton, Louise Williams, Andreas Koschinski, Marika Doucet, Chia-Chin Wu, Jie Song, Allen Kelly, Sam Booker, Graham Lee, Lewis Ross and Mike Aldridge. Thanks for your help, advice, support and friendship.

I would like to pay special thanks to those people who shared their knowledge, their experiences and their encouragement with me during my project. A special thanks to Professor Imre Vida, whose support, insight and experience continues to be an inspiration. To Dr. Mark Bailey, for his constructive comments and critical thinking into all things scientific. To Dr. Francis Burton, whose skill with programming and image analysis proved invaluable. To Dr. Sam Greenwood, for help with: cell culture, slice culture, lentiviral transduction, plasmid transfection, calcium imaging......the list goes on, thank you. To Dr. Mathis Riehle, for enjoyable discussions and his insight into the world of bio-engineering. To Dr. John Sneddon for introducing and inspiring me to study Neuroscience and to Dr. Neil Morris for giving me the opportunity to study with him at Leeds.

With particular thanks to: Kamal, for his help getting started; to Jonas, for keeping me company in the lab, day or night; to Faye, for the banter; to Craig, for the squash; to Jake, for the beer.

I take this opportunity to say thank you to my loving family, for all of their help, encouragement and patience. To my wife Tatiana, with all of my heart I say thank you, for your unwavering strength, love, support and kindness. Without you, I could not have done it. To my Mum I say thank you for everything, thank you for always being there for me, for all the encouragement, for your belief, and for all the laughs and smiles. I will never forget the things you have done for me and your hard work and sacrifice, I am forever grateful. To Mark, thank you for every lift, for every favour, for taking care of us and for being such an important part of our lives. To my Dad, thanks for your encouragement (and pessimism), for always being there to talk to, and for teaching me about the importance of friendship. To my Uncle Jude, thank you for pushing me along. To my brothers, Bic and Gareth, thanks for all the laughs and for really teaching me how to be competitive. To my Grandad Joe, Nana Marg, Nana Violet and Grandad Albert, whose love and wisdom I will cherish. A special thanks to Isaac, Tallulah, Alberta and Alex, and to my beautiful daughter Sophie whose smile makes it all worth it.

Finally, I could not finish these acknowledgements without paying thanks to some old friends and acquaintances that have made my time so much fun. To Spence, for the hitch and for "hooking me up" with Tatiana. To Matt, for being one of the best men I know. To Faraz, for being a gentleman. To Al, for all the good times. To Ed, wherever he is? To Showtime and good memories, with: Wayne, Deej, Ry, Rob, Lee, John and Nago. To Doddy, my oldest friend. To Johnny Berlin, for the music. Thanks for all the games: Rodge, Sidge, Rachel, Dave, Brendon, Barney and Tash. Thanks for all the travels: Mike, Barry, Markus, Bryce, Jason, Nick, Tony, Lisa, the Covic's, Rob and Kayo. To Ad, because I almost forgot him, and to probably still owing me money: Burridge and Spence.

Finally, to my Mother-in-Law Galina, because it's good to keep her sweet.

Author's Declaration

I declare that the work presented in this thesis is entirely my own with all exceptions being clearly indicated or/and properly cited in the context, and all citations have been provided in the reference list.

Signature: Paul Turko

The work has not been presented in part or alone for any other degree programme.

Table of contents

3. Results - The activity-dependent modulation of vesicle transport in dissociated hippocampal neurons ....page 84

Table list

Figure list

1. Introduction

2. Methods and materials

3. Results

4. Results

5. Results

Abbreviations

ACSF - Artificial cerebrospinal fluid

AKA - Automatic kymograph analysis

AMPA - 2-amino-3-(5-methyl-3-oxo-1,2- oxazol-4-yl) propanoic acid

AP - Action potential

AU - Arbitrary units

AZ - Active zone

B27 - Serum supplement

BDNF - Brain derived neurotrophic factor

bic - Bicuculline

BSA - Bovine serum albumin

Ca^{2+} - Calcium

CA1/2/3 - *Cornu Ammonis*

CBL1 - Cell body layer 1

CBL2 - Cell body layer 2

Cl^- - Chloride

CME - Clathrin mediated endocytosis

CNS - Central nervous system

CSA - Cross sectional area

CS - Coverslip

DAPI - 4',6-diamidino-2-phenylindole

DG - Dentate gyrus

DIV - Days in vitro

DMEM - Dulbecco's modified eagles medium

DNA - Deoxynucleic acid

dNTPS - Deoxyneucleotide triphosphates

DPBS - Dulbecco's phosphate buffered solution

EC - Entorhinal cortex

EDTA - Ethylenediaminetetraacetic acid

FLUO3-AM - Calcium indicator - (acetoxymethyl ester)

GABA - γ-aminobutyric acid

GBZ - Gabazine (SR95531)

GFP - Green fluorescent protein

GTP - Guanosine triphosphate

HA - Hibernate media

HC - Heavy chain

HEK - Human embryonic kidney cell

K^+ - Potassium

KIF - Kinesin super family

LC - Light chain

LDCVs - Large dense core vesicles

Lenti - Lentivirus

LF-HA - Low fluorescence hibernate media

LTP - Long term potentiation

LMT-C - Large mossy fiber terminal cluster

NA - Numerical aperture

Na^+ - Sodium

NBA - Neural basal media

MAP2 - Microtubule association protein 2

MeCP2 - Methyl-CpG-binding protein 2

MEM - Modfied eagles medium

MFs - Mossy fibers

MTs - Microtubules

NeuN - Neuronal specific nuclear protein

NMDA - N-Methyl-D-aspartic acid

NR2B - NMDA receptor subunit

NT - Neurotransmitter

PBS - Phosphate buffered solution

PCR - Polymerase chain reaction

PDHC - Primary dissociated hippocampal culture

PDMS - Polydimethylsiloxane

PEI - Polyethylenimine

PLL - Poly-l-lysine

PSD - Post synaptic density

PSD95 - Post synaptic density protein 95

PTM - post-translational modification

RPM - Revolutions per minute

SCM - Serum containing media

SNARE - Soluble NSF attachment protein receptor

STED - Stimulated emission depletion

SUB - Subiculum

SV - Synaptic vesicles

Syp - Synaptophysin

TBE - Tris/Borate/EDTA buffer

T-SNARE - Target SNARE

TSQ - N-(6-Methoxy-8-quinolyl)-ptoluenesulfonamide

VAChT - Vesicular acetyle choline transporter

VIAAT - Vesicle inhibitory amino acid transporter

VGAT - Vesicular GABA transporter

VGLUT1 - Vesicular glutamate transporter 1

VMAT - Vesicular monoamine transporter

VGLUT - Vesicular glutamate transporter

V-SNARE - Vesicular SNARE

WT - Wild type

Introduction

Chapter 1:

1.1 General introduction

Neurons are the single-cell building block of the nervous system (von Waldeyer-Hartz, 1891; Cajal, 1954), dedicated to providing fast signal propagation, through the generation and rapid conduction of electrical impulses (Hodgkin and Huxley, 1952). Neurons are connected to each other predominately by chemical synapses, specialised sites where electrical signals are converted to chemical signals (Del Castillo and Katz, 1954; Heuser et al., 1979; Jessell and Kandel, 1993). Individual neurons are capable of forming thousands of precisely placed synaptic connections. At the synapse, almost all proteins are in some way associated with either the release or subsequent detection of NT (Jessell and Kandel, 1993; Burns and Augustine, 1995; Littleton and Bellen, 1995). One of the most fundamental organelles involved in chemical neurotransmission is the synaptic vesicle (SV). (Heuser and Reese, 1973; Heuser et al., 1979; Sudhof, 2004). Neurons rely on SVs for the storage, transport of regulated release of NT, which is essential for cell signalling and neuronal function.

Although great progress has been made in understanding the interactions of synaptic vesicles at the synapse, much less it known about the transport of synaptic vesicles along the axon (Betz and Wu, 1995; Sudhof, 2004; Augustine and Kasai, 2007). However, thanks to recent advances in fluorescence microscopy and molecular biology it is now possible to "tag" and view SVs with fluorescent proteins and to image them under high resolution (Shimomura et al., 1962; Chalfie et al., 1994; Amado and Chen, 1999; Lee et al., 2008). Combining these techniques opens new doors for investigating both the mechanisms and modulation of vesicle transport.

1. 2 The Hippocampus

The hippocampus is a brain structure long believed to play a role in both learning and memory formation and represents an attractive region in which to study vesicle transport. The hippocampus has been investigated extensively for over 100 years, making it one of the most well studied brain structures (Witter et al., 2000; van Strien et al., 2009). Because of it's unique shape the hippocampus is both easy to identify and easy to isolate for experiments (Fig. 1.1). The hippocampus possesses a highly structured architecture, both in terms of connectivity and cell arrangement (Fig. 1B). This has led to the detailed connections and cell types of the hippocampus being carefully documented (Witter et al., 2000).

1.3 Major hippocampal cell types

The hippocampal formation is made up of 3 distinct sub regions: the dentate gyrus (DG), the hippocampus proper (which is further divided into the: CA3, the CA2 and the CA1 sub regions) and the subiculum (Sub) (Witter et al., 2000; van Strien et al., 2009). In the hippocampus and sub regions, neuronal cells can be categorized as either principal cells or GABAergic interneurons. Principal cells primarily communicate via excitatory synaptic transmission using the neurotransmitter (NT) glutamate; inhibitory interneurons communicate primarily using the inhibitory neurotransmitter γ-aminobutyric acid (GABA) (Curtis and Watkins, 1960; Benes and Berretta, 2001). Dentate granule cells are the principal cells of the DG, whilst pyramidal neurons are the principal cells of the hippocampus. GABAergic interneurons refer to a heterogeneous and diverse population of cells located throughout the hippocampus (Freund and Buzsaki, 1996). The DG, CA3, CA2 and the CA1 principal cells follow a strict lamination and are very well organised into their respective cell body layers (Fig. 1.1). This tight lamination makes it easy to identify specific regions and allows for orientation within the hippocampus (Witter et al., 2000).

Figure 1.1

A

Cerebellum

Cortex

Brain stem

Pre frontal cortex

Hippocampus

Bi

Bii

CA2

ori.

pyr.

CA1

rad.

Sub.

l-m.

alv.

rad.

luc.

pyr.

CA3

ori.

hil.

m.l.

EC

DG

PaS.
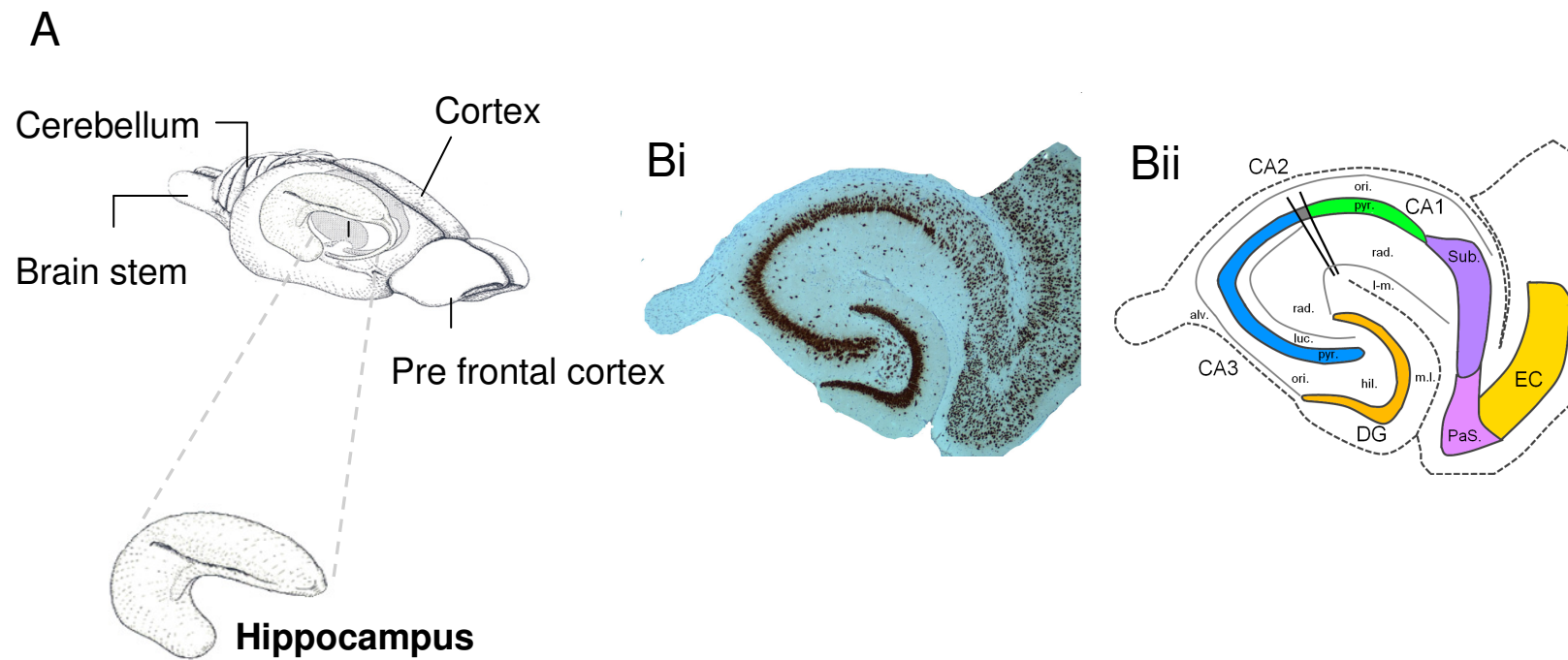
Figure 1.1 – Anatomical location and cellular organisation of the hippocampus.

The hippocampus is a distinct anatomical structure with a highly organised cellular arrangement. Figure 1.1: A schematic showing the location of the hippocampus with respect to other major anatomical landmarks in the rat brain. The inset shows an enlargement of the hippocampus, highlighting it's unique shape and structure. Figure 1.1 Bi: A cross section of the hippocampus; neurons are labelled brown following immunostaining for the nuclear neuronal protein NeuN; this highlights the distinctive cellular arrangement of the hippocampus, which can be clearly observed in the interlocking arrangement of both the granule cell and pyramidal cell body layers. Figure 1.1 Bii: A schematic representation of the hippocampus, showing the location of each cell body layer, as well as the anatomical areas. The hippocampus is divided into functionally distinct regions which are denoted by the following abrreviations: Ori. – Stratum oriens; Rad. – Stratum radiatum; Pyr. – Stratum pyramidale; l-m. – lacunosum moleculare; m-l. molecular layer; hil. Hilus; luc. – Stratum lucidum; Sub – subiculum; Pas – Parasubiculum; EC – entohinal cortex. Figure 1.1 A was adapted from: kaylab.uchicago.edu/research. Figure 1.1 B was adapted from: (Milatovic et al., 2004).

1.4 Hippocampal circuitry

How information flows through the hippocampus is a consequence of the intricate circuitry created by each cell type. A simplistic overview of excitatory connections in the hippocampus is shown in figure 1.2 (Neves et al., 2008). In this overview, the hippocampus receives major input from the superficial layers of the entorhinal cortex (EC) via the perforant pathway. After receiving input from the EC the granule cells of the dentate gyrus (DG) send abundant axonal projections, the mossy fibers (MFs), to synapse onto both pyramidal neurons and interneurons. These fibers are densely packed and form a clear band (the stratum lucidum), which runs in parallel to the cell body layer of the CA3. MFs terminate before reaching the dendritic subfield of the CA2. Mossy fiber synapses are distinctively large and synapse onto the complex spines of CA3 pyramidal neurons (Henze et al., 2002b; Danzer and McNamara, 2004). These fibers carry the major output of the DG to the CA3. Additionally, MFs also synapse onto mossy cells and numerous inhibitory interneurons (Acsády et al, 1998). To continue the circuit, CA3 pyramidal neurons project a branch of their axons (the schaffer collaterals) to synapse onto CA1 pyramidal neurons. CA1 pyramidal neurons also receive direct input from the layers III and IV of the entorhinal cortex, via a series of afferents referred to as the temporoammonic pathway (Witter et al., 1988). *In vivo,* CA3 pyramidal neurons also project their axons to the contralateral hippocampus; however, *in vitro,* these connections are severed and are no longer present. Neurons in the proximal portion of the CA3 can project reciprocal connections back to the DG (Witter, 2007). Axons from CA1 pyramidal neurons complete the "tri synaptic loop" by projecting their axons to the deep layers of the entorhinal cortex. In addition to this circuitry,

Intertwined within the excitatory networks of the hippocampus are inhibitory interneurons (INs) (Freund and Buzsaki, 1996; Markram et al., 2004) These cells synapse extensively onto principal cells and other INs. They project dense local axonal arbors, which can potentially synapse onto thousands of principal cells (Han et al., 1993; Packer and Yuste, 2011). The major role of INs is to regulate and co-ordinate network excitability, to regulate cell firing and to prevent hyper

Figure 1.2

Hippocampus   **Entorhinal cortex**

Schaffer collaterals

Temporoammonic
path

Medial

CA1

CA3

II

Lateral

III

V

DG

Associational/
commissural
fibres

Mossy fibres

Perforant
path
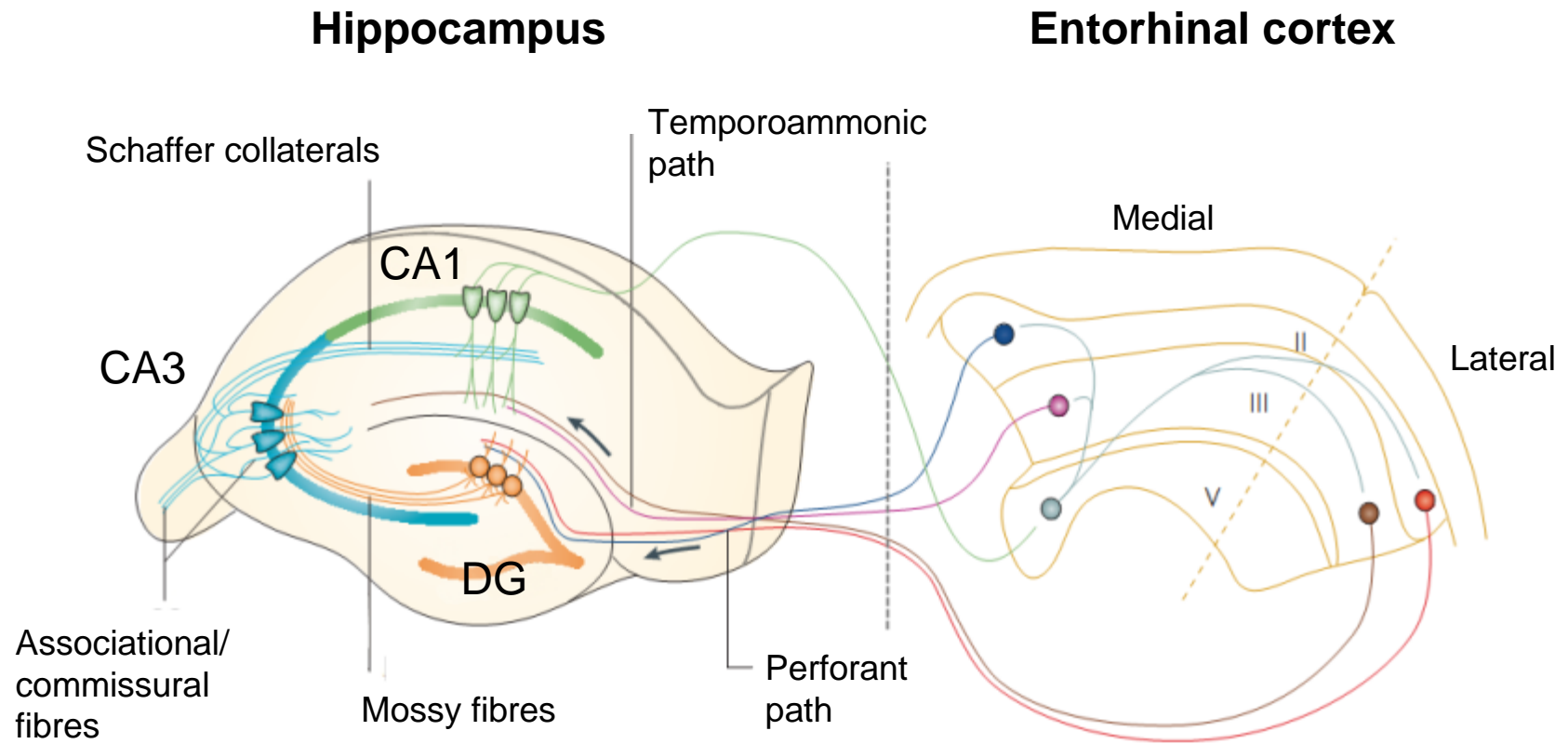
Figure 1.2 – Hippocampal circuitry.

A cartoon schematic describing the major excitatory connections of the hippocampus and entorhinal cortex. Described within this diagram is the tri-synaptic loop, consisting of: DG granule cells, CA3 pyramidal neurons and CA1 pyramidal neurons. In the tri-synaptic loop: DG granule cells (orange) project their axons (mossy fibers) to synapse onto the proximal dendrites of CA3 pyramidal neurons (light blue), along the stratum lucidum; CA3 pyramidal neurons project their axons (Schaffer collaterals) to synapse onto CA1 pyramidal neurons (green), in both the stratum oriens and stratum radiatum. CA1 pyramidal neurons then project their axons to synapse in both the subiculum and entorhinal cortex. The hippocampus makes and receives extensive synaptic contact with the entorhinal cortex. This diagram was modified from Neves et al., 2008.

excitation (Markram et al., 2004; Bartos et al., 2007). They achieve this through the precise placement of their axon onto discreet targets, their (often) fast spiking phenotype and through the regulated release of the inhibitory neurotransmitter γ-aminobutyric acid (GABA) (Han et al., 1993). GABA acts on $GABA_A$, $GABA_B$ or $GABA_C$ receptors located on either the pre and the postsynaptic neuron. The release of GABA leads to (typically in the adult) a decrease in neuronal excitability (Del Castillo et al., 1964; Bowery, 1993). Inhibitory synaptic transmission plays an important role in generating oscillations and the complex firing patterns produced by neurons in the hippocampus.

1.5 The chemical synapse

In the nervous system there are two major types of synaptic connection, the electrical synapse and the chemical synapse. Although electrical synapses play several physiologically important roles chemical synapses are far more numerous and provide the bulk of synaptic transmission. Chemical synapses are formed, typically, when the axon of one neuron makes contact with the cell body or dendrites of another neuron (Burns and Augustine, 1995; Bury and Sabo, 2011) (but see: (Watson and Bazzaz, 2001). At chemical synapses there is a distinct separation between contacting cells, an ultra thin region known as the synaptic cleft (Palay and Palade, 1955). Chemical synapses are made up of two domains: the presynaptic domain and the postsynaptic domain. Proteins in the presynaptic domain are geared towards the synthesis, storage and release of NT (Ahmari et al., 2000; Becherer and Rettig, 2006); whilst proteins in the postsynaptic domain are geared towards detecting and responding to the presence of NT (Kim and Sheng, 2004). SVs are found in abundance in the presynaptic domain and can be observed under the electron microscope. SVs appear as small (40-50nm) electron dense rings, which cluster in close proximity to the active zone (AZ) (Bodian, 1970). The synaptic vesicle membrane appears electron dense because it is packed with transmembrane proteins, of which synaptophysin is one of the most abundant (Takamori et al., 2006).

The AZ appears as an electron dense band located in and around the plasma membrane (Ahmari et al., 2000). The AZ acts as a scaffold and organisation centre for numerous proteins that facilitate vesicle fusion (for review: (Schoch and Gundelfinger, 2006)). The AZ is held in close opposition to another electron dense structure, the post synaptic density (PSD). The PSD contains a plethora of receptors and kinases specialised in transducing signals received from the presynaptic domain (Jordan et al., 2004; MacGillavry et al., 2011). Both ionotrophic and metabatrophic receptors are associated with the PSD (Tu et al., 1999; Bats et al., 2007). Ionotrophic receptors mediate fast signal transduction, whilst metabotrophic receptors tend to facilitate slow(er) signal transduction (through various down stream signalling cascades) (Curtis and Watkins, 1960; Conn and Pin, 1997; Lodge, 2009). Synaptic transmission is dependent on the selective permeability of specific receptors and ion channels to specific ions (Hodgkin and Huxley, 1952). This determines whether or not synaptic transmission is excitatory or inhibitory.

1.6 Synaptic transmission

Controlled NT release is triggered by the invasion of an action potential (AP) into the presynaptic terminal. This facilitates the opening of voltage gates calcium channels, which in turn allow calcium to enter into the cell (Lisman et al., 2007). Calcium is the signal for docked and primed vesicles at the AZ to fuse with the plasma membrane. (Fatt and Katz, 1952; Brose et al., 1992; Augustine and Kasai, 2007; Neher and Sakaba, 2008) Following fusion, synaptic vesicles expel their NT content into the synaptic cleft where it can diffuse to the postsynaptic neuron. Binding of NT to a series of complementary ligand gated receptors triggers ion channels to open and can lead to down stream signalling cascades (Pin and Duvoisin, 1995). This ultimately leads to either the depolorisation or hyperpolarisation of the plasma membrane (Hodgkin and Huxley, 1952).

A critical aspect of excitatory synaptic transmission is the ability of one neuron to elicit action potential firing in the neighbouring neuron (Lisman et al., 2007). Neurons are electrically active by virtue of a potential difference that exists across their plasma membrane (Cole and Curtis, 1939; Hodgkin and Katz, 1949; Neher and Sakmann, 1992). This gradient is maintained through the action of sodium/potassium ATPase (Na^+/K^+-ATPase) and unidirectional ion channels (Rakowski et al., 1989). Through the action of Na^+/K^+-ATPase, neurons contain a high intracellular concentration of potassium (K^+) but a low intracellular concentration of sodium Na^+. At rest, this (typically) keeps the neuron below the threshold for firing APs. The opening of AMPA receptors (following glutamate binding) permits the flow of Na^+ down its concentration gradient into the resting neuron; because of this, Na^+ causes the neuron to depolarise (Dingledine et al., 1999; Mayer, 2005). If enough AMPA receptors are activated the membrane potential of the neuron will reach threshold and begin to fire APs (Dingledine et al., 1999). This simplistic overview is a typical example of excitatory synaptic transmission.

1.7 The synaptic vesicle life cycle.

SVs contribute to neurotransmission through several cyclic steps: (1) SVs are loaded with neurotransmitter through proteins in their membrane, (2) SVs are docked and primed at the AZ, (3) SVs undergo rapid calcium dependent exocytosis of NT, (4) endocytosis recovers SVs from the plasma membrane and (5) SVs are recycled and reused for subsequent rounds of exocytosis (Heuser and Reese, 1973; Heuser et al., 1979; Ryan and Smith, 1995; Sara et al., 2002; Sudhof, 2004; Lisman et al., 2007).

In the CNS neurotransmitters are synthesised at the synapse by specific enzymes before being loaded into synaptic vesicles (Hertz et al., 1999; Mathews and Diamond, 2003). In the membrane of SVs there usually exists a single large ATP dependent transporter that determines which NTs will be loaded (Takamori et al.,

2006). Through the action of these large vesicular transporters high (millimolar) concencentrations of NT can build up within the SV (Wadiche and Jahr, 2001). Several transporters have been identified for the major neurotransmitters: GABA and glycine (VGAT), glutamate (VGLUT1, 2 and 3), monoamines (VMAT2) and acetylecholine (VAChT); all transporters are found to associate with SVs (Maycox et al., 1988; Takamori et al., 2006). These transporters define what NT will be released into the synaptic cleft. Vesicular transporters such as VGAT and VGLUT are good indicators of the type of synaptic transmission occurring at a particular synapse (Yasaka et al., 2010).

In order for SVs to mediate the rapid release of NT they must be first docked and primed at the AZ (Becherer and Rettig, 2006; Siksou et al., 2009), thus, when calcium influx occurs, SVs are well placed to immediately release NT. Although the precise mechanisms of docking and priming are still unclear, a number of proteins have been identified that play a definite role in the release process (Littleton and Bellen, 1995; Sudhof, 2004). Major contributors to the docking and priming process include: vesicular SNAREs (V-SNARES) and target SNAREs (T-SNARES) (Ungermann et al., 1999). Target SNAREs are associated with the AZ, whilst vesicular SNAREs are incorporated into the vesicle membrane. SNAP25, syntaxin and synaptobrevin are important SNAREs that form part of the trimeric complex that binds SVs to the AZ (Ungermann et al., 1999; Sudhof, 2004, 2012). Once formed, this complex is then 'primed' through ATP-dependent modifications, which renders the vesicle competent for fusion (Eliasson et al., 1997). Synaptotagmin, which is an abundant SV membrane protein is thought to account for the final conformational change needed to trigger the rapid release of NT (Brose et al., 1992; Yoshihara and Littleton, 2002), a key step in synaptic transmission. Following exocytosis, SVs are then capable of recycling away from the plasma membrane (Gandhi and Stevens, 2003).

An important step in the SV lifecycle is vesicle recycling, this permits a relatively small number of SVs to maintain synaptic transmission even during long periods of increased activity (Murthy and De Camilli, 2003; Galli and Haucke, 2004). Three major mechanisms have been proposed for how SVs recover from the plasma membrane: (1) clathrin mediated endocytosis (CME) of small SVs; (2) bulk

endocytosis of large portions of membrane; (3) "kiss and run", transient fusion with the plasma membrane. Of all three mechanisms, CME is the most well studied form of endocytosis. During clathrin-mediated endocytosis specific adaptor proteins recruit clathrin to the plasma membrane (Marsh and McMahon, 1999; Galli and Haucke, 2004). With the help of these adaptor proteins, clathrin forms a lattice that surrounds the SV (Fotin et al., 2004; Fotin et al., 2006). As this lattice begins to form it forces the vesicle to bud away from the plasma membrane (Le Roy and Wrana, 2005). Once the vesicle is fully formed, the clathrin complex is able to dissociate away before being recycled (Le Roy and Wrana, 2005). Clathrin mediated endocytosis is thought to occur during normal synaptic transmission. During periods of strong stimulation, bulk endocytosis is thought to replace a component of clathrin-mediated endocytosis (Royle and Lagnado, 2003; Clayton et al., 2008). Following strong stimulation, large amounts of irregular shaped membrane is seen to be endocytosed from the plasma membrane (Royle and Lagnado, 2003). Bulk endocytosis occurs more slowly than clathrin mediated endocytosis, but is obvious during periods of increased activity (Clayton et al., 2008). A putative third mechanism for SV recycling is: "kiss and run" (Royle and Lagnado, 2003). However, direct evidence for "kiss and run" exo/endocytosis has been difficult to acquire (Granseth et al., 2006; Rizzoli and Jahn, 2007). For example, in situations where "kiss and run" was thought to be the predominant mechanism for recycling,, CME was both necessary and sufficient for vesicle retrieval (Granseth et al., 2006; Zhu et al., 2009).

Following each mechanism of recycling vesicle protein is typically conserved or sorted back into the vesicle membrane (Wienisch and Klingauf, 2006). One way to study the transport and recycling of SVs is to tag SV membrane proteins with fluorescent probes. One particularly suitable SV protein is synaptophysin. Synaptophysin is the second most abundant transmembrane vesicle protein, which is enriched in SVs and is seen to cluster at the synapse. Around 32 copies of the protein are found per synaptic vesicle (Takamori et al., 2006). Each protein is arranged with four transmembrane domains and orientated so that both the N- and the C-terminus of the protein are located within the cytoplasm (Arthur and Stowell, 2007). Synaptophysin plays putative roles in both the competition for synapse formation and also in the efficiency of vesicle endocytosis (Tarsa and

Goda, 2002; Kwon and Chapman, 2011). However, knock out of synaptophysin does not cause an overt phenotype in mutant mice (McMahon et al., 1996). This suggests that although the protein is abundant it may also be backed up by secondary redundancy. Because of this, tagging synaptophysin with GFP should permit the visualisation of synaptic vesicles without significantly interfering with cellular activities. Previous cloning efforts have succeeded in attaching a GFP fluorescent protein to the C-terminus of synaptophysin, permitting the visualisation of vesicle transport (Pun et al., 2006). Thus, by tagging vesicles with synaptophysin-GFP it is possible to continually observe the transport of vesicles along the axon, even after they partake in exocytosis. This offers several advantages over fluorescent dyes that are typically used to study short-term vesicle dynamics (Henkel et al., 1996).

1.8 The importance of vesicle transport

Neurons because of their extensive projections and distinct polarity possess a well-developed and sophisticated transport system (Hirokawa and Noda, 2008). Vesicle transport in neurons is fundamentally more complex than in most other cell types because neurons tend to form long and elaborate processes, which can grow over great distances (Armstrong et al., 1987). Highlighting the importance of vesicle transport in neurons is the fact that deficits or disruption to vesicle transport may contribute to the development of several disease states. (Holzbaur, 2004; Chu et al., 2012). Huntington's for example, is a disease characterised by the disruption of axonal and vesicle transport. This leads to deficits in cell signalling and eventually cell death (Gunawardena et al., 2003). The same can be seen in mouse models of Alzheimer's disease, where alterations in axonal and vesicle transport are one of the earliest detectable changes that may contribute to disease progression (Stokin et al., 2005). This makes studying the physiological and pathophysiological mechanisms of vesicle transport particularly important.

1.9 Microtubules and vesicle transport

Microtubules (MTs) are long thin tube like structures, approximately 25nm in diameter; they provide a base for the movement of molecular motors throughout the cell. They are made up of repeated units of a single globular protein called tubulin, which is in turn made up of two subunits of α- and β tubulin (Borisy and Taylor, 1967; Nogales, 2000; Conde and Caceres, 2009). MTs have a stable end (minus end) and a growing end (plus end). In axons, all microtubules are positioned so that the plus end is closest to the synapse, whilst the minus end is closest to the cell body (Baas et al., 1988). In distal dendrites, microtubules possess a mixed orientation (Baas et al., 1988; Stone et al., 2008). Microtubule orientation plays an important role in directing the transport of specific motors and cargo (Kapitein et al., 2010).

The plus end of MTs is in a state of constant flux, continually breaking down and continually being rebuilt; this GTP dependent remodelling is termed "dynamic instability" and is the mechanism by which MTs can adjust their length as well as their target (Mitchison and Kirschner, 1987). Tracking proteins are found at the plus end of MTs, these proteins help to regulate and guide the growth of MTs (Akhmanova and Hoogenraad, 2005). MTs are regulated by associated proteins (MAPs). These proteins are expressed in specific compartments of the cell. For example, MAP2 is expressed exclusively in the dendrites and the cell body, whilst tau is only found in axons (Kosik and Finch, 1987).

Both microtubules and association proteins can be altered by post-translational modifications (PTM) (Bulinski and Gundersen, 1991; Ikegami and Setou, 2010; Janke and Bulinski, 2011). Some PTMs act as traffic signals for molecular motors, whilst others can alter the stability of microtubules and in turn alter the preference of specific motors for distinct regions of the cell (Ikegami et al., 2007; Ally et al., 2008; Dunn et al., 2008). Tyrosination / detyrosination cycling for example, plays a role in directing molecular motors to specific locations. Kinesin-1 is known to bind preferentially to detyrosinated tubulin, which is more abundant in axons rather than dendrites during development (Dunn et al., 2008). MTs don't simply act as a "road"

or "rail" network on which cargo is transported, but play an active role in directing the movement of molecular motors.

1.10 Molecular motors and vesicle transport

Without the help of active transport, organelles and vesicles would simply diffuse randomly within the cell and rarely reach their destination. Molecular motors are an important constituent of the intracellular transport system; through the timed hydrolysis of ATP, they are able to engage in processive motion, which allows them to walk along MTs (Hirokawa, 1998; Schief and Howard, 2001; Miki et al., 2005). A variety of motors have been discovered that depend on microtubules for motility; they are grouped into two major families, these are kinesins and dyneins (Hirokawa, 1998). Kinesins predominately drive plus end directed transport, whilst dyneins drive minus end directed transport (Schliwa and Woehlke, 2003). Each family has been shown to carry a plethora of cargos to and from the synapse, both pre- and postsynaptically. In addition, multiple dyneins and kinesins have been shown to work cooperatively or in a "tug of war" style to direct cargo transport (Kural et al., 2005). Different cargos and motors are seen to move at different speeds; vesicles for instance, are directed via fast transport, whilst larger proteins or protein complexes are transported by slow transport (Nakata et al., 1998).

Several kinesins are associated with the transport of SVs and SV precursors (Takamori et al., 2006). KIF1A and KIF1Bβ belong to the kinesin-3 family and are implicated in the transport of synaptic vesicle precursors along the axon (Yonekawa et al., 1998; Hirokawa et al., 2009). Genetic deletion of either motor leads to severe synaptic dysfunction and lethality (Niwa et al., 2008). Multiple members of each family have a direct or indirect association with SVs: KIF 5a and 5b, as well as dynein LC2 and HC1 all associate with purified SVs (Takamori et al., 2006; Hirokawa et al., 2009). KIF5b for example, binds to SVs through an interaction with SNAP25, a protein located in the vesicle membrane (Morton et al., 2010).

Recent evidence supports the idea that a deep relationship exists between motors and their cargo. This is observed in the case of the molecular motor KIF17 and it's cargo, NR2B (a subunit of the NMDA receptor). A functional blockage of KIF17 leads to a decrease in dendritic expression of NR2B (Guillaud et al., 2003). Conversely, a functional blockade of NMDA receptors leads to an increase in the expression of NR2B, but also leads to an increase in KIF17 expression (Guillaud et al., 2003). This interesting finding demonstrates a complex and reciprocal relationship between both motor and cargo. It also demonstrates that the transport system is adaptable, capable of meeting an increased demand with increased supply.

1.11 Small Rab GTPases

What regulates the binding of cargo to specific motor proteins or the targeting of specific motors to discreet intracellular domains is a series of small GTPase's belonging to the Ras superfamily of proteins (Wennerberg et al., 2005). This family of proteins co-ordinate almost all aspects of membrane trafficking. One of the most important members of the Ras family of proteins is the Rab family of GTPase's. Following the binding of GDP or GTP, the proteins function as molecular switches to determine cargo release, trigger additional posttranslational modifications or alter motor protein direction (Stenmark and Olkkonen, 2001; Mizuno-Yamasaki et al., 2012). Over 60 Rab proteins are expressed in human cells and show a distinct and unique expression pattern on each organelle, which serves to direct organelles through the transport system; examples of identified Rab proteins include: Rab 5, which is required for vesicle fusion to endosomes, Rab 1, which is required for vesicle fusion to the Golgi apparatus and Rab 8, which is required for vesicle fusion to the plasma membrane (Mizuno-Yamasaki et al., 2012). Acting in unison with association proteins, the Rab superfamily of proteins essentially tag and confer an identity to the vesicle membrane (Corbeel and Freson, 2008). In the brain, Rab3A is the most abundant small GTPase and is highly enriched on

synaptic vesicles and plays a key role in the efficiency of exocytosis as well as trafficking vesicles to the synapse (Leenders et al., 2001); Rab3A is known to modulate synaptic transmission and synaptic plasticity (Schluter et al., 2006). The importance of the Rab proteins are underlined by a number of knock-down or knock-out studies, which often produce offspring with diminished synaptic transmission, stark synaptic-structural anomalies or postnatal lethality (Schluter et al., 2004). Overall, the Rab superfamily of proteins play an essential role in directing vesicle transport between the different plasma membrane domains.

1.12 Postsynaptic structural plasticity

In response to various forms of external stimuli, dendritic spines have the ability to rapidly alter their structure (Engert and Bonhoeffer, 1999; Yuste and Bonhoeffer, 2001). They do this by either extending out, changing shape or retracting back to the dendrite and live imaging experiments have revealed that it can take just a matter of seconds for a spine to extrude from and then return the dendritic shaft (Majewska et al., 2000). Dendritic spines are also seen to extend out and initiate rapid synapse formation onto nearby stationary axons (Ziv and Smith, 1996). Although dendrites are capable of rapid motility, under normal conditions (*in-vivo*) they appear to be quite stable (Grutzendler et al., 2002); when investigating dendritic spine turnover in the visual cortex Grutzendler and colleagues reported low levels of dendritic spine turnover in the adult (<4% turnover); a finding that was confirmed by (Holtmaat et al., 2005). They suggest that dendritic spines are able to preserve their structure and location for many weeks to many months, but reserve the ability to undergo rapid structural changes.

Dendritic spine structural modifications are amenable to modulation by external stimuli; for example, animals housed in an enriched environment, with increased sensory input, show a marked increase in spine density (Johansson and Belichenko, 2002). Also, the generation of LTP with high frequency stimulation is correlated with a local increase in dendritic extensions (Engert and Bonhoeffer,

1999). The release of caged glutamate repeatedly near dendritic spines also leads to a pronounced and prolonged increase in their size (Kasai et al., 2003). Conversely, epileptiform activity leads to a decrease in the number of dendritic spines; with up to 50% of spines being seen to reversibly retract over several days (Zha et al., 2005).

These experiments suggest that dendritic spines are capable of responding to changes in activity with rapid modifications to their structure. Yet, they also suggest that dendritic spines can remain stable for long periods. This stability can be sustained for many weeks or many months and may even last for the life time of the animal. The ability to grow and form new connections is an attractive mechanism for how new information might get stored and encoded within neuronal networks (Holtmaat and Svoboda, 2009).

1.13 Mossy fiber structural plasticity

Historically, evidence for presynaptic structural plasticity has been derived from studying discrete axonal projections in the visual cortex (Bence and Levelt, 2005; De Paola et al., 2006). More recently however, attention has shifted to studying other axonal subtypes, including the mossy fibers of the hippocampus (De Paola et al., 2003; Lawrence and McBain, 2003; Galimberti et al., 2006). Mossy fibers are of interest for a number of reasons: firstly, synapses formed between mossy fibers and CA3 pyramidal neurons are some of the largest in the brain, which can reach volumes of hundreds of cubic micrometers (Pierce and Milner, 2001; Bischofberger et al., 2006; Galimberti et al., 2006); Secondly, in addition to their sparse connectivity with principle cells, mossy fibers also synapse extensively with local inhibitory interneurons (Lawrence and McBain, 2003); a single mossy fiber typically forms only 10-18 different large terminal complexes (LMT-Cs) with pyramidal neurons, but can form ten times as many synapses onto interneurons (Acsady et al., 1998). It is thought that these extensive inhibitory synapses allow

Figure 1.3

Ai

synaptic vesicles

Mossy fibre synapse

mfb

Large thorny excrescence

Aii

mfb

B

Mossy fibre
terminals

40
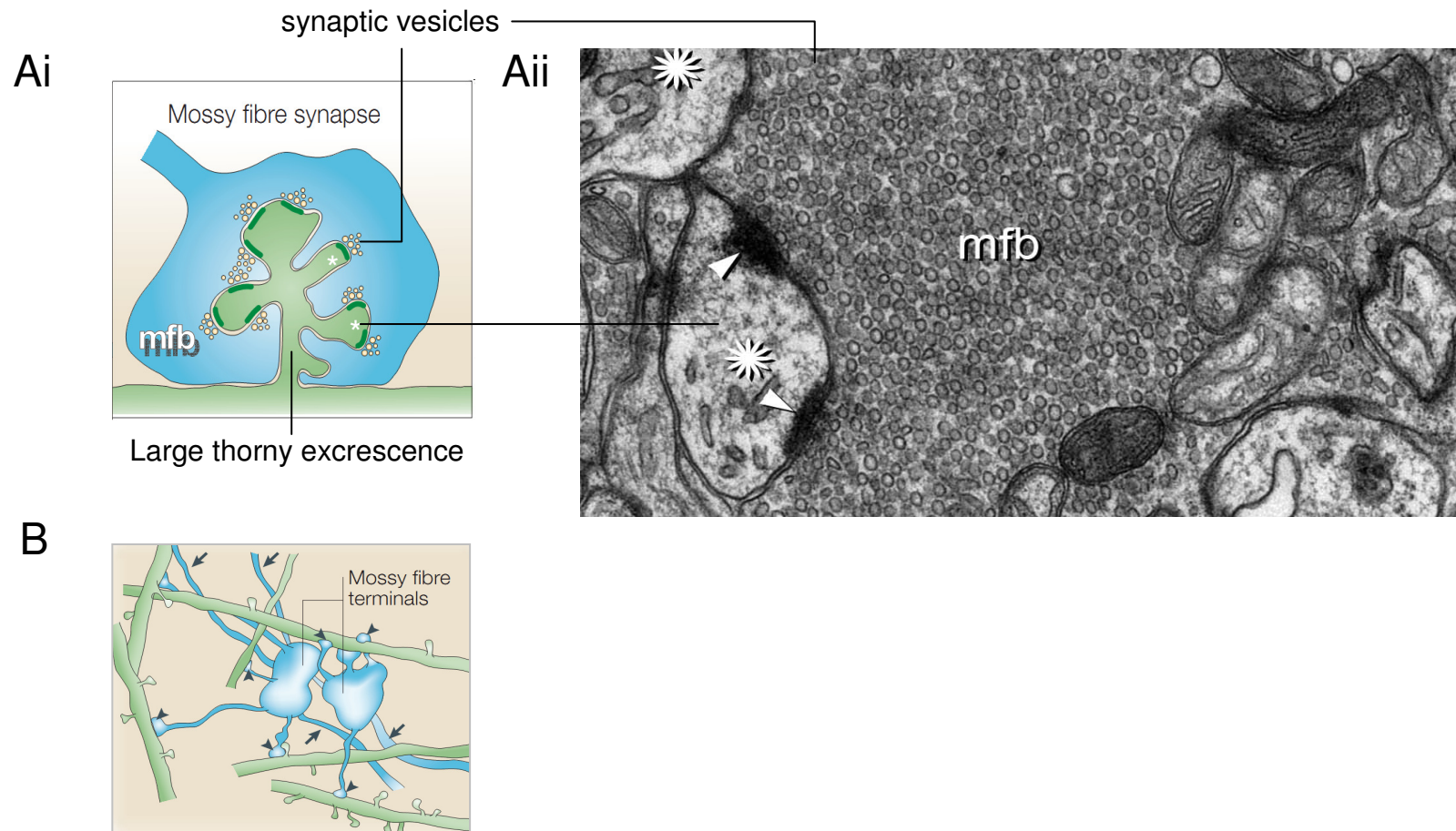
Figure 1.3 - **Structure and composition of large mossy fiber terminals.**

Dentate granule cells synapse onto CA3 pyramidal neurons by forming large complex mossy fiber terminals that engulf CA3 thorny excrescences, which are prominent on the apical dendrites of CA3 pyramidal neurons; this process is depicted in figure 1.3 Ai, which shows a large mossy fiber terminal (blue) synapsing onto the thorny excrescence of a CA3 pyramidal neuron (green). Clusters of synaptic vesicles, at presynaptic release sites, are shown in yellow. Figure 1.3 Bi: An example electron micrograph showing a large mossy fiber terminal (mfb), which is densely packed with synaptic vesicles (labelled). The mossy fiber terminal in this image is in close proximity to two post synaptic elements (asterix) containing post synaptic densities (white arrows). Figure 1.3 B: A schematic of mossy fiber terminals (blue) synapsing onto the dendrites of inhibitory interneurons. Mossy fibers synapse far more numerously onto inhibitory interneurons by projecting small filopodia like extensions to target the shaft of inhibitory interneuron dendrites (Acsady et al., 1998) . Figure 1.3 Ai and figure 1.3 B were modified from (Nicoll and Schmitz, 2005). Figure 1.3 Aii was modified from: research.mssm.edu/cnic/hamzei-sichani.

mossy fibers (granule cells) to buffer the spread of epileptiform activity through the hippocampus (Lawrence and McBain, 2003).

During development, mossy fibers show significant structural plasticity, which can persist even into the adult (Galimberti et al., 2006; Gogolla et al., 2007). Filopodia can extend out or retract over tens of microns and large mossy fiber terminal complexes (LMT-Cs) can entirely re arrange their structure (De Paola et al., 2003). These changes can be rapid and transient, occurring over seconds to minutes, or they can be persistent (De Paola et al., 2003). LMT-Cs increase in both size and complexity during development, a process that is enhanced in animals that are housed in an enriched environment (Galimberti et al., 2006). An interesting observation is that LMT-Cs show pronounced individual plasticity and turnover, but overall, the total number of LMT-Cs appears to be stable (De Paola et al., 2003). A study imaging LMT-Cs in adult mice found that very few terminals appeared or disappeared over a 15 day period (De Paola et al., 2003). In agreement with this, another study imaged LMT-Cs for several months and found that less than 1% of terminals appeared to be dynamic (Galimberti et al., 2006). This persistent stability mirrors that of dendritic spines.

Like dendritic spines, MFs also show enhanced structural plasticity in response to external stimuli. For example, acute glutamate application increases the number of motile filopodia and also the rates at which individual terminals remodel (De Paola et al., 2003). High frequency stimulation (100Hz) serves to increase terminal dynamics with a similar effect to that of glutamate (De Paola et al., 2003). This means that MFs can adapt to different stimuli input by altering their structure. This physiological structural plasticity is seen at other synapses too and represents a way in which cells can fine tune their output to the signals they receive.

Under normal conditions structural changes appear as subtle re-arrangements of axon collaterals. However, following periods of aberrant neuronal activity, such as during an epileptic seizure, MFs are seen to sprout extensive filopodial extensions, which can grow for hundreds of microns. These filopodia can even extend into the molecular layer of the dentate gyrus, a region that is usually devoid of mossy fiber synapses (Sutula et al., 1998; Scharfman et al., 2003). This produces recurrent connections that are not normally present, as seen in both animal models of

epilepsy, as well as patients suffering from temporal lobe epilepsy (Sutula et al., 1998; Molnar and Nadler, 1999; Lynd-Balta et al., 2004), The presence of these recurrent connections is thought to be a significant risk factor for future epileptic seizures. However, the underlying molecular mechanisms are poorly described. For instance, it is not yet known how vesicle transport reacts to a period of epileptiform activity, even though vesicle transport plays a critical role in both cell growth and neurite extension (Matsuzaki et al., 2011).

1.14 Cellular basis of epilepsy

Epilepsy is a severe and potentially debilitating neurological condition, in which patients suffer from recurrent seizures, or as a consequence of a previous seizure have an increased chance of suffering further seizures (McNamara, 1994). Several neurological disorders that stem from cellular malfunctions appear to predispose the sufferer to an increased likelihood of experiencing an epileptic episode. This is the case in the metabolic disorder Phenylketonuria, where because of a mutation in the enzyme phenylalanine hydroxylase there occurs a build-up of toxic metabolites within brain tissue. This metabolite build-up can cause significant cell damage and can heighten the chances of suffering future seizures (van Spronsen, 2010). In another disorder, KCNQ2 encephalopathy, the expression of a mutated voltage gated M-type potassium channel with diminished activity leads to neurons becoming hyper excitable (Weckhuysen et al., 2012). This leads to a damaging amount of epileptiform activity in neonates. Hyper activity also occurs when the activity of certain ion channels is enhanced. For example, a mutation in the β_1 voltage gated sodium channel subunit also significantly increases the chances of neuronal tissue developing epileptic seizures (Wallace et al., 1998).

Aside from ion channel malfunction and metabolite build up, there are other aberrant cellular changes that can upset the balance between excitation and inhibition; for example, increased glutamate receptor expression is correlated with

an increased chance of seizures, as is a disruption in vesicle localisation to the presynaptic vesicle density (Li et al., 1995; Zhang et al., 2004). Interestingly, in the pre-synaptic domain, as a result of epileptiform activity, both the release probability and the number of release sites for synaptic vesicles increases (Upreti et al., 2012). This results in increased NT release and can predispose neuronal networks to future seizures (Upreti et al., 2012).

Although many cellular alterations and malfunctions have been identified that can increase the likelihood of developing seizures, in many cases the importance or sequence of these events has yet to be investigated. In particular, the role of intracellular transport, which is essential for supplying receptors to the cell membrane, for regulating the number of vesicles at the synapse and for mediating structural plasticity, has been largely neglected in the pathogenesis of epilepsy. It is therefore important to observe the consequences of epileptiform activity on the transport of vesicles, to see if vesicle transport is affected by levels of neuronal activity that significantly alter other cellular systems.

1.15 Summary and aims

Intracellular transport is essential for maintaining the structure, function and survival of neurons. Disrupted axonal transport may contribute to disease progression in a number of neurodevelopmental disorders. It is therefore important that we understand both the physiological and pathophysiological contribution of axonal transport to cellular function, as well as understanding how different cell processes might regulate or alter vesicle transport. Synaptic vesicles have been characterised extensively in terms of their anatomy and function, yet data pertaining to the transport of synaptic vesicles along the axon is scarce. In the past, many labs have used non-neuronal cell lines to gather data on vesicle transport, which they extrapolated in order to build models for how vesicle transport could be accomplished in the axon. Although informative, novel methods now permit vesicle transport to be investigated directly and repeatedly in the axons of living neurons, which provides precise information about vesicle dynamics.

Using these methods, our goal was to repeatedly investigate the important transport properties of synaptic vesicles in the axon. In particular, we aimed to: (1) identify and characterise the long--term transport properties of synaptic vesicles, (2) to investigate whether vesicle transport could be modulated by changes in neuronal activity, (3) to probe for possible vesicle trafficking deficits in certain disease models and (4) to develop novel assays for focusing the study of vesicle transport onto specific neuronal cell types.

As described above, neurons demonstrate substantial pre and postsynaptic structural plasticity as a result of changes in neuronal activity. For example, increased activity leads to altered receptor expression, changes in morphology and can trigger second messenger cascades that lead to further cellular adaptations. Although much is known about the synaptic changes that occur as a result of increased neuronal activity, very little is known about how vesicle transport adapts. However, because increased neuronal activity leads to increased synaptic transmission and because synaptic transmission relies on vesicle transport, it is likely that vesicle transport would also be affected by increased

neuronal activity. Based on this, we hypothesised that vesicle transport rates would be significantly enhanced by increased neuronal activity, because of the demand for new cargo at the synapse. Any change to vesicle transport would have a significant impact on cell function given the essential role vesicle transport plays in various cellular processes. It is therefore important that we investigate physiological and pathophysiological adaptations of vesicle transport to changes in neuronal activity.

Methods and materials

Chapter 2:

2.1 Animals and procedures

All experiments and procedures were approved by the Ethical Review committee for the University of Glasgow and were performed in accordance with the United Kingdom Animals and Scientific Procedures Act 1986. All neonates were terminated under schedule 1.

2.2 Sterile practice

Strict sterile practice was adhered to at all times. All glass was steam autoclaved at $121^{o}C$ for a minimum of 20 minutes and all media was filtered using 0.2um Sartorius filters. All tools and equipment including disposable blades were first sprayed with 70% ethanol before entering the fume hood. All tools that came into contact with biological tissue, were first submerged into standard 1% Virkon concentrated media in a 50ml falcon tube, followed by two five minute washes in 70% ethanol. This prevented fungal and bacteria growth in the incubator. No anti-fugal or anti-bacterial agents were required in the culture media and cultures were checked every day for contamination. Incubators were cleaned once per month and fume hoods were cleaned before each dissection.

2.3 Primary hippocampal cell culture

To produce primary dissociated cultures we used methods similar to those presented by (Gan et al., 2011), with some modification. Hippocampi were rapidly removed from postnatal (P0 – P2) Wistar and Sprague Dawley rat pups or BALB/c mouse pups and placed into ice cold home made buffer solution. All hippocampal tissue was then mechanically and chemically dissociated. A #22 scalpel was used for the mechanical dissociation, by making approximately 20 flat crisscrossing cuts on the lid of a sterile 35mm petri dish into the tissue. Papain dissolved in

homemade-buffer (1.5mg/ml) was used for chemical dissociation. The chopped tissue was transferred to 2.5mls of $37^{o}C$ papain solution by a P3 pasteur pipette and allowed to incubate for 20-25 minutes. The media was maintained at $37^{o}C$ to promote the enzymatic action of papain. Following papain incubation, hippocampal tissue was transferred to a 15ml falcon tube containing 2mls of pre-warmed bovine serum albumin (BSA) solution made up in homemade-buffer (10mg/ml). BSA acts to halt the enzymatic action of Papain. Hippocamapal tissue was repeatedly and gently triturated several times in BSA solution using a small tipped plastic Pasteur pipette (Appletonwood Scientific, USA). This was repeated a further two more times into separate tubes containing 2mls of BSA. Finally, 6mls of BSA cell suspension was collected into a single 15ml falcon tube. The 6ml cell suspension was centrifuged at 3000rpm for 3 minutes and at $4^{o}C$ to form a small dense pellet of tissue. The buffer was carefully drained off (without disturbing the tissue pellet) and replaced with 3ml's of pre warmed neural basal A media supplemented with 1ml B27 and 0.5ml L-glutamine. Cells were suspended into NBA culture media using a P1000 pipette by gently triturating the media (approximately 30 times). After allowing the cells to settle they were then filtered through 2 cell sieves to reduce dirt and debris. Once filtered, cells were then plated onto 18x18mm pre treated Poly-L-lysine (PLL) coated cover slips (20µg/ml) in 35mm Petri dishes. Cells were left to adhere for 1 hour before the addition of 2ml of pre warmed NBA to each dish. Cells were inspected for health and general appearance, in healthy cultures neurite outgrowth was already clear at this stage. Cell cultures were incubated at $37^{o}C$ / 5% CO_2 in a humid incubator. Cell culture media was changed every 7 days; 1ml of the culture media was replaced with 1ml fresh NBA media. Dissociated cultures were made from only one animal at a time and were plated at density of 25000 cells / cover slip, in a 50µl droplet. If necessary, 30 – 40 cover slips could be prepared per dissection.

100 cover slips were prepared for cell culture by batch coating them in PLL. First a stock solution of PLL (5mls at 200µg/ml), made up in distilled water and stored at -$20^{o}C$, was defrosted and made up to 50mls using double distilled H_2O. This solution was then filter sterilised and added to a sterile 50ml falcon tube, along with 100 autoclaved glass cover slips. Cover slips and media were then gently

shaken, inverted and disturbed for 3 hours so that the media could reach all faces of the cover slip. After this, the media was then drained off, leaving only coated cover slips behind. These were then washed 3 times in sterile double distilled water and allowed to dry thoroughly on pre sterilised blue roll inside the fume hood

To produce a standardised cell culture protocol we used a haemocytometer to make cell count estimates prior to plating (LW Scientific, Inc. 800/726-7345). This produced a consistent plating density between experiments. Following the manufacturer's instructions for the haemocytometer, 100µl of a 3ml dissociated cell suspension from of a pair of neonate hippocampi was gently mixed 1:1 with trypan blue in an epindorf tube. 8µl-10µl of the trypan cell suspension was loaded into both grids of the haemocytometer using a p20 micropipette between the cover slip and the slide. Cells were counted in 5 grid regions from both grid sections and averaged by 10 to get a single value. This value was then multiplied by 2 to account for the 1:1 addition of trypan blue and then multiplied by 1×10^4 to get a value for cells per ml. The cells were then suitably diluted in fresh complete NBA media to achieve a consistent cell density of one million cells/ml. 50µl of this suspension was then added to each cover slip to plate around 50000 cells. This consistency was maintained unless otherwise stated

2.4 Organotypic hippocampal slice culture

Organotypic slice cultures were prepared using methods adapted from (Stoppini et al., 1991) using the interface method. Briefly, hippocampi were rapidly removed from male postnatal day P6 – P8 BALB/c (WT or Mecp2$^{Stop/y}$) mice and added to ice-cold serum containing media (SCM). Individual hippocampi were carefully transferred to the cutting plate of a McIlwain tissue chopper using a wide bore P3 pasteur pipette. On average, 12 structurally sound and undamaged 400µM transverse slices could be reliably produced per animal. After cutting, slices were washed off the cutting plate into a 50ml petridish, using a P3 pasteur pipette filled with chilled serum containing culture media (SCM). The petri dish and slices were then placed into the refrigerator for approximately one hour, a suggested step to

improve slice viability (Galimberti et al., 2006). After one-hour incubation at 4^oC, slices were then viewed under a dissection microscope (Nikon: SMZ 645) inside a fume hood. After visual inspection for general appearance and the presence of undamaged cell body layers, suitable slices (4 per well) were transferred to a 6 well tissue culture plate containing three porous culture inserts (Millicell, Millipore, PICM03050). Four small removable squares of membrane (0.5x0.5cm) were cut from a single Omnipore filter (JHWP02500, 25mm, Millipore) and laid onto each culture insert. A single slice was placed carefully onto each small membrane square. This allowed slices to be manipulated without causing any damage. Each well containing an insert was incubated with 1ml of pre warmed SCM. Cultures were incubated at 37^oC / 5% CO_2 in a humid incubator over night. After 24 hours serum containing media was replaced with 1ml of serum free media. Cell culture media was then changed every 2 to 3 days.

2.5 Separate cell culture of DG and CA3 cell body layers

To produce separate and defined cell cultures, it was first necessary to dissect out individual cell body layers from freshly produced acute hippocampal slices. Hippocampal slices were produced as described in paragraph 2.4. Dissection of individual cell body layers was performed under a stereo-dissecting microscope (Nikon; SMZ 645) in a 90mm petri-dish, containing chilled complete Hibernate A media (Brain bits ltd; UK; HA). Only undamaged and intact slices were chosen for dissection. Both the DG and CA3 cell body layers were dissected out using a fine tip 25g or 13g microlance needle (BD bioscience; 0.5mm x 25mm). Each individual cell body layer was collected in a separate 35mm petri-dish, also containing chilled complete Hibernate A media. Following dissection, each collection of cell body layers were individually dissociated as described in paragraph 2.3. Following dissociation, only the DG granule cell population was transduced with either lenti-GFP or lenti-syp-GFP ($1x10^6$ I.U.). Cells were triturated gently for 10s to facilitate even distribution of the virus. Following this, 50µl of the DG granule cell suspension was plated at a density of $8x10^4$ cells / ml on only one side of the wall;

CA3 cells were plated at the same volume and density on the opposite side of the wall. Cells were allowed to adhere for 1 hour before each side was gently washed with complete NBA. Following this, both the upper and lower magnetic components were carefully removed, using a pair of fine tip Dumont forceps (Fine scientific tools; UK). To do this, the wall was gently peeled upwards, so as to not disturb the cell body layers, before being lifted away. The lower segment of magnet was also removed from below the cover slip. The cultures were then fed with 2mls of pre-warmed complete NBA and left to incubate.

The magnetic wall used to separate each cell body layer was created from commercially available Halbach array magnets (first 4 magnets, UK; FTA45024A). The top and bottom magnets (described in figure 5.1) were cut to different widths; the upper magnet was cut to either 0.5x15mm or 1mmx15mm, whilst the lower magnet was cut to 5x15mm. The lower magnet was arranged so that it's magnetic field was directed upwards, whilst the magnetic field of the top magnet was directed downwards. This produced a tight seal that restricted the mixing of solution from each cell body layer (see fig 5.3).

2.6 Lentiviral preparation

Using standard molecular cloning techniques synaptophysin-GFP cDNA was obtained by PCR amplification from Thy-1-spGFP (Pun et al., 2006). Synapsin-1 promoter cDNA was obtained by PCR amplification from pXCXSynI (Glover et al., 2002). Synaptophysin-GFP and GFP cDNA were cloned into the plenti(pll4.2) lentivirus backbone by ligation, downstream of the synapsin-1 promoter, at restriction sites EcoR1 and Nhe1 (figure 2.1). Recombinant viral particles containing plenti(pll4.2) constructs expressing synapsin-1-synaptophysin-GFP or synapsin-1-GFP cDNA were then transfected into human embryonic kidney 293 (HEK) cell culture for viral particle production (paragraph 2.8 methods). GFP was fused downstream of synaptophysin at the C-terminus, which produces fluorescence in the cytoplasmic domain (Johnston et al., 1989). A graphical summary of each viral plasmid is described in figure 2.1. Viral vectors were a kind gift from Professor Kumlesh K. Dev. Kamal K. E. Gadalla produced the viral particles used in this project.
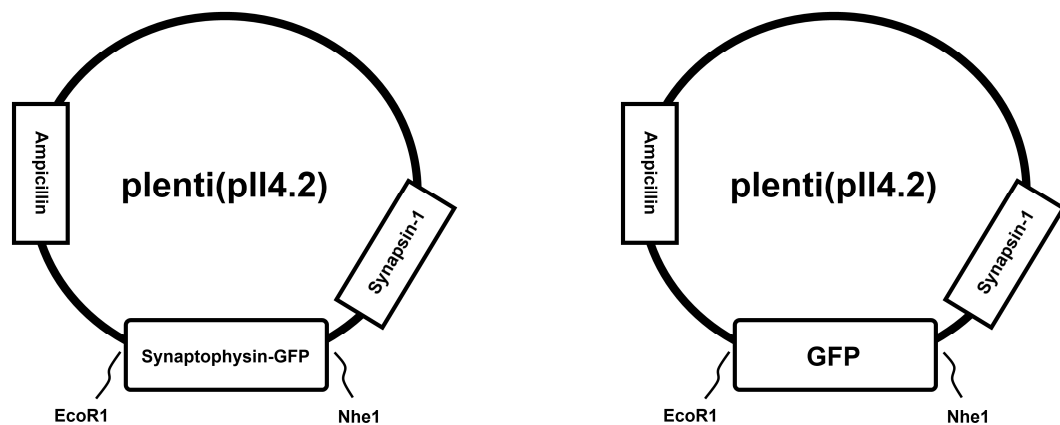
Figure 2.1 - Schematic diagram of lentiviral constructs

Both synaptophysin-GFP and GFP were driven under the synapsin-1 promoter, in the plenti (pll4.2 backbone) with ampicillin resistance. A ligation reaction was used to insert Syp-GFP and GFP between EcoR1 and Nhe1 restriction sites.

2.7 HEK cell culture

Human Embryonic Kidney cells (HEK 293T) cells were recovered from liquid nitrogen and transferred to a cell culture suit by a container of dry ice. The cells were then allowed to warm gently at room temperature for 2 minutes before being warmed more vigorously at 37^oC in a heated water bath until defrosted. Once defrosted HEK cells were transferred to a sterile fume hood and into 9ml's of pre incubated (37^oC and 5% CO_2) complete DMEM. Once mixed in the DMEM the cell suspension was then centrifuged for 4 minutes at 4000rpm. The supernatant was discarded and the HEK cells were re-suspended into 1ml of pre incubated complete DMEM. The HEK cell suspension was then added to a pre-incubated T150ml flask with 30ml of complete DMEM and disturbed to allow even plating. The plate was then incubated over night at 37^oC and 5% CO_2 before the media was changed. Cell growth was checked daily and inspected for contamination or over confluency. Once the cells had reached a confluency of around 75-80% they were passaged into a new container. To perform passage, the old media was discarded and cells were washed in DPBS to remove excess serum before being incubated with 3ml's of trypsin for 3 minutes. After incubation cells were washed in DMEM complete media and pipetted up and down to facilitate the dispersal of cells. To estimate cell counts a hemocytometer was used as per the manufacturers instructions (LW Scientific, Inc. 800/726-7345). After this ($8x10^6$ cells) were added to a tissue culture flask for subsequent cell culture. Cells reached 75-80% confluency after approximately 24 hours and were then suitable for plasmid transfection.

2.8 HEK 293T cell transfection

After a suitable confluence had been achieved HEK cells could then be transfected to produce viral particles. A PEI solution was made up to allow transfection of viral plasmids. 1µl of PEI was added to 5mls of OptiMEM, mixed several times by inversion and then sterile filtered into a fresh 50ml falcon tube.

The DNA plasmids were then added to 5mls of OptiMEM; lenti vector (40µg), packaging plasmid (pMDLg/PRRE) (20µg), envelope plasmid (pMD$_2$G) (10µg) and rev plasmid (pRSV-REV) (10µg). The OptiMEM / DNA media also mixed by inversion several times followed by sterile filtration into a fresh 50ml falcon tube. OptiMEM PEI was then added to OptiMEM DNA drop wise, mixed several times by inversion and left at room temperature for 20-25 minutes to allow the precipitate to form. The HEK cell media was removed and replaced with the PEI / DNA mix, and left for 4 hours in the incubator. After incubation, cells were checked for visible formation of a black precipitate. If this was confirmed, all media in the plate was discarded and replaced with 30mls of fresh complete DMEM. Transfected cultures were left to express viral particles in the incubator for 48hrs. After 48hrs media was removed into a sterile 50ml falcon tube, 30mls of fresh media was replaced and the cultures were returned to the incubator. The media containing viral particles was centrifuged at 4000rpm for 4 minutes to form a cell pellet, only the media was filter sterilised to a fresh 50ml falcon tube, the cell pellet was sprayed with Virkon and discarded. The viral media was placed in the refrigerator over night. The following day the rest of the media was collected like the first day; the plate was sprayed with Virkon and discarded. The viral suspensions were mixed together before being ultra-centrifuged at 27000rpm for 2hrs (4^oC). They were re-suspended into 100-200µls of DPBS and stored in 10µl aliquots in the -80°C freezer.

2.9 Bacterial transformation

An aliquot of chemically competent DH5α bacterial cells (Invitrogen 18265-017) were recovered from frozen in the –80°C freezer in preparation for plasmid transformation. A single aliquot was then transformed using 10-100ng of plasmid. After mixing several times the cells were allowed to sit on ice for 30 minutes. The bacterial mix was then heated at 42°C for 30-45 seconds before being incubated on ice for 3 minutes. After cooling, 900µl of LB media was added to each tube and left to incubate for 60-90 minutes at 37°C in a shaking incubator. 100µl of

transformed cells were then spread on agar containing suitable antibiotics and left over night at 37°C; the next day a single colony was then sub cultured for a maxi-prep as per the manufacturers instructions (QIAGEN, Crawley, UK). A minimum of 1µg of DNA was collected after purification measured using a spectrophotometer (Nano-drop1000, Thermo Scientific, USA).

2.10 Standard PCR

Standard PCR reactions were carried out in a volume of 25-50µl using either hot star PCR buffer (QIAGEN, Crawley, UK) or phire 5X buffer (New England BioLabs, Ipswich, UK). DNA plasmid concentrations used for PCR ranged from 100pg-10ng with 0.25µM dNTPS and 0.5µM concentrations of both forward and reverse primers. PCR conditions were modified slightly depending on the polymerase used, the primers needed and the construct size.

2.11 Gel electrophoresis

According to their size DNA molecules were separated on Agarose gel using electrophoresis. Agarose (0.8-1.0% (w/v) was added to 100ml of 0.5XTBE buffer and heated in a microwave on full power until all the Agarose had dissolved. After allowing time for the solution to cool, Ethidium bromide (Sigma E-1510) was then added at 200ng/ml to facilitate the visualisation of DNA, post electrophoresis, under U.V. light. The Agarose solution was placed in a horizontal loading tray and allowed to solidify for 1hr at room temperature. After the gel had solidified DNA samples were mixed with 1XDNA loading dye and carefully loaded to each lane of the gel. One lane was reserved for the running of 300-600ng of a DNA size ladder. After approximately 1hr of electrophoresis at 100-120volts/cm the gel was removed carefully from the loading tray and visualised under a U.V. light source (254nm wavelength). An image of the gel was captured for post-hoc analysis to

determine of how far each lane of DNA had run. All bacterial stocks were stored in 25% glycerol at -80°C.

2.12 Transduction of dissociated cell cultures

Dissociated cell cultures were transduced with lentivirus at DIV0. Stock solutions of lenti-syp-GFP or lenti-GFP were diluted to a working concentrations of $1x10^6$ or $1x10^8$ I.U/ml. Viral particles were added directly to freshly dissociated cell cultures prior to plating; falcon tubes containing cells and viral particles were then gently triturated to ensure even distribution of viral particles. Dissociated cultures were then left to express the lentiviral construct for a minimum of seven days prior to imaging.

2.13 Focal lentiviral injection into the DG cell layer

To investigate vesicle dynamics at mossy fiber synapses, lenti-syp-GFP was selectively targeted to the dentate gyrus via focal and controlled injection of viral particles. Slices were transferred in Hibernate A media to an inverted microscope with a protective sterile plastic cover. Micro capillaries with a tip diameter of 5μm were back filled with lenti-virus ($2x10^7$ infectious units) from a 75μl stock until 3/4 full. Micro capillaries were then held in place by stable manipulators attached to the microscope. Micro capillaries were fabricated using the P-97 micropipette puller (Sutter instruments company). Viral particles were injected using medical air regulated by a Pico-Sprizter system. The Pico-Spritzer was set to perform low pressure (0.5-1.5 psi) 3 second bursts upon command; this allowed for a slow and steady release of the viral solution. Several sparse injections were made along the cell body and molecular layer, under visual inspection, using x4 magnification. Capillary tips often became blocked, so a "clean tip" command was issued to the Pico-Spritzer that would engage a short high pressure burst to clean the tip. After

Figure 2.1

Confocal stack

1. **Image enhancement**

Subtract background	Enhance contrast	3D median filter
[50 pixel]	[N.A. 0.4%]	[1 pixel]

2. **Automatic threshold and segmentation**

Stable count thresholding

(Russel et al, 2009)

Binary output

3. **Volume measurement**

Object counter 3D

(Bolte and Cordelières, 2006)

Identified particles

4. **Data manipulation**

Excel / Graph pad prism
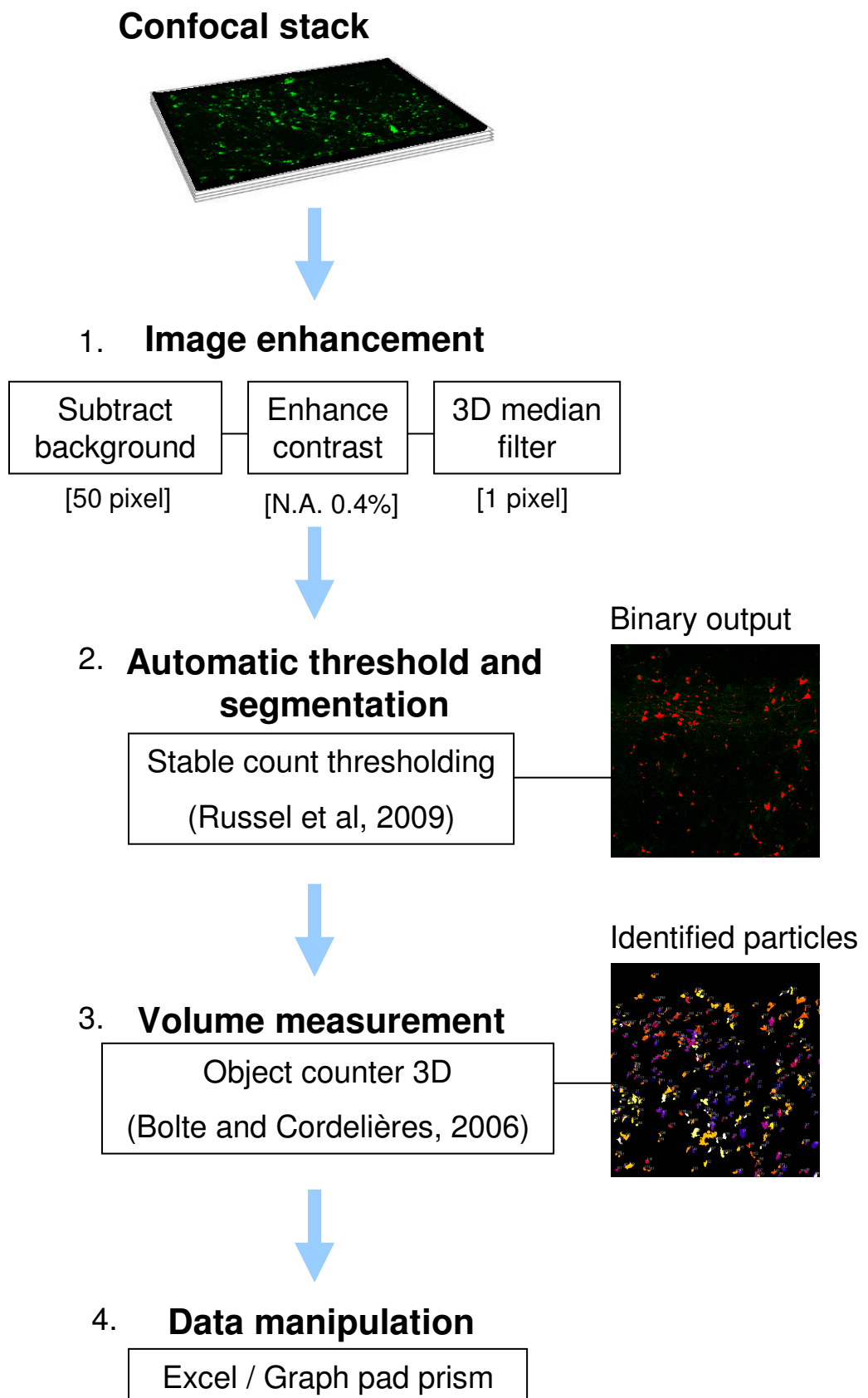
Figure 2.1 - **A workflow for automatically analysing the volume of syp-GFP positive vesicle clusters.**

To analyse the volume of syp-GFP positive vesicle clusters obtained in confocal stacks, it was necessary to develop a workflow for enhancing, segmenting and then measuring the volume of individual vesicle clusters automatically. Figure 2.1 summarises this workflow. Image enhancement was the first step in image processing. All settings used in this workflow were the default settings given by image J and stated in section 1. Image enhancement was used to improve signal to noise and to filter out spurious signal. Following image enhancement, automatic segmentation was achieved by incorporating the "stable object count" algorithm created by Russell et al, 2009. This algorithm identifies objects of interest in an image stack by incrementally increasing the threshold value of the stack and counting the number of thresholded pixels at each increment; when the pixel value becomes stable with successive increases in threshold, objects of interest are estimated to be distinguished from background noise. This provides a deterministic and impartial threshold value for estimating the distribution of large vesicle clusters. Following automatic thresholding, object counter 3D was then used to measure the volumes of individual vesicle clusters (Bolte and Cordelieres, 2006). Data was then output and processed in excel.

injections, slices were quickly returned the incubator and left to express for 7-10 days before live imaging, drug treatment or immunocytochemistry.

2.14 Immunocytochemistry

Cover slips containing cultured cells were fixed in 4% paraformaldehyde (PF) at DIV10-14 for 10 minutes. After fixation, PF was washed out of the cell culture using three 10-minute washes in double salt PBS. Various primary antibodies were dissolved in double salt PBS containing 0.3% Triton X. Cultures were incubated with primary antibodies for 24hrs (concentrations shown in table 2.3). Following incubation, cell cultures were washed with three further 10-minute washes in double salt PBS. Specific secondary antibodies were then applied for three hours (see figure 2.4). These were also washed away by three 10-minute washes in double salt PBS. Cultures were then mounted onto glass slides using home-made vector shield and sealed with varnish. DAPI was included in the vector shield to help identify nuclei and to aid in cell quantification.

To identify the origin and location of syp-GFP positive clusters in dissociated culture we performed immunolabelling for MAP2, GFP and also VGLUT1. MAP2 (1:1000) was used to identify cell bodies and dendrites to see if identified syp-GFP positive clusters were accumulating in their expected location. VGLUT1 (1:2000) was used as a marker for synaptic vesicles and GFP (1:1000) was used to improve signal to noise levels of syp-GFP.

Organotypic cultures were fixed and washed in a similar way to dissociated cultures but with slight adjustments to fixation and antibody incubation times. An additional blocking step was also included to reduce background fluorescence. Organotypic slices were fixed for 1hr in 4% PF before three 10-minute washes in double salt PBS. Slices were then blocked in normal goat serum (10%) for 1hr. Primary antibodies were left on for 3 days. Secondary antibodies were left on for 24hrs.

To improve the signal to noise level of the syp-GFP signal, organotypic slices injected with syp-GFP were immunostained for GFP (1:1000). Slices were also immunostained for NeuN to help identify cell body layers (1:500) and the location of the stratum lucidum.

2.15 Imaging of large vesicle clusters

Immunolabelled cultures were then imaged using a confocal laser-scanning microscope equipped with a Krypton-Argon laser (Bio-Rad; UK). Slice cultures were viewed using a X60 lens (NA 1.3). Image stacks were produced with an XY pixel value of 0.16μm and optical sections were captured at a z-interval of 0.2μm. To sample within the dynamic range of the 8 bit system, sub-saturating grey scale values were obtained by adjusting laser intensity and gain between experiments. Images were captured as close to the Nyquist sampling rate as was feasible. In order to quantify large vesicle clusters in organotypic slices, three regions were chosen that sequentially ran along the stratum lucidum. Image stacks were captured from the top 80-90 optical sections (≈20μm) of the slice. This provided clear image stacks of large vesicle clusters located along the stratum lucidum. Images stacks were saved as .TIF files before being analysed using Image J / FIJI.

2.16 Live imaging overview

In order to visualise vesicle dynamics in axonal projections over time slice cultures were imaged at 14-17 days post-transduction. Dissociated cell cultures were taken 10 – 14 days post-transduction with lenti-synaptophysin-GFP and imaged using a CCD camera (Orca R2; Hamamatsu, UK), connected to an upright microscope (Nikon SMZ 645; Tokyo, Japan). Fluorescent illumination was produced by a

fluorescent LED system (OptoLED; Cairn research, Kent, UK) at approximately 498nm and filtered to allow peak emission transmission of approximately 520nm (filter set; Chroma, VT, USA). Slice cultures were constantly perfused with ACSF that was bubbled with 95% O_2/ 5% CO_2 and warmed using an inline heater and controller to 34^oC - 37^oC (Warner instruments, UK). Dissociated cell cultures were imaged without the need for flow, in Hibernate A media and Hibernate A low fluorescence media (HA / LF-HA; Brain bits ltd, UK), which are modified culture media that can maintain pH under ambient atmospheric conditions (Brewer and Torricelli, 2007). Cell cultures were heated using a thermo-regulated metal jacket to 37^oC also controlled by a heating controller (Warner instruments, UK). Organotypic cultures were viewed using a Nikon x60 plan fluor water immersion NA 1.0 and dissociated cultures were imaged using a Nikon x100 Oil immersion NA 1.3. When searching for a suitable region of interest the lowest possible power needed to visualise the cultures was used and this was used for the least possible amount of time.

All imaging systems were controlled using the image J freeware plug-in μ manager (Image J; NIH, USA).

2.17 Live imaging – dissociated culture

To image vesicle dynamics along axonal segments, two different imaging protocols were used. One protocol was designed to capture highly motile particles, whilst the other protocol was designed to capture the long-term dynamics of large vesicle clusters. Particles and clusters had different temporal characteristics so each protocol captured images at a different frequency. To quantify the movement of motile particles we used both short frequency (duration (D) = 60s) and high frequency (Interval between frames (I) = 0.6s) image capture. In order to minimise bleaching we kept power on the OptoLED system (P = 20Au) and exposure (E = 150ms) as low as possible. We used a high binning rate (B=4) to improve signal to noise. This provided smooth particle tracks and particles that did not fade. Two

high frequency trafficking videos were taken at T=0hrs and T=10hrs. The second video was taken approximately 5 minutes after the first, but with a lower frequency and longer duration (D=120s and I=1.2s). This video was used as a reference for identifying stationary vesicle clusters. Using these videos we were able to sample vesicle transport from the same axonal segment over 10hrs. Axons chosen for imaging were long, straight and free from damage. Axons that were broken, damaged or that showed no particle movement were ignored. To minimise photo-bleaching, axons were exposed to no more than 40s of light during the entire imaging protocol.

To image the dynamics of large vesicle clusters we used low frequency optical sectioning to image the entire z-axis of the axonal segment. This minimised the spurious effects of drift. Approximately 10-30 optical sections (0.3μm z-step) were used to capture each axonal segment. Exposure and fluorescence were kept to a minimum during experiments (E=200ms and P=20Au). Using these settings it was possible to sample vesicle cluster dynamics at T=0hrs and T=10hrs with no evidence of bleaching. Images were captured at 1024x1024 resolution. All experiments, control and treated, were interleaved to decrease variability.

2.18 Live imaging - organotypic slice culture

In order to track the size and distribution of large vesicle clusters over time we used optical sectioning (0.3μm z-step) to repeatedly image vesicle clusters for several hours. We measured individual vesicle clusters every hour for six hours in the presence or absence of 20μm gabazine (gabazine; SR95531; Tocris, UK). Image stacks were captured repeatedly from a single region in the stratum lucidum. Approximately 80-90 optical sections were used to capture the entire structure of vesicle clusters in the area. To establish a baseline for cluster size, control stacks were captured at T=0hrs and T=1hrs prior to gabazine application. Control experiments were interleaved between GBZ treated experiments. Images

were processed using blind deconvolution (Huygens, UK) before being assessed and measured for changes in volume over time. We used a Nikon plan fluor objective (x60) to image in vesicle clusters. All cultures were imaged under low-medium power and exposure, to minimise bleaching (B=2, E=200ms and P=30AU).

2.19 Analysis of vesicle cluster dynamics (dissociated culture)

To quantify the movement of vesicle clusters over time we used FIJI/imagej (NIH; USA) to generate max projection images of axonal segments at T=0hrs and T=10hrs and compared the location of vesicle clusters. Vesicle clusters were identified for their size (greater than the width of the axon) and their short-term stability (stable for >5 minutes) (De Paola et al., 2003). Max projection images were concatenated using FIJI so that T=0hrs was frame one and T=10hrs was frame two. Images were then flattened as a colour RGB, which generated a single merged image that allowed the dynamics of vesicle clusters to be easily visualised (Fig 3.5 – B). To estimate the size of vesicle clusters, we measured the maximal cross sectional area (CSA) (from a flattened max image projection) of each vesicle cluster at T=0hrs and T=10hrs. Images were manually segmented using Imagej/FIJI. Only stable vesicle clusters were assessed for a change in size.

2.20 Analysis of motile particle dynamics (dissociated culture)

Time-lapse video of particle transport was analysed using "Automatic kymograph analysis" (AKA), a custom made software, was a kind gift from (Mukherjee et al., 2011). Vesicle transport was analysed along a 50µm length of axon. Smooth axons were automatically traced in AKA, but axons containing many large vesicle clusters were traced manually using FIJI.

To trace axons manually, videos containing vesicle transport were loaded into FIJI and converted to a max projection image. This max projection image was then used as a template to identify the position of the axon. The axon was traced in white, whilst the background was labelled black. Images were saved as a single TIF file before being loaded in AKA. In order to analyse motile particle transport, an image stack containing 100 frames and representing 60s worth of high frequency video (I = 0.6s) was loaded into AKA, accompanied by a black and white trace of the axon. The white axon was then highlighted and automatically overlaid to the video. This generated a kymograph of vesicle transport along the axon. This kymograph was automatically adjusted for good contrast within AKA. Particles were tracked automatically using AKA, but occasionally some tracks were missing. Manual adjustment of tracks was possible and spurious tracks were deleted. Large stationary vesicle clusters were ignored.

2.21 Analysis of vesicle cluster dynamics (organotypic culture)

To measure the volume of vesicle clusters over time, we used Huygens Essential to manually crop out and analyse individual vesicle clusters. Simultaneous analysis of all vesicle clusters was not possible due to poor signal to noise. Individual clusters were first cropped at the same xyz co-ordinates through each time point. All deconvolution was done using default iteration and was based on an estimated point spread function given by: x60 objective (n.a., 1.0), excitation wavelength (488nm), emission wavelength (520nm) and a refractive index of the imaging media (1.33). Deconvolution improved signal to noise sufficiently to allow an estimate of vesicle cluster volume. Clusters were identified using manual thresholding and were rendered in 3D. Volumes were measured in the Huygens analysis suite.

2.22 Analysis of large vesicle clusters (organotypic culture)

To measure the volume of vesicle clusters along the stratum lucidum it was necessary to automate an analysis workflow. This workflow is summarised in figure 2.1 and consists of four main steps: 1) Image enhancement. 2) Automatic threshold and segmentation, 3) Volume measurement and 4) data manipulation. The goal of image enhancement was to improve the contrast of vesicle clusters (enhance contrast 0.4%), to remove noise (3D median filter, 1 pixel) and to correct for uneven background illumination (subtract background, 50 pixel rolling ball). This produced clear vesicle clusters that could be reliably thresholded in step two. To accurately and automatically threshold image stacks we applied an algorithm that was used previously in the quantification of fluorescent images (Russell et al., 2009). This algorithm determines the "best" threshold level for each confocal stack. In simple terms, it counts the number of voxels in an image stack whilst simultaneously increasing the threshold level, when the voxel count becomes stable it assumes that objects of interest have been identified from background noise, the image is then thresholded at this level. Automatic thresholding removed the potential error that can derive from manual segmentation. After accurate segmentation, 3D object counter (a widely-used plugin for ImageJ/FIJI) was used to count the number of segmented voxels in each vesicle cluster (Bolte and Cordelieres, 2006). The volume of each segmented cluster was then analysed before being individually numbered for future reference. Data output was analysed in Microsoft Excel. Fluorescent objects with a volume less than $2\mu m^3$ were ignored, as these likely represent small motile particles rather than vesicle clusters. Fluorescent objects greater than $15\mu m^3$ were classified as large vesicle clusters, in line with previous estimates for the volume of large mossy fiber terminals (Bischofberger et al., 2006). A distribution of these terminals as shown in (figure 4.4). All steps in the workflow were incorporated into an analysis macro created using ImageJ.

2.23 Calcium imaging

Calcium imaging was used to check for network activity in dissociated cultures. Calcium spikes have been shown to correlate well with the induction of action potential firing (Smetters et al., 1999) and can serve as a measure for culture activity (Ivenshitz and Segal, 2010). To this extent, calcium imaging was used to test for bic-induced neuronal activity. Cultures were loaded with 2.5μM Fluo-3 AM ester (Biotinum; UK) for 60mins in complete NBA culture media at 37°C. The cells were then washed and allowed to sit for 30 minutes in low fluor HA buffer at 37°C before being imaged; this improved loading by allowing sufficient time for de-esterification of the AM ester. Using a X20 Nikon NA 0.45 objective lens, a single region was randomly selected from the cover slip and imaged for 60s at 100hz. This provided calcium spikes that could be reliably reconstructed. Cultures were then treated with 20µm bic or vehicle before being imaged for a further 60s. The number of cells firing action potentials was expressed as a proportion of the total number of stained cells.

2.24 Electrophysiology

To check for activity in organotypic slices, we used field recordings to measure population spikes in the region of the CA3. Briefly, organotypic slice cultures were transferred to an imaging chamber and held in place using a platinum ring. Slices were submerged in oxygenated (95%O_2/5%CO_2) flowing ACSF (2mls/minute) at 34°C. Under x20 magnification a recording electrode was then placed into the CA3 cell body layer. Control recordings were made for 15 minutes before the application of 20µm bic. Slices were recorded for 1hr following bic treatment. Recording electrodes contained 0.5M NaCl. Field potentials were sampled at 10kHz and filtered at 1kHz. Head stage connectors were passed through an Axoclamp B amplifier and a Brownlee amplifier (gain, 10) (model 440; Brownlee Precision, USA). A humbug noise eliminator was used to remove 50Hz noise (Quest scientific, UK). Data were captured using a NDAQ A-D board (National Instruments, UK).

2.25 Genotyping of *Mecp2*^{Stop/y} mice

Bird et al., University of Edinburgh, created the Mecp2-stop mouse model used in this project (Guy et al., 2001). In this model, all Male Mecp2$^{Stop/y}$ mice have truncated mRNA, which disrupts Mecp2 protein expression, whilst females express an X-linked mosaicism of truncated protein. Shih-Ming Weng, Glasgow University; used PCR to confirm the genotypes of all mice used in this study. Methods were performed as described previously (Weng et al., 2011). DNA was collected from tail samples taken prior to cell culture. Primers used for genotyping were developed by (Guy et al., 2007). These were used to differentiate between WT and Mecp2$^{Stop/y}$ litter mates (Fig 4.6).

2.26 Statistics and data handling

All statistical tests were performed using Minitab or Graphpad prism. Graphs were created in Graphpad prism. Tables and charts were managed using Microsoft Excel. The statistical tests performed in the thesis were as follows: unpaired student T-test, paired student T-test, Wilcoxon-matched pairs test, one way ANOVA (analysis of variance), two-way ANOVA (analysis of variance) and Mann-Whitney non-parametric. When comparing between two normally distributed data sets an unpaired or paired student's T-test was applied to look for significant differences between the means. When comparing between the means of three or more normally distributed samples, a one-way or two-way ANOVA test was applied. The Wilcoxon-matched pairs test was used to test for differences in the median value of two non-normally distributed samples. The Mann-Whitney non-parametric test was applied to unpaired, non-normally distributed data to test whether the median value's of two samples were significantly different.

Table 2.1 - Equipment for viral preparation

Type:	Equipment list:	Supplier:	Cat. #
HEK cells	Human embryonic kidney cells	ATCCCRL	11268
Media	Sodium Pyruvate	Sigma	S8636
	Fetal bovine serum (FBS) heat inactivated	Sigma	F9665
	DMEM (high glucose, no glutamine, with sodium Pyruvate)	Sigma	D6546
	Trypsin / EDTA 0.25%	Sigma	T4049
	Polyethylenimine (PEI)	Sigma	408727
	Trypan blue solution (0.4%)	Sigma	T8154
	Phosphate buffer solution (PBS) 1X w-out calcium	Invitrogen	14190-0942.47
	L-Glutamine	Invitrogen	25030-024
	Pen-Strep 10K units	Invitrogen	15140-1225.61
	Optimem-1 W/Glutamax-1	Invitrogen	51985-026
Plasmids	Plasmid pMD2.G	Addgene	12259
	Plasmid pMDLg/pRRE	Addgene	12251
	Plasmid pRSV-Rev	Addgene	12253
Disposable	TC FLASK 150CM VENTED	Corning	430825
	Nunc Cryo-tube vial	Sigma	V7759
	Syringe filter (0.2um / 25mm)	Sartorius	16534k

Table 2.2 - Enzyme supply list

Enzyme list:	Supplier:	Cat. #
GoTaq hot start Polymerase -	Promega	M5001
Thermo-start high performance PCR mater mixes	Thermo-scientific	AB-1147
Phire hot start DNA polymerase	NEB	F-120s
Crimson Taq DNA Polymerase	NEB	M0324G
T4 DNA ligase	Invitrogen	15224/017
Rapid DNA ligation kit	Roche	11 635 379 001
T4 DNA ligase	NEB	0202S

Table 2.3 - Primary antibody list

Antibody	Species	Dilution	Source
NeuN	Mouse	1:500	Millipore, UK
MAP2	Mouse	1:1000	Sigma
GFP	Sheep	1:1000	AbD Serotec
Calbindin	Rabbit	1:1500	Gift from Dr Imre Vida
VGLUT1	Rabbit	1:2000	Synaptic-Systems
Synaptophysin	Mouse	1:500	Chemicon

Table 2.4 - Secondary antibody list

Antibody	Species	Working dilution	Source
Alexa 488	Sheep	1:500	Biotium
Alexa 488	Mouse	1:500	Jackson laboratories
Alexa 567	Mouse	1:500	Jackson laboratories
Alexa 647	Rabbit	1:500	Jackson laboratories
Alexa 647	Mouse	1:500	Jackson laboratories

2.27 Equipment and solutions

Dissociated culture:

Item:	Cat. No.
- Papain;	SIGMA - P4762 -100MG
- BSA	SIGMA - A9418 -10G
- Pasteur pipettes 1ml	Greiner - 612399 - 1ml
- Falcon tube - 15ml	Corning - 430790
- Fine tip Pasteur pipette	Appleton woods UK - KC257
- NBA	INVITROGEN - 10888-022 - 500ml
- B27 (x50)	INVITROGEN - 17504-044 -10ml
- L-glutamine 10ml	VITROGEN - 25030-024 - 200mM
- Poly-L-lysine	INVITROGEN - P6282 - 5MG
- 35mm Petri dish	Greiner - 627102
- Trypan Blue	SIGMA - T8154-100ML

Organotypic culture:

Item:	Cat. No.
- Millicell slice culture inserts	PICM03050
- Mc Ilwain tissue chopper	ICKLE Engineering Co. UK
- L-Glutamine	SIGMA - G7513 - 200mM/100ml
- Neural basal-A media	INVITROGEN - 10888-022 – 50ml
- B27 (x50)	INVITROGEN - 17504-044 – 10ml
- Hanks Buffered Salt Solution	INVITROGEN - 14170-088 - 500ml
- MEM	INVITROGEN - 21090-022 – 500ml
- HORSE SERUM	INVITROGEN - 26050-088 – 500ml
- OPTI-MEM – GLUTAMAX	INVITROGEN 11058-021 – 500ml

Home made cell culture buffer:

NaCl	116 mM
KCl	5.4 mM
$NaHCO_3$	26 mM
NaH2PO$_4$	1.3 mM
$MgSO_4.7H_2O$	1 mM
$CaCl_2.2H_2O$	1 mM
$EDTA.2Na.2H_2O$	0.5 mM
Glucose	25 mM
pH	7.4
Osmolarity	350mOsm

Dissection media (DM):

OPTI-MEM with HEPES   50ml

Glucose   27.5mM

Serum culture media (SCM):

Heat inactivated horse serum   25ml

Hanks buffered salt solution   12.5ml

OPTI-MEM with HEPES   12.5ml

Glucose   27.5mM

HEPES   5mM

Serum free culture media (SFCM):

Neural basal A	48.5ml
B27	1ml
L-Glutamine	0.5ml
Glucose	27.5mM
HEPES	10mM

Low fluorescence Hibernate buffer (LFHA):

Low fluorescence HA	48.5ml
B27	1ml
L-Glutamine	0.5ml

Complete Hibernate buffer:

Hibernate A   48.5ml

B27   1ml

L-Glutamine   0.5ml

Artificial cerebrospinal fluid (ACSF):

NaCl   125 mM

KCl   2.5 mM

$NaHCO_3$ 25 mM

NaH2PO$_4$ 1.24 mM

$MgSO_4.7H_2O$ 1 mM

$CaCl_2.2H_2O$ 2 mM

Glucose   25 mM

Complete DMEM:

DMEM   500ml

Fetal Bovine serum (FBS)   50ml

L-Glutamine   5ml

Antibiotics Pen.-Strept.   5ml

Sodium Pyruvate   5ml

PBS x10 stock:

NaCl   1.37 M

KCl   27mM

Na_2HPO_4 80mM

KH_2PO_4 20mM

Double distilled water   1L

pH 7.4

Phosphate buffer:

Dissolve the following in 800ml distilled H_2O:

NaCl   8g

KCl   0.2g

Na_2HPO_4 1.44g

KH_2PO_4 0.24g

Adjust volume to 1L with additional distilled H_2O.

pH   7.4.

Bacterial solutions:

Luria-Bertani (LB) medium:

Bacto-tryptine	3%
Bacto-Yeast extract	0.5%
NaCl	1%

LB agar:

LB media	-
Agar	7-10%

Ampicillin stock solution:

Ampicillin	25 mg/ml in water
	(Working concentration is 50ug/ml)

SOB media:

Bacto-tryptine	2%
Bacto-Yeast extract	0.5%
NaCl	10mM
KCl	0.25mM
$MgCl_2$	10mM
$MgSO_4$	10mM
pH = 7	

SOC media:

SOB media	-
Glucose	0.04%

Alkaline lysis solutions:

Solution I (re-suspension solution)):

glucose   50 mM

tris-HCL (pH 8.0)   25 mM

EDTA   10 mM.

Storage - 4°C

Solution II (Lysis solution):

NAOH   0.2mM

1% SDS

Solution III (neutralization solution) 3M KAC:

potassium acetate   294.45 g

glacial acetic acid   115 ml

Water   885ml

Results

Chapter 3:

Activity-dependent modulation of synaptophysin positive vesicles in dissociated hippocampal neurons

3.0 Introduction

Synaptic vesicles (SVs) play a vital role in both the storage and release of neurotransmitter and are responsible for the quantal nature of NT release (Del Castillo and Katz, 1954; Heuser and Reese, 1973; Heuser et al., 1979; Sudhof, 2004; Augustine and Kasai, 2007). Most NT release at the synapse occurs via the calcium sensitive exocytosis of SVs (Fatt and Katz, 1952; Brose et al., 1992; Augustine and Kasai, 2007; Neher and Sakaba, 2008). Proteins located in the membrane of SVs and at the active zone (AZ) are sensitive to changes in calcium, which acts as a chemical signal for the controlled release of NT (Brose et al., 1992; Taubenblatt et al., 1999). Following release, SVs can then recycle and refill in preparation for new rounds of exocytosis (Heuser and Reese, 1973; Haucke et al., 2011). As a result of recycling small quantities of SVs can maintain synaptic transmission even during periods of increased activity (Murthy and De Camilli, 2003; Galli and Haucke, 2004).

At the synapse vesicle recycling permits self-sustaining neurotransmission. However, vesicle recycling is insufficient for indefinitely maintaining synaptic transmission (Yonekawa et al., 1998; Ma et al., 2009; Sharma et al., 2012). Over time it becomes necessary for proteins at the active zone and in the vesicle membrane to be replaced or modified (Speese et al., 2003). Although protein production in the axon is widely accepted, the bulk of protein is still produced in the cell body (Brittis et al., 2002). Neurons must therefore transport this newly synthesised protein over long distances to the synapse. Nascent protein is delivered in transport vesicles or tubulo-vesicular structures, which are transported by molecular motors (Yonekawa et al., 1998; Ahmari et al., 2000; Hirokawa and Noda, 2008; Hirokawa et al., 2009). These vesicles are seen to transport precursor proteins out to the synapse, where they can be functionally integrated into either the plasma membrane or synaptic vesicles. Disrupting the movement of transport vesicles significantly disrupts synaptic transmission, which can ultimately lead to cell death.

As well as delivering transport vesicles, molecular motors also work in unison to shuttle SVs and large dense core vesicles (LDCVs) (Zhou and Misler, 1995; Yonekawa et al., 1998; Hokfelt et al., 2000). These vesicles are often delivered to sites representing new or existing synaptic contacts (Sabo et al., 2006). A bi-directional "tug of war" occurs between different motor families, which facilitates the precise placement of SVs (Hendricks et al., 2010). As seen from electron micrographs SVs are usually transported in small packets, these mobile packets form part of a shared pool that can move between neighbouring synapses (Krueger et al., 2003; Fernandez-Alfonso and Ryan, 2008; Staras et al., 2010; Herzog et al., 2011). Interestingly, evidence suggests that mobile SVs may partake in exocytosis away from the synapse (Krueger et al., 2003; Ratnayaka et al., 2011) and that in response to acute membrane depolarisation SVs can undergo both exocytosis and endocytosis at non-discreet sites along the axon (Ratnayaka et al., 2011). This form of activity-dependent modulation has been examined in acute experiments, but has not been examined in long-term experiments. Thus, we still do not know how increased neuronal activity will alter the transport of vesicles over time.

AIMS

The aims of this chapter were as follows: (1) To develop an assay for studying the transport of synaptophysin (syp) positive vesicles in the axons of primary hippocampal neurons. (2) To use this assay to investigate how synaptophysin positive vesicles are transported over time. (3) To examine how the transport of synaptophysin positive vesicles can be modulated by changes in neuronal activity. (4) To investigate the effects of increased neuronal activity on the long-term dynamics of synaptophsin positive vesicle clusters. We hypothesised that increased neuronal activity would alter the dynamics of synaptic vesicle clusters and of transport vesicles transiting along the axon. This is based on numerous activity-dependent structural changes observed at CNS synapses and because synaptic transmission is known to rely heavily on synaptic vesicle transport.

Figure 3.1

A
GFP
20μm

Bi
Syp-GFP
20μm

Bii
Syp-GFP
5μm
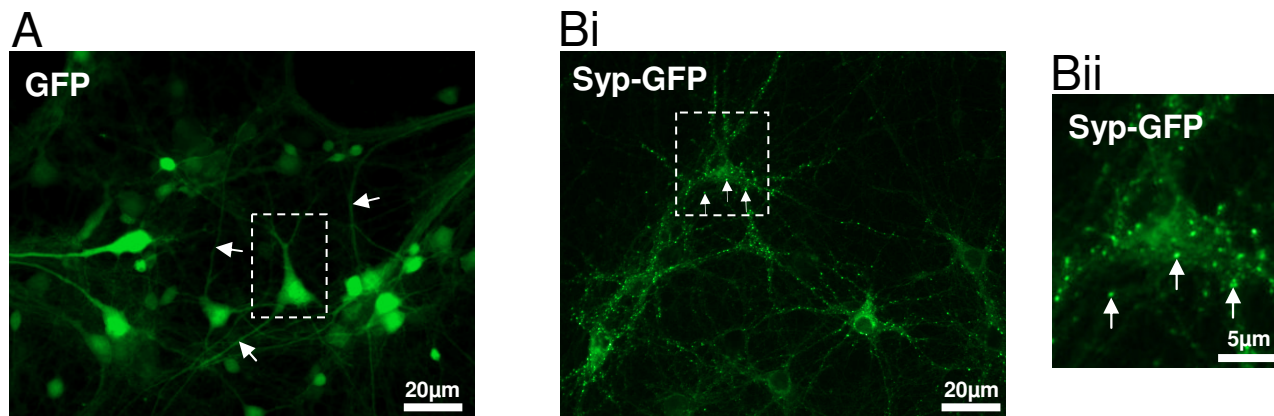
Figure 3.1 – Testing the functionality of lentiviral constructs (lenti-GFP and lenti-synaptophysin-GFP) in primary dissociated hippocampal culture.

To test the functionality of our lentiviral constructs we transduced primary dissociated hippocampal cultures (PDHC) at DIV0 with a high concentration of either lenti-GFP or lenti-synaptophysin-GFP (lenti-syp-GFP) (>1x10^6 infectious units/ml). PDHC were then incubated with lentiviral particles for 10 days before being imaged. **A)** A micrograph showing GFP expression in PDHC. As expected, GFP is expressed in a diffuse manner, both in the cell body, as well as in long neuronal processes (white arrows). **B)** Micrographs showing lenti-syp-GFP expression in PDHC. Syp-GFP accumulates into bright clusters, which are located in close proximity to cell bodies and proximal dendrites (white arrows). This pattern of expression suggests that the syp-GFP fusion protein is reporting the correct location of synaptophysin.

3.1 Characterisation of lenti-GFP and lenti-synaptophysin-GFP

To check the functionality of lentiviral constructs primary hippocampal cultures were produced and transduced at DIV0 with a high concentration of either lenti-GFP or lenti-syp-GFP ($1x10^6$ infectious units/ml) (Fig 3.1). Cell cultures were monitored daily for the expression of GFP. In agreement with (Ehrengruber et al., 2001) we found that lentiviral constructs were reliably observable by DIV7 (post transduction). Infection of cells with lenti-GFP led to diffuse cytoplasmic labelling of the entire cell body as well as axonal and dendritic processes (Fig 3.1 A). In contrast, cells infected with lenti-syp-GFP showed characteristically bright syp-GFP positive puncta located in close proximity to cell bodies and neurites (Fig 3.1 B). To confirm the identity of these puncta we immunostained fixed cultures for endogenous synaptophysin. We found that syp-GFP positive clusters were positive for synaptophysin (Fig 3.2), which suggests that lenti-syp-GFP is driving the correct expression of both GFP and syp-GFP. We did observe some synaptophysin positive clusters that were negative for syp-GFP, an observation that can be explained by the fact that not all neurons were transduced by the lentivirus. Overall, we found that both lentiviral constructs were functioning as expected and that syp-GFP successfully labels synaptophysin positive vesicle clusters.

3.2 syp-GFP positive accumulations co-localise with VGLUT1 in close proximity to MAP2 positive neurons

As an additional check to confirm the identity and location of syp-GFP positive clusters we immunostained primary hippocampal dissociated cultures transduced with lenti-syp-GFP, for vesicular glutamate transporter 1 (VGLUT1) and microtubule-associated protein 2 (MAP2). VGLUT1 is known to label synaptic vesicles located at excitatory synapses in the hippocampus and the cortex, whilst MAP2 has been shown to label the proximal dendrites and cell bodies of neurons (Bernhardt and Matus, 1984; Herzog et al., 2006). Supporting the idea that lenti-

Figure 3.2
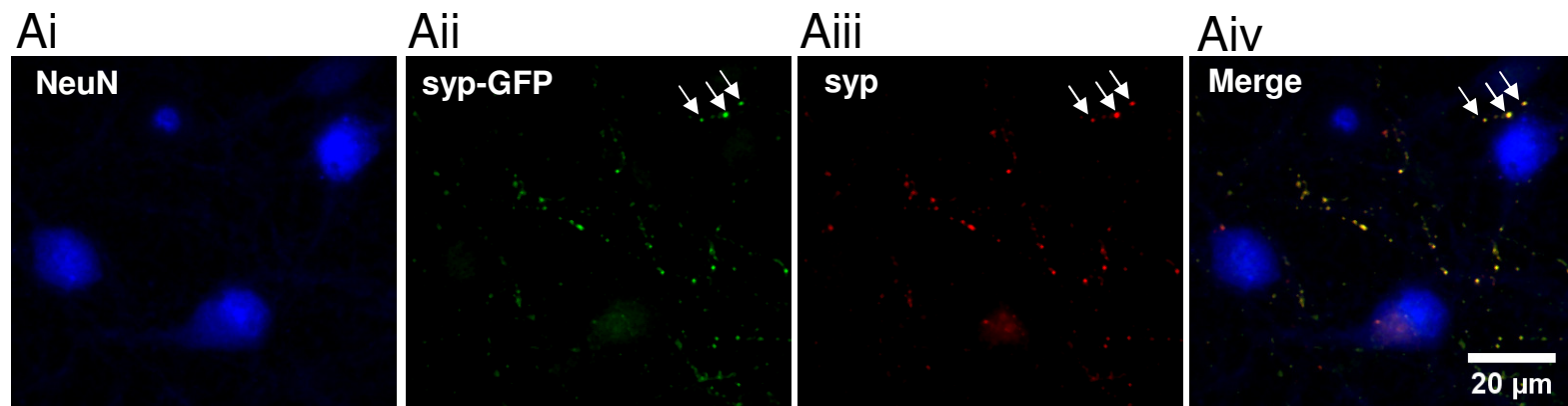
Figure 3.2 – Lenti-synaptophysin-GFP reliably labels synaptophysin positive synaptic vesicle clusters.

Synaptophysin immunolabelling was used to confirm the identity of syp-GFP positive accumulations. Primary dissociated hippocampal cultures (PDHC) transduced with lenti-syp-GFP were immunolabelled for NeuN (a neuronal marker) and synaptophysin (syp) at DIV10. **Ai)** A micrograph showing NeuN labelling. NeuN labels (diffusely) the soma and nucleus of neurons. **Aii)** A micrograph showing syp-GFP positive accumulations. **Aiii)** A micrograph of the same region showing synaptophysin immunolabelling. **Aiv)** A merged image of Ai-Aiii). Yellow accumulations denote an overlap between our transgene (syp-GFP) and the presence of synaptophysin (syp) (white arrows highlight an example of syp-GFP and syp co-localisation). This suggests that lenti-syp-GFP is driving the correct expression of synaptophysin-GFP.

syp-GFP is tagging synaptic vesicles, we find that syp-GFP positive puncta co-localise with VGLUT1 positive puncta in close proximity to MAP2 positive dendrites and cell bodies (Fig 3.3). This suggests that bright syp-GFP positive puncta are likely to be presynaptic clusters of vesicles. This is in agreement with Fletcher et al., (1991) who showed that synaptophysin positive vesicles tend to cluster together in close proximity to post synaptic neurons. From this, we can conclude that lenti-syp-GFP has assumed the endogenous position of synaptophysin.

3.3 synaptophysin-GFP is trafficked along axonal processes and accumulates into stationary vesicle clusters

After validating that syp-GFP was being correctly expressed by our lentiviral constructs, we then used live imaging to reveal the active transport and dynamics of syp-GFP. Figure 3.4 describes the characteristics of syp-GFP transport. We found that syp-GFP was transported in the form of "small motile particles" that moved bi-directionally along axonal processes. These particles were transported rapidly, moving with a median velocity of $0.4\pm0.04\mu m/s$. Motile particles showed characteristic processive movement, moving continuously and without stopping through several successive frames of capture. As well as being transported along the axon, syp-GFP positive particles were also seen to accumulate into GFP positive axonal swellings, as shown in figure 3.3 these swellings were VGLUT1 positive; making it likely that they were in fact clusters of synaptic vesicles. These clusters likely represent pre-synaptic vesicle accumulations. Two control videos, separated by a 5 minute interval, revealed that these vesicle accumulations were stationary; an example is shown in figure 3.4 B; a persistent stable vesicle cluster is marked with a blue arrow, whilst several small motile particles were marked with either green or red arrows. syp-GFP accumulations were considered to be synaptic vesicle clusters if they were larger than the width of the axon and stationary between two successive control videos. All other syp-GFP positive

Figure 3.3
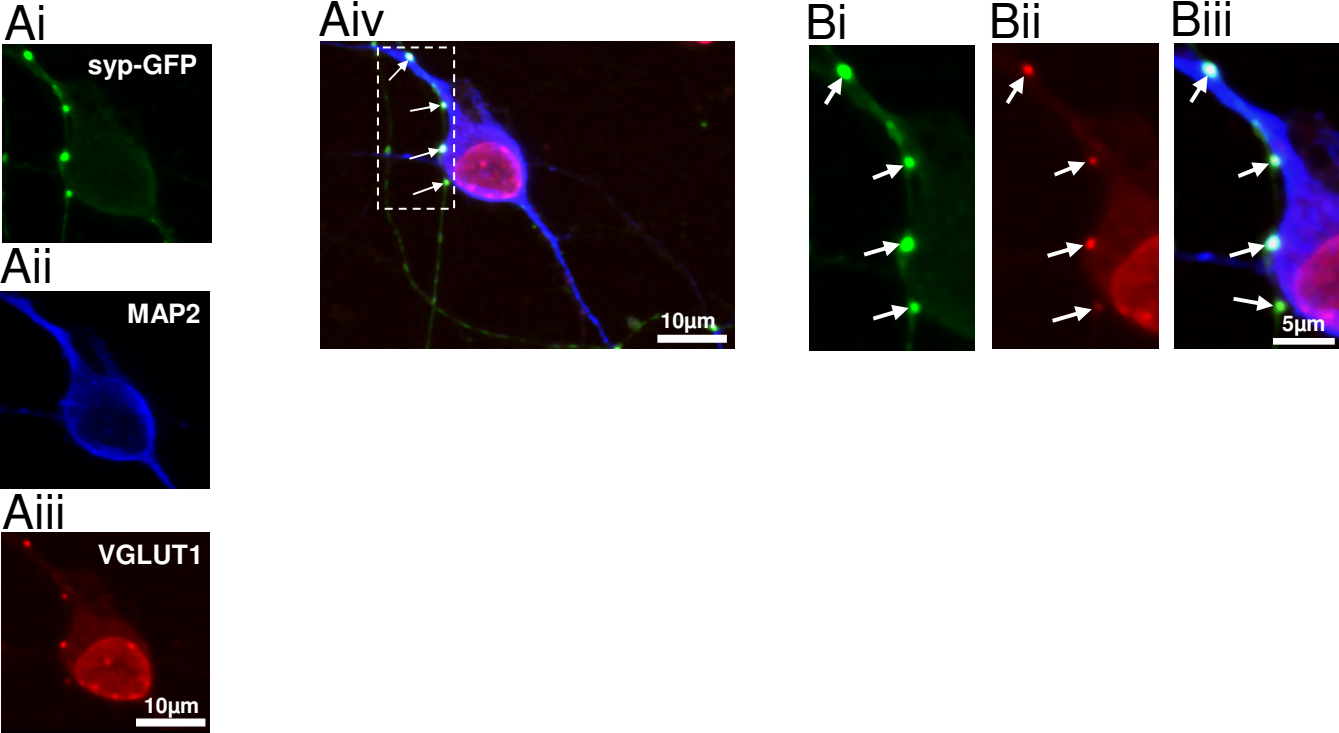
Figure 3.3 – Synaptophysin-GFP positive vesicle clusters co-localise with the vesicular glutamate transporter-1 (VGLUT1) in close proximity to cell bodies and dendrites.

Immunolabelling for vesicular glutamate transporter-1 (VGLUT1) and microtubule association protein-2 (MAP2) was used to confirm the location and identity of syp-GFP positive vesicle clusters. Primary dissociated hippocampal cultures (PDHC) transduced with lenti-syp-GFP at DIV0 were immunulabelled at DIV10 for MAP2 (which labels the cell body and dendrites of neurons) and VGLUT1 (which labels excitatory synaptic vesicles). **Ai)** A micrograph showing syp-GFP expression. **Aii)** A micrograph showing MAP2 expression (blue). **Aiii)** A micrograph showing VGLUT1 expression (red). **Aiv)** A merged image of syp-GFP, VGLUT1 and MAP2 expression. **B)** Three micrographs that are an enlargement of the checker-boxed region shown in Aiv. White arrows denote the co-localisation between syp-GFP (Bi green) and VGLUT1 (Bii red). Syp-GFP accumulates into vesicle clusters that are located in close proximity to MAP2 positive dendrites. These vesicle clusters co-localise with VGLUT1. Syp-GFP therefore labels (as expected) vesicle clusters in the presynaptic element of putative excitatory synapses.

particles were classified as "motile particles" and analysed for their movement characteristics.

3.4 The majority of vesicle clusters are stable for at least 10 hours

Synaptophysin-GFP is a useful marker of long-term vesicle dynamics because it is located within the membrane of synaptic vesicles and is recycled back into the membrane during endocytosis (Takamori et al., 2006; Kwon and Chapman, 2011). This property was exploited so that synaptic vesicle dynamics could be observed over time. Figure 3.5 describes the dynamics of synaptic vesicle clusters over 10hrs under basal levels of activity, for this experiment motile particles were ignored and only stationary vesicle clusters were analysed for changes in movement.

To assess vesicle cluster dynamics over time, we counted the number of vesicle clusters at 0hrs and then at 10hrs from the same axonal segment. We wanted to establish how stable vesicle were under control conditions. We found that there were approximately 6 vesicle clusters for every 50μm length of axon. We normalised the total number of vesicle clusters to 50μm because of the slight differences in the length of each axon measured. Over 10hrs, we observed no change in the total number of vesicle clusters /50μm (Fig. 3.5 C). At T=0hrs, we vesicle cluster density was 6.11±0.780 vesicle clusters/50μm; at T=10hrs, this value did not significantly differ: 6.15±0.982 clusters/50μm (p=0.93, paired student t-test, n=25, 11 experiments). Although vesicle cluster density appeared stable over 10hrs, we did notice some vesicle cluster rearrangement. Taking this into account, we then investigated the dynamics of individual vesicle clusters. We found that the majority of vesicle clusters (72%±10.2%) showed no apparent movement over 10hrs (Fig 3.5 - Cii). The remaining clusters fell into two categories: those that appeared (new) or those that disappeared (lost). "New" clusters (0.98±1.395 clusters/50μm) accounted for 13.7%±3.92% of the total clusters imaged and "lost" clusters (1.02±0.403 clusters/50μm) accounted for

Figure 3.4
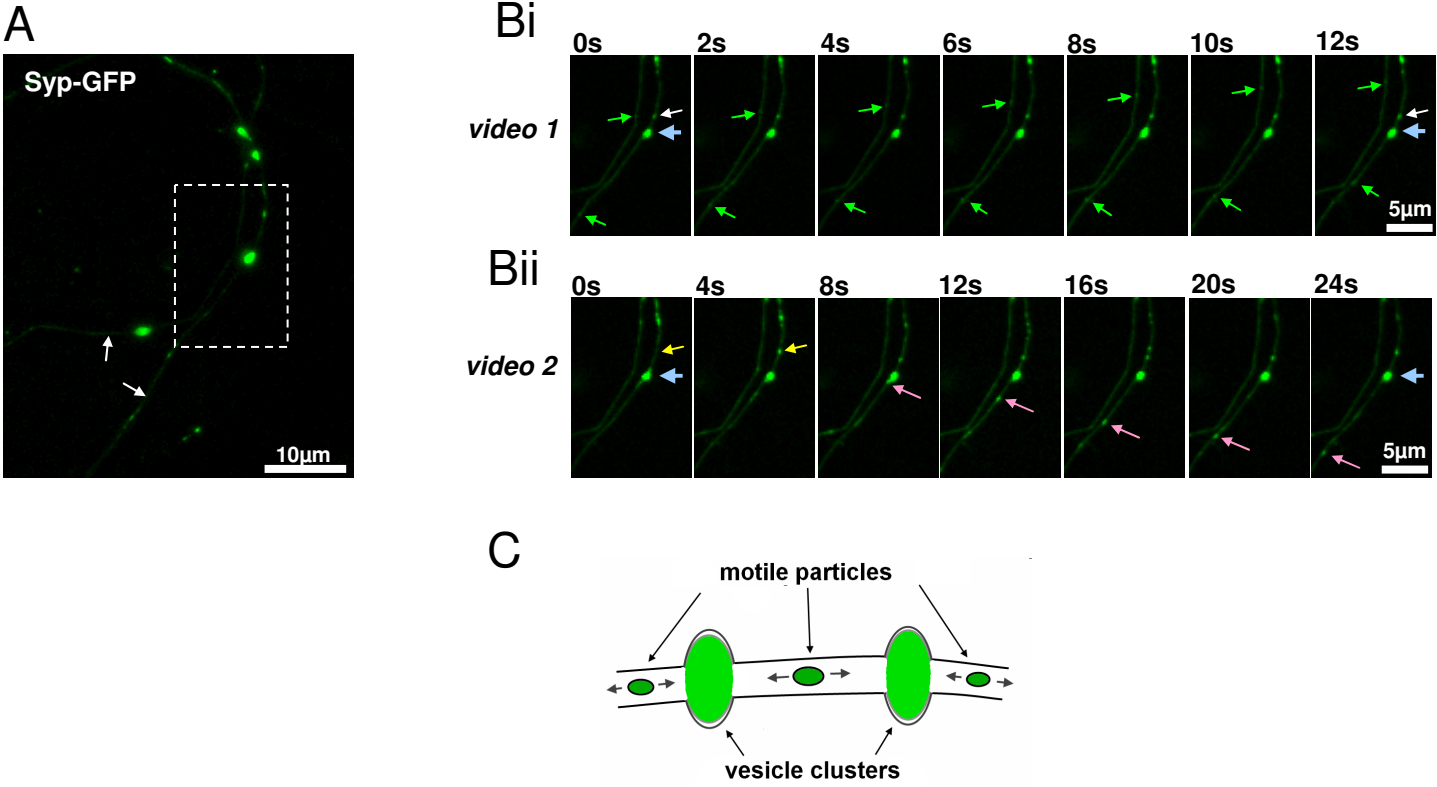
Figure 3.4 – Motile synaptophysin-GFP positive particles show rapid bi-directional transport and accumulate into large vesicle clusters.

Time lapse video (≈0.5-1.5Hz) was used to observe and quantify the dynamics of syp-GFP in living primary dissociated hippocampal cultures (PDHC) at 37°C. PDHC were imaged at DIV10-14 (post transduction with lenti-syp-GFP). **A)** A representative micrograph showing two syp-GFP positive axons (white arrows) that were chosen for live imaging. Time lapse videos were taken 5 minutes apart to visualise vesicle transport and vesicle cluster dynamics. **B)** Excerpts taken from each video are shown at different frequencies. **Bi)** An excerpt from video 1 showing seven sequential images captured every 2 seconds. The anterograde movement of motile particles is tracked by two green arrows (the cell bodies associated with each axon is located below the field of view to the left). A stationary vesicle cluster (which is larger than the width of the axon) is denoted by a blue arrow. A GFP positive particle that is temporarily stationary is denoted by a white arrow. **Bii)** Excerpts taken from a second video, captured of the same region, 5 minutes later (video 2). To sample vesicle trafficking for a longer period of time the interval between images in this excerpt is longer (4s). A syp-GFP positive motile particle (moving in the retrograde direction) is tracked by a pink arrow. The same vesicle cluster shown in video 1 is still stationary in video 2 (blue arrow).The previously stationary motile particle seen in video 1 is now seen to move in video 2 (yellow arrow). **C)** A cartoon schematic summarising the movement characteristics of both small motile particles and vesicle clusters. For the purpose of analysis: vesicle clusters were classified as being larger than the diameter of the axon and were stationary for at least 5 minutes; all other GFP positive accumulations were classified as being motile particles. Motile particles were trafficked bi-directionally along axonal processes and could be intermittently stationary.

14.3%±5.66% of the total clusters imaged. We observed that most vesicle clusters were therefore stable, whilst a subset of clusters were in a state of dynamic equilibrium, disappearing and appearing in equal quantity.

After quantifying the dynamics of individual vesicle clusters we then assessed the dynamic movement characteristics of individual axons. Each axonal segment (25 in total) was assessed for a change in cluster dynamics over 10hrs. A proportion of axons, 10 out of 25 (40%), showed no change in vesicle cluster number and showed no evidence of vesicle cluster movement, these axons were classified as being completely "stable" (no movement / no change in number). All other axons, 15 out of 25, were classed as being "dynamic" (60%), because they showed some evidence of vesicle cluster movement. Of the dynamic axons, 3 showed a net increase in total cluster number (12%), whilst 4 showed a net decrease (16%). The remaining 8 axons showed no net change in the number of vesicle clusters (32%), in these axons we observed a balance between the number of new and lost vesicle clusters. In summary, the majority of axons (60%) contained dynamic vesicle clusters. However, most axons (72%) maintained a consistent number of vesicle clusters. Taken together, this suggests that vesicle clusters are in state of dynamic equilibrium, with the majority of axons showing a dynamic turnover, whilst being capable of maintaining a consistent number of vesicle clusters.

3.5 Axonal segments show consistent particle dynamics

As well as investigating the long-term dynamics of synaptic vesicle clusters we also captured short (1 - 2 minute) high frequency (1.5Hz) videos of vesicle transport (Fig 3.6). Videos of the same axonal segment were captured at T=0hrs and T=10hrs in order to asses how vesicle transport changed over time (supplementary videos: 1 and 2). To analyse the rate and quantity of vesicle transport, videos of vesicle transport were converted to kymographs (Fig 3.6 Aii). In these static representations of vesicle transport it was possible to track motile particles and to measure the number and velocity of particle tracks.

Figure 3.5

A

vesicle clusters

Bi

0hr   10hr   Merge

10µm

Bii

0hr   10hr   Merge

New

Stable

Lost

5µm

Ci

P = 0.93

clusters / 50µm

n=25   n=25

0hr   10hr

clusters / 50µm

0hr   10hr

Cii

stable
new
lost

P=0.0006
**

clusters / 50µm

n=25

dynamic

Ciii

Stable
Net increase
Net decrease
No net change

axons imaged

40%   } stable

12%
16%   } dynamic
32%

99
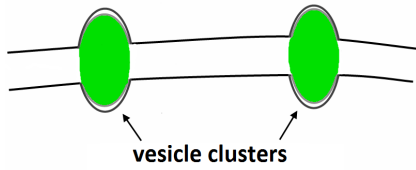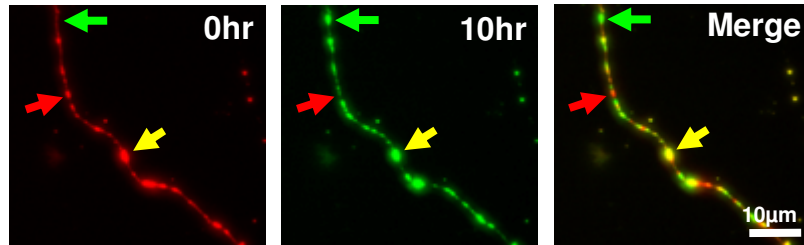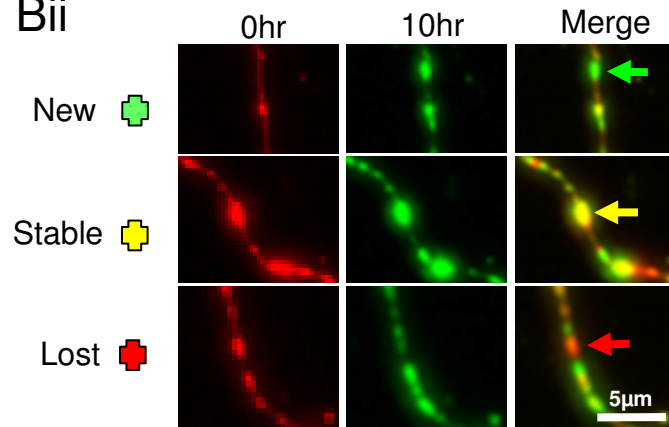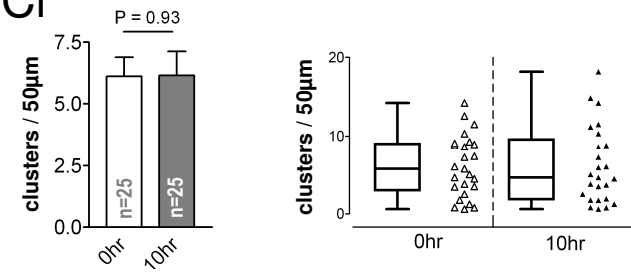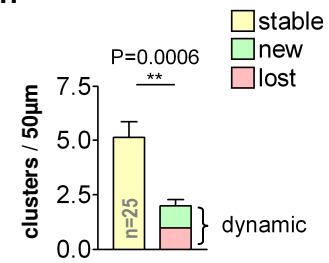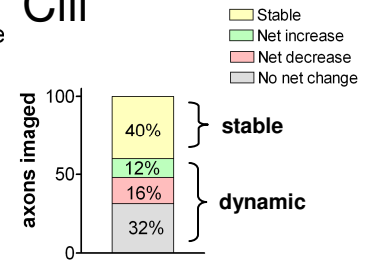
Figure 3.5 – Under control conditions synaptic vesicle clusters are in a state of dynamic equilibrium.

To establish basal levels of synaptic turnover, we imaged the long-term dynamics of syp-GFP positive vesicle clusters. We repeatedly imaged sections of axon, maintained at 37°C, at DIV10-14 (following transduction with lenti-syp-GFP). **A)** For this analysis, small motile particles were ignored and only vesicle clusters were analysed. Vesicle clusters were identified as being larger than the diameter of the axon and stationary for at least 5 minutes (see figure 3.3). **Bi)** Representative micrographs showing vesicle cluster dynamics in a single axon over 10hrs. The axon at 0hrs is pseudo-coloured red. The same axon at 10hrs is pseudo-coloured blue. The merged image highlights any change in location of vesicle clusters over time. New clusters appear green, vesicle clusters that have not moved (stable) appear yellow and vesicle clusters that have disappeared/moved appear red. Each of these events is shown in Bii). **Bii)** Enlarged micrographs of vesicle clusters seen in Bi). In the merged image: green denotes that a new cluster has developed over 10hrs, red denotes that a cluster has disappeared over 10hrs and yellow denotes that the same cluster is present at 0hrs and 10hrs. Vesicle cluster dynamics were used to estimate synaptic stability and turnover under control conditions. **Ci)** A bar chart and scatter plot summarising vesicle cluster density / 50 μm at 0hrs and 10hrs. Under control conditions we observed no change in the average density of vesicle clusters / 50 μm (p=0.93, paired student t-test, n=25, 11 experiments). There was no net increase or decrease in the number of vesicle clusters. This suggests that the number of synaptic connections made by these axons over 10hrs remains consistent. **Cii)** A bar chart summarising the dynamics of individual vesicle clusters over 10hrs. The majority of vesicle clusters were found to be stable and were present in the same location over 10hrs (yellow). There were significantly more stable clusters than there were dynamics clusters; stable clusters accounted for approximately 72.5 ±10.6% of all clusters; whilst dynamic clusters accounted for just 27.5 ±6.9% of all clusters (p=0.0006, paired student t-test, n=25, 11 experiments). Of the dynamic clusters, 13.7% ±3.92% were newly formed, whilst 14.3% ±5.66% were lost over the period of 10hrs. **Ciii)** A summary plot of all axons used in these experiments and their vesicle cluster dynamics over 10hrs. Axons were pooled into two main groups, those that showed no movement (40%) (stable) and those that showed some movement (60%) (dynamic). The majority of axons (72%) (grey and yellow) showed no increase or decrease in the number of vesicle clusters over 10hrs.

Under control (basal) conditions we found no significant difference in the trafficking characteristics of motile particles between 0hrs and 10hrs. We observed no change in the median velocity (or the "rate" of transport) of motile particles over 10hrs. At T= 0hrs we calculated median velocity as 0.4±0.04µm/s; where as at 10hrs, we calculated median velocity as 0.3±0.03µm/s (p=0.053, paired student t-test, n=15, 11 experiments) (Fig 3.6 – Bii). We found no change in the trafficking density of motile particles (or "quantity" of transport). The trafficking density remained unchanged after 10hrs (no change in the number of moving particles /50µm, 0hrs =17±2 particles / 50µm to 10hrs = 19±3 particles / 50µm (p=0.49, paired student t-test, n=15, 11 experiments) (3.6 – Biii). Total mean displacement of particles also remained unchanged over 10hrs. (no change in total mean displacement, 0hrs = 1.96±0.216µm; 10hrs = 1.78±0.24µm (p=0.27, paired student t-test, n=15, 11 experiments) (3.6 – Biv). Under control conditions we found no significant alteration in vesicle transport.

3.6 GABA$_A$ antagonist bicuculline increases network activity

In order to investigate the effects of increased neruonal activity on vesicle dynamics we treated cell cultures with the GABA$_A$ receptor antagonist bicuculline (bic) (20µM), to block inhibition and to increase network activity (Fig 3.7). Blocking inhibitory network activity has been shown to: induce burst firing, increase firing frequency and has been used as tool for investigating long-term activity dependent changes in the dissociated culture (Arnold et al., 2005; Karmarkar and Buonomano, 2006; Qiu et al., 2012). Bicuculline treatment has been used previously to generate burst firing and to increase neuronal activity for over 24hrs (Arnold et al., 2005). To confirm bic induced activity calcium imaging was used to measure the number of cells firing calcium spikes in response to treatment with 20 µM bic. Calcium spikes are well correlated to action potential firing (Smetters et al., 1999). The number of cells firing calcium spikes significantly increased following 15 minute treatment with 20µM bic. We detected an increase in calcium spiking

Figure 3.6

Ai

motile particles

Aii

0hr   10hr

raw

tracked

10μm

20s

Bii

Median velocity

P = 0.053

n=15   n=15

0hr   10hr

Biii

Traffic density

P = 0.49

n=15   n=15

0hr   10hr

Bi

Movement ratio

P = 0.56

n=15   n=15

0hr   10hr

P=0.56

0hr   10hr

Biv

Mean displacement

P = 0.269

n=15   n=15

0hr   10hr
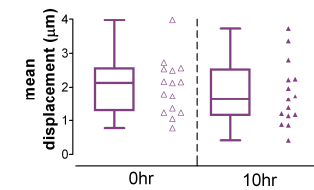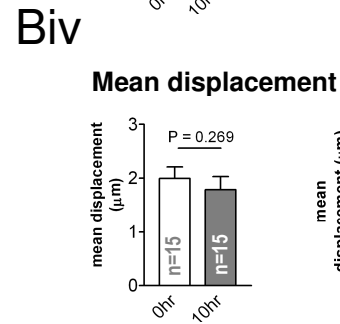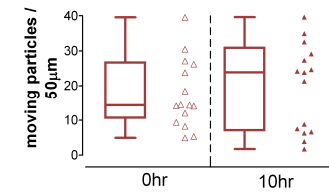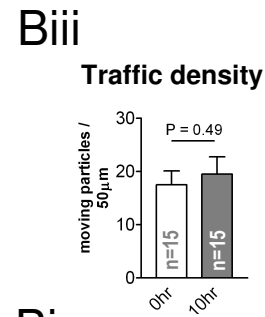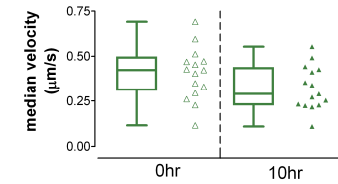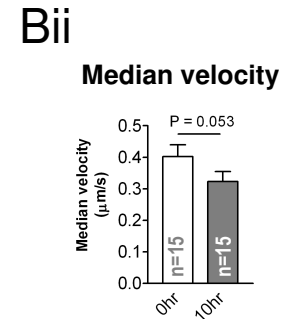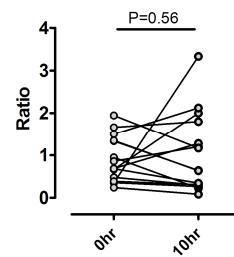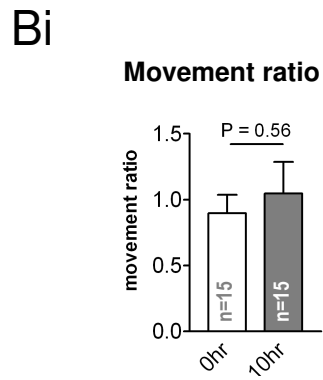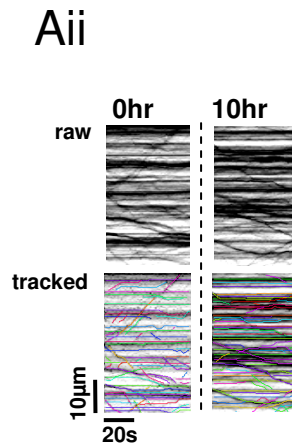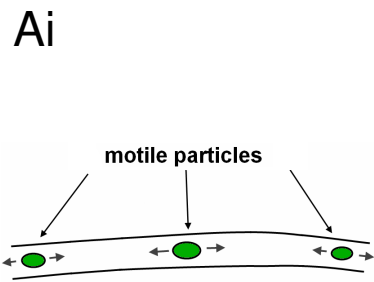
Figure 3.6 – Axonal segments show consistent particle dynamics.

To establish basal levels of vesicle transport, we repeatedly imaged syp-GFP positive particles in the axons of syp-GFP transduced primary dissociated hippocampal neurons at 10-14 days (maintained at 37°C). For this analysis, large vesicle clusters were ignored (see figure 3.3) and only small motile particles were analysed (depicted in the cartoon shown in **Ai)**. To quantify the movement parameters of small motile particles we generated kymographs from time lapse video showing syp-GFP transport. Kymographs are a static representation of movement over time. **Aii)** Two representative kymographs showing the recorded trajectories of motile particles for 60s (at T=0hrs and at T=10hrs). Several quantitative measures of motile particle transport can be made by manually tracing the trajectories produced by each individual particle (tracked). The direction and slope of the lines indicate the velocity of the particle. A flat horizontal line indicates a stationary particle. Four measures that describe the general movement of motile particles are shown in B. **Bi)** A graph and scatter plot summarising the proportion of moving to stationary particles. The number of moving particles was divided by the number of stationary particles. There was no significant change in particle movement over 10hrs (p=0.56, paired student t-test, n=15, 11 experiments), suggesting that the proportion of particle transport was consistent. **Bii)** A bar chart (left) and a scatter plot (right) summarising the median velocity of moving particles. No change significant change in velocity was observed over 10hrs (p=0.53, paired student t-test, n=15, 11 experiments). **Biii)** A bar chart (left) and scatter plot (right) summarising the trafficking density of moving particles. No change was observed in the number of moving particles / 50µm, over 10hrs (p=0.49, paired student t-test, n=15, 11 experiments). **Biv)** A bar chart (left) and scatter plot (right) summarising the mean displacement of all particles. Mean displacement did not change over 10hrs (p=0.269, paired student t-test, n=15, 11 experiments). All measured movement parameters for syp-GFP positive particles showed no change over 10hrs.

from 1.4±0.62 cells / field, in control recordings (3.2%), which increased to 4.6±1.49 cells / field following treatment with bic (14.1%) (p=0.046, paired student t-test, n=4, 3 experiments). We calculated the proportion of cells firing action potentials from a population of both neurons and glia.

3.7 Increased activity leads to more dynamic vesicle clusters

To test whether increased activity would have an effect on vesicle cluster dynamics, axonal segments were imaged before and after 10hrs treatment with 20µM bic (Fig 3.8). Following bic treatment we observed no change in the total number of vesicle clusters per 50µm length of the axon. At 0hrs vesicle cluster density was 6.5±0.69 clusters/50µm, whilst at 10hrs vesicle cluster density remained unchanged at 6.2±0.87 clusters/50µm (p=0.55, paired student t-test, n=17, 11 experiments). In addition, there was no change in the absolute number of stable vesicle clusters, between control and bic treated cultures (Fig 3.8 Aii / Bii). In control cultures there were 5.1±0.76 stable clusters/50µm (yellow clusters), whilst in bic treated cultures there were 4.54±0.81 clusters/50µm (yellow clusters); p=0.607, unpaired student T-test). However, bic treatment did increase the proportion of dynamic vesicle clusters compared to control (Fig 3.8 C). In control cultures the number of dynamic vesicle clusters was 28±6.89%, whilst in bic treated cultures this increased to 44±8.46%; p=0.0261, unpaired student t-test. The increase in the proportion of dynamic clusters came as the result of a proportional increase in the appearance of both new and lost clusters (dynamic clusters). Following bic treatment the proportion of newly formed clusters was 20%±5.4%, whilst the proportion of clusters seen to disappear was 24%±5.4%, p=0.27, paired student T-test. This "balanced turnover" accounted for an increase in the number of dynamic clusters without an increase in overall vesicle cluster density. Bic treatment therefore increased the number of dynamic vesicle clusters without altering cluster stability or overall vesicle cluster density.

Figure 3.7
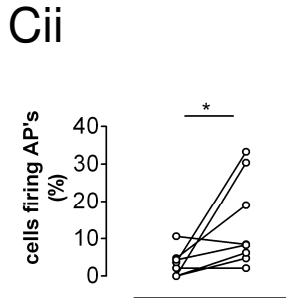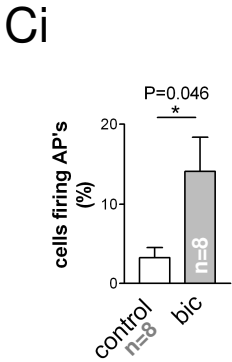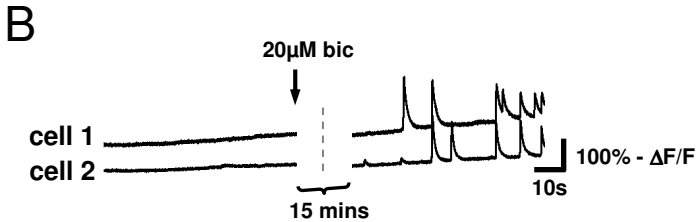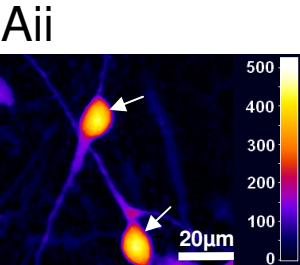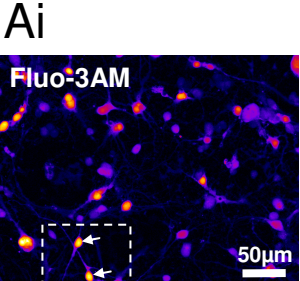
Figure 3.7 – GABA$_A$ antagonist bicuculline increases the number of cells firing calcium spikes in primary dissociated hippocampal culture.

To assess network activity in dissociated cultures treated with the GABA$_A$ receptor antagonist bicuculline (bic), Primary dissociated hippocampal cultures (PDHC) were batch loaded with the calcium sensitive dye Fluo-3AM (2.5µM) for 60 minutes prior to imaging. **Ai)** A typical low power micrograph of a loaded PDHC (pseudo-coloured fire for better contrast). **Aii)** An enlargement of the checker-boxed region seen in Ai). White arrows indicate two cells that have been sufficiently loaded with Fluo-3AM. Attached scale bar gives a reference for intensity (fluorescence intensity is measured in arbitrary units, AU). **B)** Representative traces from two cells, before and after treatment with 20µM bic. Cell 1 and Cell 2 were imaged for 1 minute at 100Hz using a x20 objective under control conditions (left). Cultures were then treated with bic (20µM). Following 15 minutes of incubation with bic, cultures were then re-imaged (right). Bic treatment increased the number of cells that showed calcium spiking. **Ci)** A bar chart (left) and a scatter plot (right) summarising the proportion of cells showing calcium spikes / field. The number of cells firing calcium spikes / total number of cells was quantified for each field. There was an increase in the number of cells firing calcium spikes (p=0.046, paired student t-test, n=8, 3 experiments). This indicates an increase in network activity, because calcium spiking correlates well to action potential firing.

When looking at the effect of increased activity on vesicle cluster dynamics in individual axons (Fig 3.8 – E) we found that bic induced activity significantly increased the proportion of dynamic axonal segments. In control cultures we observed that 15 out of 25 axons (60%) had dynamic vesicle clusters, whilst in bic treated cultures we found that 15 out of 17 axons (88%) had dynamic vesicle clusters (p=0.0013, Chi-squared test). In addition, we also observed a decrease in the number of axons that were able to maintain their exact cluster density over 10hrs. In control cultures most axonal segments maintained a consistent number of vesicle clusters over 10hrs (72%). However, following bic treatment only 18% maintained a consistent cluster density, most axons (53%) showed a net decrease in the number of vesicle clusters after 10hrs. This suggests that bic treatment alters vesicle cluster turnover by increasing the number of dynamic vesicle clusters and may lead to a decrease in vesicle clusters. .

3.8 Increased activity leads to smaller vesicle clusters

As well as investigating vesicle cluster dynamics we also investigated whether or not vesicle cluster size was altered in response to increased activity. We did this by measuring the maximal cross sectional area of each stable vesicle cluster at 0hr and at 10hrs. Under control conditions we detected no change in cluster size over 10hrs. Average cross sectional area at 0hrs was $12.8\pm1.57\mu m^2$, whilst at 10hrs it was $12.5\pm1.49\mu m^2$ (p=0.10, Wilcoxon-matched pairs test, n=126, 11 experiments). Following treatment with 20μm bicuculline we detected a significant decrease in the average cross sectional area of stable vesicle clusters, vesicle clusters decreased in size from $14.7\pm1.67\mu m^2$ at T=0hrs, to $12.1\pm1.41\mu m^2$ at T=10hrs (p=0.0042, Wilcoxon-matched pairs test, n=80, 8 experiments). This equated to a $17.8\pm6.78\%$ decrease in vesicle cluster size following 10hrs treatment with bic.

Figure 3.8
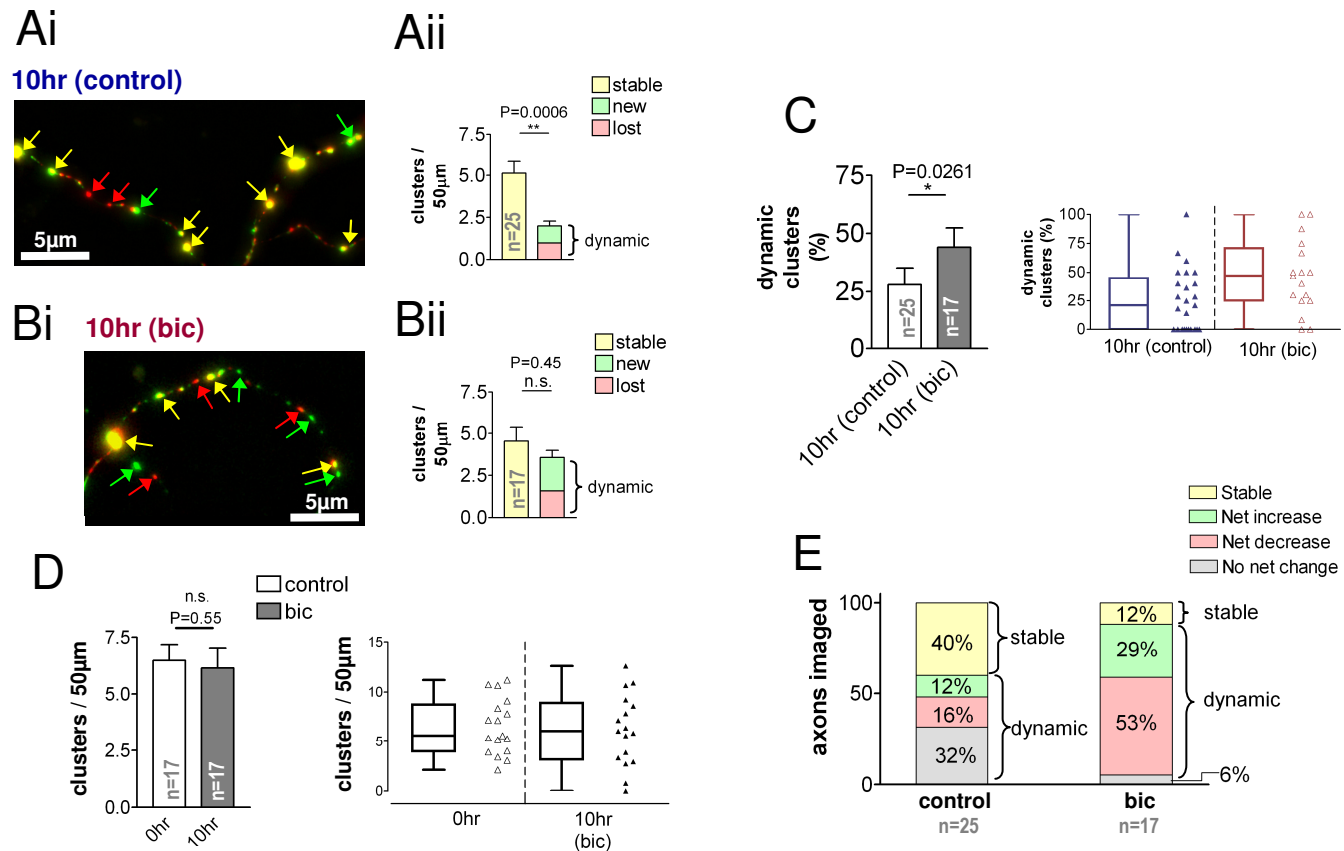
Figure 3.8 – Increased network activity leads to dynamic vesicle clusters.

To study the effect of prolonged increased activity on vesicle cluster dynamics we treated primary dissociated hippocampal cultures (PDHC) with the GABA$_A$ receptor antagonist bicuculline (bic) for 10hrs. **Ai)** An example micrograph showing vesicle cluster movement over 10hrs under control conditions. **Bi)** An example micrograph showing vesicle cluster movement over 10hrs following 20µM bic treatment. Yellow arrows indicate stable clusters, green arrows indicate newly formed clusters and red arrows denote clusters that have moved / disappeared. **Aii)** A bar chart summarising vesicle cluster dynamics under control conditions. Under control conditions there are significantly more stable clusters / 50µm that there are dynamics clusters (p=0.0006, paired student t-test, n=25, 11 experiments). **Bii)** A bar chart summarising vesicle cluster dynamics during prolonged bic induced activity. Bic induced activity leads to an increase in the number of dynamic vesicle clusters. Meaning there is no longer significantly more stable clusters / 50µm vs dynamic clusters; number of stable clusters /50µm = 4.5±0.8; number of dynamic clusters 50µm = 3.6 ±0.44 (p=0.45, paired student t-test, n=17, 11 experiments). **C)** A bar chart (left) and scatter plot (right) summarising the increase in dynamic clusters seen in bic treated PDHC. In bic treated cultures there are a greater number of dynamic vesicle clusters compared to control; in control cultures we observed that 28±6.9% of vesicle clusters were dynamic, where as in bic treated cultures we observed that 44±8.4% of vesicle clusters were dynamic (p=0.261, unpaired t-test, n=42, 11 experiments). **D)** A bar chart and scatter plot summarising vesicle cluster density / 50 µm at 0hrs and 10hrs. Bic induced activity did not alter the average density of vesicle clusters /50 µm over 10hrs (p=0.55, paired student t-test, n=17, 11 experiments). This suggests that although there are more dynamic clusters, these clusters remain in a state of dynamic equilibrium at least for 10hrs. **E)** A summary plot of all axons used in these experiments and their vesicle cluster dynamics over 10hrs, including control axons (left) and bic treated axons (right). We observed a significant increase in the number of dynamic axons between control and treated cultures.

3.9 Increased activity does not alter the movement of motile particle

To test whether increased activity would alter the transport of motile particles we used high frequency (1.5Hz) video to capture vesicle transport before and after 10hrs treatment with 20μM bic. Under these conditions we found no detectable change in the trafficking characteristics of motile particles over 10hrs. Each trafficking characteristic is summarised in fig 3.9 and in table 3.1 (below). Under these conditions, motile particle movement was not affected by bic induced increased activity and there was no change in either the rate or quantity of vesicle transport. We found that each of the measured transport characteristics were consistent before and after treatment with bicuculline.

	0hrs (n=6, 5 experiments)	10hrs (bic) (n=6, 5 experiments)
Movement ratio (moving/stationary)	0.98 ±0.216	0.93 ±0.300 (p=0.88)
Median velocity (μm/s)	0.45 ±0.054	0.48 ±0.094 (p=0.81)
Traffic density (moving particles/50μm)	17.8 ±5.77	19.25 ±7.28 (p=0.73)
Mean displacement (μm)	1.96 ±0.333	1.98 ±0.302 (p=0.95)

Table 3.1 – Summary of trafficking characteristics in response to 10hrs bicuculline (20μM bic) treatment.

Figure 3.9
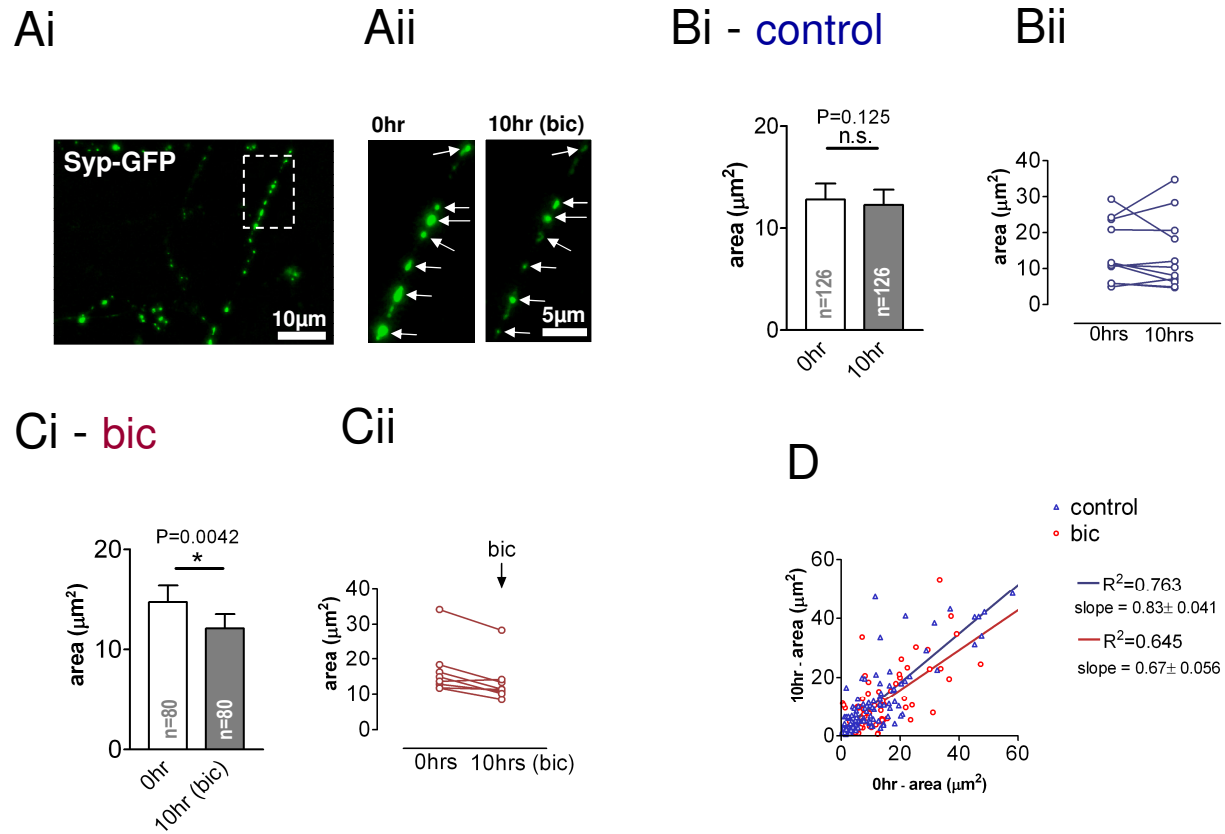
Figure 3.9 – Increased neuronal activity leads to smaller vesicle clusters.

To test the effect of increased neuronal activity on the size of vesicle clusters, we measured the maximal cross sectional area of stable vesicle clusters at T=0hrs and T=10hrs (with or without 20µM bic). **Ai)** A low power representitive micrograph of a lenti-syp-GFP transduced axon chosen for living imaging. **Aii)** An enlargement of the checker-boxed region shown in Ai) captured at T=0hrs. Stable vesicle clusters are highlighted by white arrows. **Aiii)** An enlargement of the checker-boxed region shown in Ai) captured at T=10hrs following 20µM bic treatment. Vesicle clusters appear visably smaller. **Bi)** A bar chart summarising the maximal cross sectional area of vesicle clusters at T=0hrs and T=10hrs under control conditions. **Bii)** A scatter plot summarising the average maximal cross sectional area of vesicle clusters / cover slip under control conditions. Under control conditions there was no change in vesicle cluster size over 10hrs (p=0.125, Wilcoxon-matched pairs test, n=126, 9 experiments). **Ci)** A bar chart summarising the maximal cross sectional area of vesicle clusters at T=0hrs and then at T=10hrs (following treatment with 20µM bic). Vesicle clusters are significantly smaller in the bic treated cultures (p=0.0042, Wilcoxon-matched pairs test, n=80, 6 experiments). **Cii)** A scatter plot of the average maximal cross sectional area of vesicle clusters / cover slip at T=0hrs and then at T=10hrs (following treatment with 20µM bic). **D)** A scatter plot showing the maximal cross section area ($µm^2$) of individual vesicle clusters measured at T=0hrs (x axis) and T=10hrs (y axis). Vesicle clusters from bic treated cultures are shown in red. Vesicle clusters from untreated cultures are shown in blue. Control (blue), slope = 0.83±0.041 (R^2 = 0.7633). Bic treated (red) = 0.67±0.056 (R^2=0.645). Increased neuronal activity leads to a decrease in size of vesicle clusters.

3.10 Discussion

Although many aspects of vesicle transport are well described, for instance, we already know that particular vesicles are transported to specific locations within the cell (Horton and Ehlers, 2003; Al-Bassam et al., 2012) and we also know that different types of vesicles can be transported at different rates (Macosko et al., 2008), what we know less about is how vesicle transport is regulated, especially in response to changes in neuronal activity. Our aim therefore was to monitor syp-GFP positive vesicles, which are relevant for synaptic transmission and to see how the transport of these vesicles could be modulated.

To achieve this, we transduced a dissociated cell culture assay with lenti-syp-GFP, in order to visualise syp positive vesicles. We used this assay to establish that vesicle transport rates were consistent over time (see figure 3.6) and that vesicle transport was surprisingly insensitive to changes in neuronal activity (figure 3.10), generated by treatment of the $GABA_A$ receptor antagonist bicuculline, a compound that is known to increase neuronal activity (Arnold et al., 2005) and to trigger structural modifications at the synapse (Qiu et al., 2012). Interestingly, although vesicle transport was unaffected by bicuculline treatment we did observe a significant increase in the number of dynamic synaptophysin positive vesicle clusters (Fig 3.8), as well as a decrease in size of stable vesicle clusters (Fig 3.9). Vesicle cluster turnover was more than 15% higher in cultures treated for 10hrs with bicuculline. Given that synaptophysin positive vesicle clusters immunolabelled positive for VLGUT1 and are found in close proximity to MAP2 positive dendrites (Fig 3.3), an increase in vesicle cluster dynamics may be indicative of an increase in synaptic turnover. Taken together these observations hint at the possibility that vesicles located at the synapse and vesicle being transported along the axon may be differentially modulated by increased neuronal activity.

Figure 3.10

A
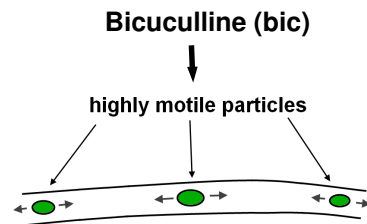
Bi
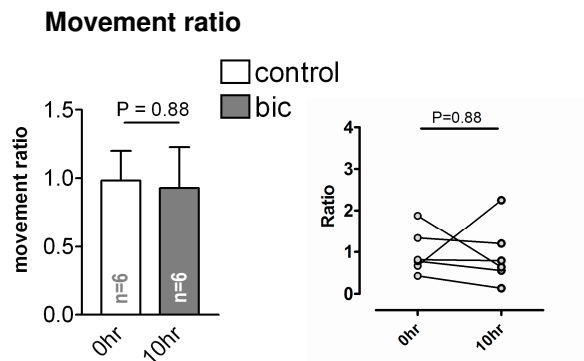
Bii
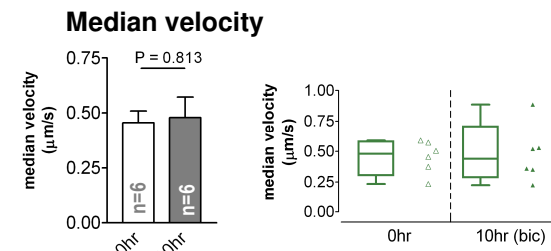
Biii
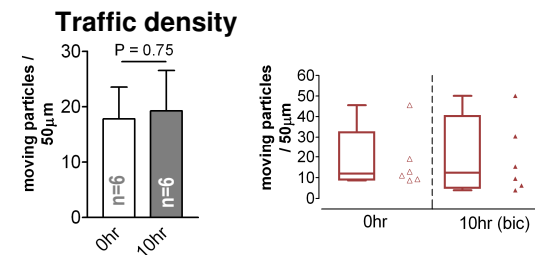
Biv
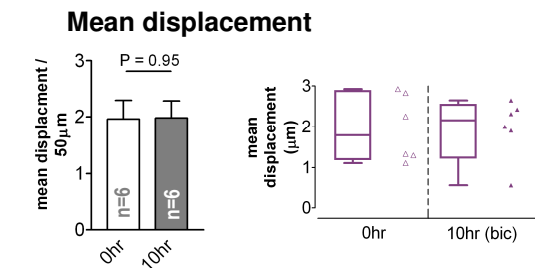
Figure 3.10 – Increased neuronal activity does not alter the movement characteristics of motile particles.

To study the effect of prolonged increased activity on motile particle dynamics we treated primary dissociated hippocampal cultures (PDHC) with the $GABA_A$ receptor antagonist bicuculline (bic) for 10hrs. For this analysis, large vesicle clusters were ignored (see figure 3.3) and only small motile particles were analysed (depicted in the cartoon shown in A). Analysis was performed on kymographs of time lapse video showing syp-GFP transport (see figure 3.6). **Bi)** A graph and scatter plot summarising the proportion of moving to stationary particles. The number of moving particles was divided by the number of stationary particles. There was no significant change in particle movement over 10hrs (p=0.88, paired student t-test, n=6, 5 experiments); this suggests that vesicle transport remains consistent during periods of increased activity. **Bii)** A bar chart (left) and a scatter plot (right) summarising the median velocity of moving particles. No significant change in velocity was observed over 10hrs (p=0.813, paired student t-test, n=6, 5 experiments). **Biii)** A bar chart (left) and scatter plot (right) summarising the trafficking density of moving particles. No change was observed in the number of moving particles / 50µm, over 10hrs (p=0.75, paired student t-test, n=6, 5 experiments). **Biv)** A bar chart (left) and scatter plot (right) summarising the mean displacement of all particles. Mean displacement did not change over 10hrs (p=0.95, paired student t-test, n=6, 5 experiments). Increased neuronal activity induced by 20µM bic treatment (for 10hrs) did not alter the movement parameters of motile particles.

Under basal levels of activity the transport of synaptophysin positive vesicles was consistent over time

In this chapter we utilized an assay for studying the transport of vesicles relevant for synaptic transmission. Our aim was to investigate how the transport of syp-GFP positive vesicles changes over time and in response to increased neuronal activity. After transducing neurons with lenti-syp-GFP we observed the movement of highly motile particles that were seen to traffic bi-directionally along long thin neuronal processes. The speed of the these vesicles, their bi-directional transport and their accumulation into vesicle clusters is consistent with what has been reported previously for synaptophysin positive vesicles (Nakata et al., 1998; Bury and Sabo, 2011)(De Paola et al., 2003). We validated that GFP correctly labelled synaptophysin positive vesicles by immunolabelling transduced cultures for endogenous synaptophyin (see figure 3.2); in addition, we also identified that vesicle clusters were likely to be presynaptic vesicle clusters because they co-localised with VGLUT1 and were found in close proximity to MAP2 positive dendrites (see figure 3.3).

Once satisfied that syp-GFP was functioning as expected we then examined control cultures and measured the consistency of synaptophysin positive vesicle transport. This was done to establish basal rates of vesicle transport, prior to increasing neuronal activity, to test whether vesicle transport rates were stable over time. as can be the case during early stages of development (Macosko et al., 2008). We observed no signficant change in either the rate or quantity of vesicle transport over 10hrs, neither the trafficking density nor the median velocity of vesicle transport was significantly altered by increased neuronal activity (see figure 3.10). Consistent vesicle trafficking may be a consequence of cell culture age, because by DIV10-DIV14 *in vitro* most rapid cell growth may already have begun to plateau or slow down (Basarsky et al., 1994; Papa et al., 1995), thus, by this time point the demand for vesicle transport may have wained. During development rapid cell growth places a significant demand on the supply of new vesicles to the synapse. However, as development progresses vesicle transport appears to slow down (Macosko et al., 2008). If cell growth is consistent or stable then vesicle transport could also be consistent or stable. In addition, because by this time point

most neurons will have already formed and recieved synaptic connections (Tokioka et al., 1993; Basarsky et al., 1994) this too might decrease the demand on vesicle trafficking (Schoch and Gundelfinger, 2006). Recent experiments suggest that vesicles are continually being transported from the cell body along the axon and out towards the synapse and are only captured or retained by synapses when required (Shakiryanova et al., 2006). If this is the case then the supply of vesicles may far out weigh the demand for new cargo at the synapse, because excess vesicles are likely to be transported in reserve for when demand is increased, which might explain why vesicle transport appears to be consistent.

Under basal levels of activity, vesicle cluster density is consistent and the majority of vesicle clusters appear to be stable

In addition to monitoring the transport of motile particles we also set out to measure changes in synaptic turnover by quantifying the long-term dynamics of clusters of synaptic vesicles. Vesicle clusters were identified from time-lapse video based on their size (larger than the width of the axon) and because they were stationary for longer than a period of five minutes. This identification criteria is based on previous analysis of synaptophysin positive vesicle transport, which also identified that syp-GFP formed into two separate popuations (highly motile packets and stationay clusters) (De Paola et al., 2003). We identified that vesicle clusters were likely to be located at presynaptic sites, because vesicle clusters immunolabelled positive for VGLUT1, which is a vesicular transporter present in the membrane of vesicles located at mature synapses (Herzog et al., 2006). In addition, we also found that vesicle clusters were located in close proximity to MAP2 positive dendrites and cell bodies (MAP2 labels a subset of excitatory and inhibitory neurons in culture). Our observations support the idea that syp-GFP clusters at presynaptic sites (Fletcher et al., 1991).

In order to investigate the effects of increased neuronal activity on vesicle cluster dynamics we set out to establish basal levels of vesicle cluster turnover. To do this, we identified vesicle clusters in time lapse video and then analysed their dynamics over 10hrs. We found that most (75%) vesicle clusters did not appear to

move over 10hrs and thus were considered to be stable. All other clusters were considered to be dynamic, because they either appeared or disappeared over 10hrs. Interestingly, we found that dynamic clusters appeared and disappeared in equal proportions, which meant that overall vesicle cluster density remained consistent. We therefore observed putative synaptic turnover, which appeared to be in a state of dynamic equilibrium.

Previous studies have found, and depending on the developmental stage, that synapse numbers can be in a state of decline, at a plateau, or in a state of growth. In networks that are developing the number of new synapses outweighs the number of lost synapses, so vesicle cluster density slowly increases (Okabe et al., 1999; De Paola et al., 2003). In our experiments we observed mostly stable vesicle clusters over a period of 10hrs, which suggests that most rapid early developmental growth may have already occurred, being instead replaced by balanced turnover. This turnover likely reflects the formation and dissolution of synaptic connections, given that vesicle clusters are strongly associated with clusters of post synaptic AMPA receptors (Ripley et al., 2011). Overall then, we find that under basal levels of activity, both vesicle transport rates and putative synapse numbers remain consistent over a period of 10hrs. We find that most vesicle clusters are stable, but a proportion show balanced turnover, some that has been previously, both *in vitro* and *in vivo* (Trachtenberg et al., 2002; De Paola et al., 2003; Kondo and Okabe, 2011). We report that in pure hippocampal cultures during basal levels of activity that vesicle transport rates are consistent and that vesicle clusters are in a state of balanced turnover.

Bicuculline induced an increase in neurons firing calcium spikes

Our strategy for studying the effects of increased neuronal activity on vesicle transport was to relieve cell cultures of $GABA_A$ mediated synaptic inhibition by applying the $GABA_A$ receptor antagonist bicuculline (20µM) to our dissociated cell cultures. Bicuculline treatment is known to promote increased neuronal activity in both hippocampal slice cultures and in dissociated neuronal cell cultures (Sokal et al., 2000; Arnold et al., 2005; Uva et al., 2005; Li et al., 2007). Bic treatment has

also been widely used to study activity dependent changes at the synapse (Zha et al., 2005; Qiu et al., 2012). In particular, prolonged (>24hrs) bic treatment is seen to significantly alter the expression levels of presynaptic vesicular transporters VGLUT1, VGLUT2 and VIAAT (De Gois et al., 2005), as well down regulating the postsynaptic expression of glutamate receptors (Qiu et al., 2012). In organotypic slices GABA$_A$ receptor antagonists (bicuculline or gabazine) are known to produce repetitive epileptiform activity (Samoilova et al., 2003), whilst in dissociated cultures they have been shown to induce burst firing, which leads to a prolonged increase in neuronal activity (Sokal et al., 2000; Arnold et al., 2005). To measure the effect of bicuculline treatment in our dissociated cultures we used the calcium sensitive dye Fuo3-AM (5µM) in conjunction with live imaging to detect and count the number of cells firing calcium spikes. Calcium spikes are well correlated to action potential firing and therefore offer a good indication of cell culture activity (Smetters et al., 1999). Following 15 minute bicuculline treatment we observed an approximately 4 fold increase in the number of cells per field firing calcium spikes. A representative trace recorded from two neurons is shown in figure 4.7 B, in this trace calcium spikes were induced following the application of bicuculline. Calcium spikes were characterised by a sharp and rapid upstroke phase (<200ms) and a characteristic decay phase (Smetters et al., 1999). Unfortunately, because of bleaching, phototoxicity and the buffering action of calcium sensitive dyes, calcium imaging was only suitable for gathering short samples of activity (minutes to hours). We were therefore unable to continuously observe how neuronal activity developed during bicuculline treatment. Fortunately however, this has been investigated previously using multi electrode recordings, which have been used to repeatedly capture cell culture activity over a period of 24hrs (Arnold et al., 2005); based on these data bicuculline treatment elevates neuronal activity and triggers burst firing for at least 24hrs (Arnold et al., 2005). This suggests that for the duration of our imaging experiments (10hrs) neuronal activity should be elevated by bic treatment.

The transport of synaptophysin positive vesicles was unaffected by an increased in neuronal activity

After establishing that vesicle transport rates were consistent under basal levels of activity we then investigated the effect of increased neuronal activity on the transport of synaptophysin positive vesicles and the dynamics of vesicle clusters. We hypothesised that increased neuronal activity would produce a detectable change in vesicle transport. However, after imaging vesicle transport in the same axonal segment over 10hrs and in the presence of bicuculline we found no detectable change in either the rate or quantity of vesicle transport. We found that: vesicle trafficking density, median velocity and mean displacement were not significantly differerent from control (Fig 3.10). This was a surprising finding considering the numerous pre and postsynaptic activity-dependent changes that can be onserved in the CNS as a result of increased neuronal activity (Trachtenberg et al., 2002; De Paola et al., 2003; Mizrahi et al., 2004; Zha et al., 2005; de Wit et al., 2006; Minerbi et al., 2009; Ratnayaka et al., 2011; Qiu et al., 2012) and the suggestion that vesicle transport rates are directly affected by acute depolarisation (Krueger et al., 2003; de Wit et al., 2006; Ratnayaka et al., 2011).

One possible explanation for a lack of detectable changes in vesicle transport is that bicuculline induced activity was insufficient to exceed the transport capabilities of the neuron. Given the importance of vesicle transport for maintaining synaptic transmission, neurons are likely to have a 'large working safety margin' for ensuring the adequate supply of vesicles to the synapse. Supporting this idea is the observation that (at any given time) almost all synaptophysin positive vesicles were localised to the axon and were rarely seen in the cell body, and almost never found in dendrites . This suggests that most synaptophysin positive vesicles once produced are immediately directed into the axon and set in motion towards the synapse. Functionally, this would ensure a constant supply a vesicles towards the synapse and would offer a practical way for storing vesicles or protein, other than in the cell body. It is possible that this constant supply of vesicles may already be travelling at a sufficient rate to accommodate any increased demand generated by bicuculline treatment. To test this possibility further it would be necessary to push neuronal networks to produce even higher levels of activity, which could be done

by manually applying localised high frequency electrical stimulation or by repeatedly stimulating neuronal networks with microelectrode arrays. Microelectrode arrays are advantageous because they can be used to stimulate large numbers of neurons repeatedly and at a particular frequency (Hales et al., 2012).

Previously it has been suggested that vesicle transport rates can be modulated by acute and local depolarisation, both high potassium levels (Krueger et al., 2003; de Wit et al., 2006) and high frequency stimulation (Ratnayaka et al., 2011) have been used depolarise the plasma membrane, whilst studying axonal transport. As a consequence of both of these applications vesicle transport rates were seen to reversibly slow or stop, which was observed using pH sensitive fluorescent dyes that were used to track the short-term movements of vesicles and to examine the rate and location of exocytosis. The authors concluded that vesicles could stop and release NT at extrasynaptic sites and that this was directly attributable to acute depolarisation. Unfortunately, in the case of potassium chloride it was not possible to rule out that high osmolarity was causing a decrease in vesicle transport, rather than depolarisation alone. Also, in the high frequency stimulation experiments the authors only focused their analysis on moving vesicles that appeared to slow in response to increased activity and did not investigate how the entire population of vesicles responded to increased activity. Until now, we did not know how a population of synaptophysin positive vesicles would react to a prolonged increase in neuronal activity. Our findings do not immediately support the hypothesis that vesicle transport is sensitive to an increase in neuronal activity. However, our experiments looked at the long-term changes of vesicle transport, where as the above studies investigated acute and rapid changes occurring shortly after focal depolarisation. It is possible that vesicle transport did respond to an increase in activity in our experiments, but had already returned to basal levels prior to 10hrs. To investigate this further it would be necessary to perform constant surveillance of vesicle transport in response to increased activity. Although useful this is especially difficult, particularly when dealing with the axonal transport of extremely small (<80nm) vesicles. Overall, we did not observe a detectable change in vesicle transport in response to a pharmacological induction of increased neuronal activity.

Figure 3.11
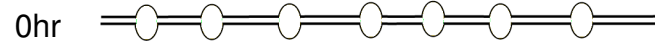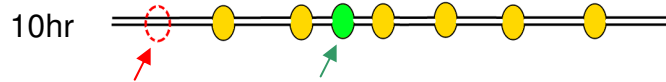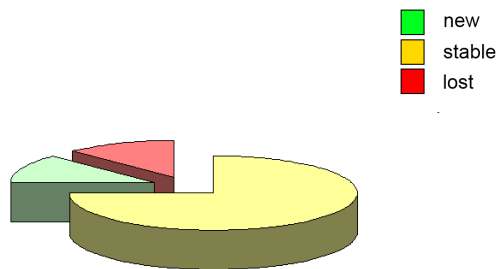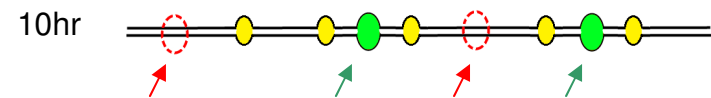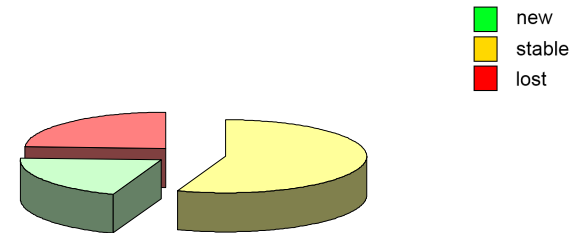
Figure 3.11 – Vesicle cluster size and dynamics are altered by increased neuronal activity (summary).

Live imaging revealed changes in vesicle cluster dynamics and size following 10hrs treatment with bicuculline (20µm). Figure 3.11 A and B summarizes data presented in chapter 3. The diagrams shown in A and B represent axonal processes containing vesicle clusters. The diagrams in Aii and Bii highlight the three possible vesicle cluster configurations: either stable (yellow), new (green) or lost (red). Red and green arrows highlight dynamic vesicle clusters. Aii/Bii: Dynamic vesicle clusters are increased following bic treatment, whilst stable vesicle clusters decrease in size. Aiii/Biii – A pie chart summarising the relative proportions of dynamic vesicle clusters and stable clusters. Increased neuronal activity increases the proportion of dynamic vesicle clusters.

Increased neuronal activity alters vesicle cluster dynamics but not vesicle transport dynamics

An interesting observation presented in this chapter was that vesicle cluster dynamics but not motile particles dynamics were selectively altered by increased neuronal activity. Increased activity did not alter vesicle transport but did alter vesicle cluster dynamics, by increasing balanced synaptic turnover by more than 15% and by reducing the size of stable vesicle clusters. This finding hints at the possibility that each vesicle population (clusters vs motile particles) may be differentially modulated by changes in activity. Supporting this idea is the fact that transport vesicles and synaptic vesicles are structurally distinct (Tsukita and Ishikawa, 1980). Vesicles located at the synapse are small, clear and round and are known to be sensitive to changes in activity (Bodian, 1970; Brose et al., 1992). In contrast, many vesicles that are transported along the axon, are large, have an irregular shape and resemble tubulo-vesicular structures (Tsukita and Ishikawa, 1980; Nirenberg et al., 1995; Hirokawa, 1998). These vesicles are seen to carry synaptophysin, but only in its precursor form, which is not necessarily functional (Hirokawa, 1998). Given that the primary role of these vesicles is to deliver cargo from the cell body to the synapse it is distinctly possible that they are not sensitive to changes in neuronal activity. If true, this could explain why we detected no change in vesicles transport, but why other studies did. Previous studies have mostly used FM1-43 (a pH sensitive dye, which labels recycling vesicles) to observe activity-dependent changes in vesicle transport (Ratnayaka et al., 2011). Vesicles that become loaded with FM1-43 must already be actively participating exo / endocytosis and are therefore likely to be synaptic vesicles, thus, it is then no surprise that this subset of vesicles is sensitive to future bouts of increased activity. However, in our experiments if synaptophysin-GFP labels both transport vesicles and synaptic vesicles (Pennuto et al., 2003), then only a fraction of our syp-GFP positive vesicles may actually be sensitive to changes in neuronal activity. This could explain is why we were unable to detect a change in vesicle transport but why we could detect changes the in the dynamics of vesicle clusters.

Overall, our results suggest that specific populations of vesicles may have different sensitivities to changes in neuronal activity. Our results support the idea that

transport vesicles and synaptic vesicles have very different functional roles. Our results are important for future studies that focus on vesicle transport, because we show that it may be necessary to design novel fluorescent probes in order to investigate the transport of each vesicle population independently.

Increased activity increases synaptic turnover and decreases the size of stable vesicle clusters

In this chapter we described how increased neuronal activity increases vesicle cluster turnover without altering the total number of vesicle clusters. This finding was not surprising as there are already many examples in both young and old animals that synaptic "turnover" can be promoted by increased activity. In developed neuronal networks the number of synaptic connections cannot increase indefinitely, neurons must therefore rearrange or strengthen existing connections. This is thought to play at least some role in the process of learning and memory. Our results suggest that rather than promoting a net increase or decrease in synaptic connections, increased activity seems to trigger the re-arrangement of existing synaptic connections, which may lead to a rearrangement of the network.

In addition to increased turnover another particularly interesting observation described in this chapter was that the size of stable vesicle clusters seemed to get smaller following increased activity. We found that stable vesicle clusters decreased in size by around 20% following bicuculline treatment. Vesicle clusters in control cultures did not decrease in size, which rules out the detrimental effects of photobleaching as an artefact. In addition, we also interleaved our experiments, so that control experiments and treated experiments were performed one after the other and from the same culture, which was done to help minimise variation between experiments.

Unfortunately, it is still not clear what happens to vesicle clusters that makes them appear smaller. One promising idea is that the synaptophysin-GFP fusion protein, located within the vesicle membrane, gets slowly lost from the vesicle membrane following repeated rounds of vesicle fusion and recycling. This is known to happen

to other vesicle proteins, which are essential for synaptic transmission, including synaptobrevin, a binding partner for synaptophysin (Taubenblatt et al., 1999; Dittman and Kaplan, 2006). Synaptobrevin is found in higher quantities in the plasma membrane following periods of increased activity (Dittman and Kaplan, 2006). Imaging the plasma membrane and synaptic vesicle membrane under ultrahigh resolution is necessary to answer what happens to these vesicle clusters following increased activity.

3.11 Conclusions

I conclude that the vast majority of synaptophysin-GFP positive vesicles that are transported along the axon in a mixed population of hippocampal neurons are insensitive to a prolonged increase in neuronal activity. I conclude that these vesicles differ from synaptic vesicles in their sensitivity to increased neuronal activity. I say this, because only vesicle cluster dynamics and not transported vesicles were affected by a prolonged increase in neuronal activity. Our observations seem may highlight important functional differences that exist between these two vesicle populations.

Chapter 4:

Activity-dependent modulation of hippocampal-mossy fiber vesicle clusters

4.0 Introduction

In chapter 3 we found that vesicle cluster dynamics and vesicle cluster size were significantly altered by changes in neuronal activity, whilst the transport of small motile particles remained unaffected. To better understand this finding we opted to investigate vesicle transport in a specific cell type making known synaptic connections. We chose to study vesicle transport in the axons of dentate gyrus (DG) granule cells, the mossy fibers (MFs), which possess a well-characterised anatomy and form defined synaptic connections (Frotscher, 1985; Claiborne et al., 1986; Acsady et al., 1998). MFs run in a tight bundle along the stratum lucidum (S.L.) and form large distinct synapses onto the complex spines of CA3 pyramidal neurons, as well as forming numerous, smaller, *en-passant* and filopodial synapses onto GABAergic interneurons (Claiborne et al., 1986; Chicurel and Harris, 1992; Acsady et al., 1998; Galimberti et al., 2006). MF-CA3 synapses are distinctively large (>15µm^3) evenly spaced and are densely packed with synaptic vesicles (Bischofberger et al., 2006). This makes them experimentally accessible for both live imaging and electrophysiology.

In the past MF development and structural plasticity have been studied extensively using histological stains that take advantage of their high zinc content (Babb et al., 1991; Proper et al., 2000). More recently however MF development has been studied using fluorescent reporter genes, such as GFP and membrane bound GFP, which have been used to visualise and repeatedly image MF terminals (Galimberti et al., 2006; Holtmaat and Svoboda, 2009). This has revealed several interesting and previously unknown aspects of MF development and structural plasticity. For instance, live imaging experiments have revealed that MFs can remain structurally plastic even into adulthood and that MF development is enhanced by living in an enriched environment (Galimberti et al., 2006). In addition it appears that MF complexity is associated with higher scores in learning and memory tasks, which hints at the importance of MF plasticity in the formation of spatial-memory (Ramirez-Amaya et al., 2001).

Aside from the physiological role of MFs in normal brain function, MFs may aslo play a significant role in the pathophysiological progression of temporal lobe

epilepsy (Sutula et al., 1988; Babb et al., 1991; Sutula et al., 1998; Lynd-Balta et al., 2004; Holmes, 2009). In response to epileptiform activity, in both human and animal patients, MFs are seen to sprout extensive filopodial projections (Sutula et al., 1988; Santhakumar et al., 2005). These projections can eventually develop into recurrent granule cell-to-granule cell synaptic contacts, which are only present following epileptiform activity and are thought to be a significant risk factor for developing future seizures (Holmes et al., 1999; Frotscher et al., 2006). Unfortunately, the mechanisms that lead to mossy fiber sprouting and the development of aberrant synaptic contacts are poorly understood (Babb et al., 1991) and can take many days to develop following seizure onset (Cavazos et al., 1991). Interestingly, recent observations from our collaborators in Ireland (Kumlesh K. Dev; Trinity College Dublin; unpublished observations) suggest that prior to MF sprouting vesicle transport deficits may already exist as a result of epileptiform activity. This could produce serious and detrimental consequences to cell function, especially because vesicle transport plays such an essential role in various cellular processes. Unfortunately, because most previous studies have focused on the structural rather than the functional changes that occur within mossy fibers as a result of epileptiform activity and because no studies have specifically investigated the transport of vesicles within mossy fibers there exists a lack of knowledge regarding the effects of epileptiform activity on the transport of mossy fiber vesicles. Never-the-less it is known that epileptiform activity can trigger a plethora of aberrant cellular changes that can alter network function, such as irregular ion channel expression and increased NT release (Li et al., 1995; Wallace et al., 1998; Upreti et al., 2012). These changes, because they are intrinsically linked to the intracellular transport system may lead to alterations in vesicle transport, thus, we hypothesised that vesicle transport and vesicle localisation would be significantly altered as a result of epileptiform activity. Altered vesicle transport could represent a novel target for therapies that may halt or reverse the aberrant changes that occur as a result of epileptiform activity.

MeCP2 is one of the most abundant nuclear and neuronal proteins (Guy et al., 2011). MeCP2 plays a key role in gene regulation, acting as both a repressor and enhancer of transcription (Nan et al., 1997; Su et al., 2012). Absence or disruption of MeCP2 expression leads to structural and functional plasticity deficits as well as

several synaptopathies (Asaka et al., 2006; Smrt et al., 2007; Kline et al., 2010; Weng et al., 2011). Endogenous MeCP2 mutations lead to the development of a severe neurological condition, Rett syndrome (Guy et al., 2001). Female MeCP2 knock out mice recapitulate both the progression and the symptom development observed in Rett syndrome (Guy et al., 2007; Ricceri et al., 2008), this includes a delayed onset and a propensity for developing seizures. In hemizygous mice overt symptom onset occurs at around 8 weeks, but prior to this, functional deficits appear scarce (Guy et al., 2007). However, because in the early stages of a number of neurological disorders vesicle transport deficits appear as one of the earliest detectable changes (Holzbaur, 2004; Chu et al., 2012) we hypothesised that it may be possible to detect vesicle trafficking deficits in neurons lacking MeCP2.

Aims

The aims of this chapter were to investigate vesicle trafficking in the axons of dentate granule cells, the mossy fibers. Specifically the aims were: (1) to establish a live imaging assay in which to study vesicle trafficking specifically in hippocampal mossy fibers, (2) to investigate the effects of epileptiform activity on the transport and dynamics of synaptophysin positive vesicles and vesicle clusters and (3) to use this assay to probe for possibly early vesicle transport deficits in neurons lacking the essential nuclear proteins MeCP2.

Figure 4.1

Ai

Lenti-Syp-GFP injection

CA1

DG

CA3

distal

proximal

Bi

Bii

Biii

rad.

luc.

CA3

rad.

luc.

CA3

20µm

rad.

luc.

CA3

proximal ←→ distal

Ci

Syp-GFP

5µm

Cii

2µm

Ciii

2µm
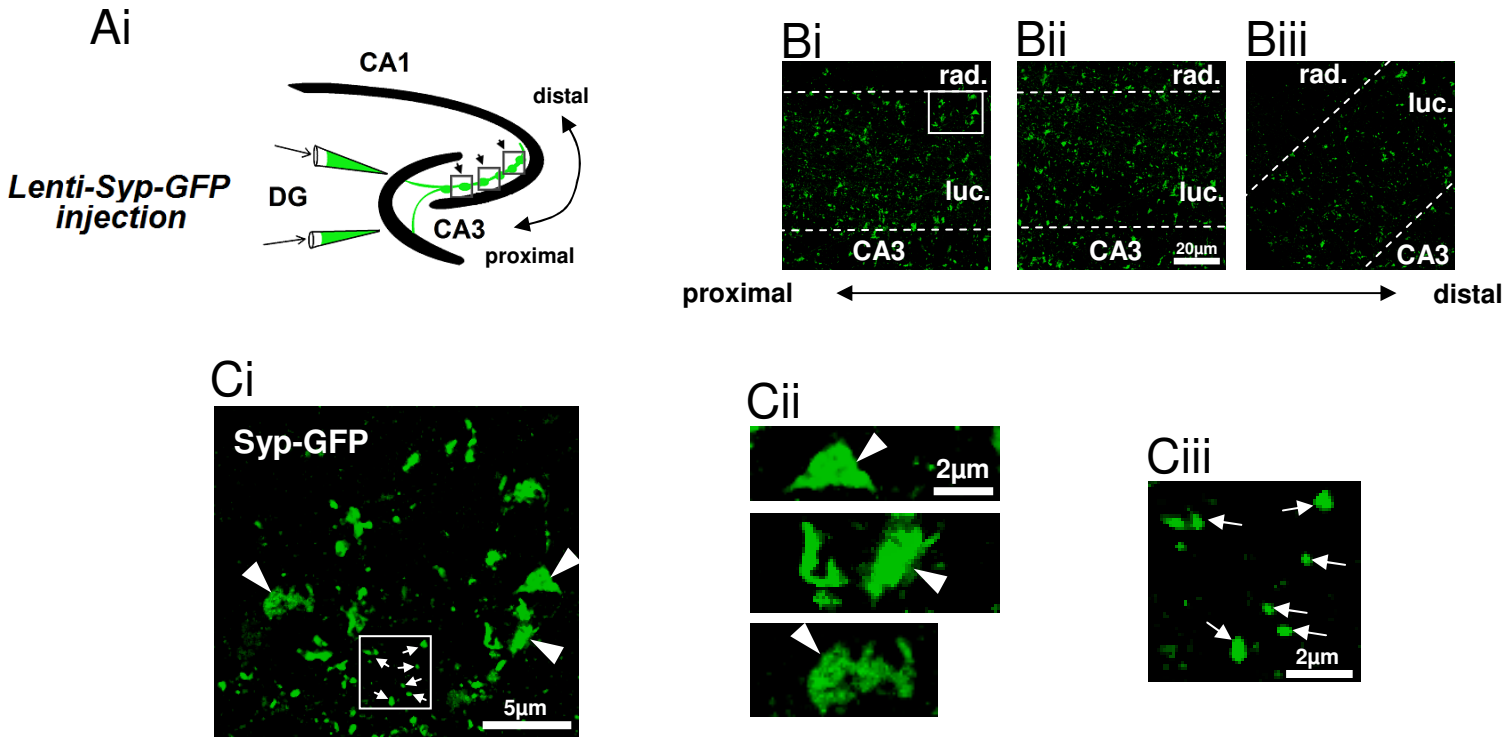
Figure 4.1 – Targetted transduction of dentate granule cells (with lenti-syp-GFP) reveals syp-GFP accumulations running along the stratum lucidum.

In order to study vesicle dynamics in a single axon subtype type (the mossy fiber), hippocampal organotypic slices were selectively injected with lenti-syp-GFP into the dentate gyrus (DG) at DIV7. **Ai)** A cartoon schematic of the injection process. A micropipette containing lenti-syp-GFP (>1x10^6 infectious units/ml) was micromanipulated under low power magnification (x4 objective) into the DG cell body layer. Lenti-syp-GFP was then pressure injected at equal intervals along the cell body layer (100-200μm spacing). Thick black lines indicate the cell body layers (DG, CA3 and CA1). Thin green lines indicate transduced axons (running in parallel to the CA3 cell body layer). Black squares (with black arrows) indicate sequential regions of interest running along the stratum lucidum. **B)** Three micrographs taken from these regions of interest are shown. Labelled are the stratum radiatum (rad.), stratum lucidum (luc.) and the CA3 cell body layer. **Ci)** An enlarged image taken from Bi), which shows individual syp-GFP positive vesicle clusters of varying size. **Cii)** Large vesicle clusters are shown by large white arrow heads. **Ciii)** An enlarged image of the white square box shown in Ci). Several small vesicle clusters are marked by white arrows. This distribution of terminals is typical for mossy fibers axons running along the stratum lucidum (Acsády et al, 1998).

4.1 Specific granule cell transduction with lenti-syp-GFP

To study vesicle trafficking in specific cell types we injected hippoccampal organotypic slices at DIV7 with lenti-syp-GFP specifically into the DG cell body layer. The injection process was modified from (Ehrengruber et al., 2001) and is depicted by a cartoon schematic shown in Figure 4.1 A. Following the injection, slice cultures were left to incubate until DIV14 before being processed. To characterise the expression pattern of syp-GFP we immunostained organotypic hippocampal slices at DIV14 for the neuronal marker NeuN. Injected slices showed extensive syp-GFP labelling running along the stratum lucidum. Abundant syp-GFP positive vesicle clusters were evident in close proximity to the CA3 cell body layer. Supplementary video 3 gives an overview of syp-GFP expression in the hippocampus. syp-GFP positive axons can be seen emerging from the DG cell body layer and traversing the hilus, from here axonal processes can be seen to run in parallel to the CA3 cell body layer where they are then seen to terminate before reaching the CA1 cell body layer, coinciding with the anatomical location of mossy fibers.

4.2 Increased activity does not detectably alter the volume of vesicle clusters over 5hrs

After identifying syp-GFP positive axons running along the stratum lucidum we then visualised vesicle transport using live imaging. Although we had initial success in observing vesicle transport in mossy fiber axons (see supplementary video 4), follow up videos failed to produce clear images of vesicle transport. This was attributed to our wide-field microscope being unsuitable for imaging fluorescent signals in thick tissue. Many videos suffered from drift and had poor signal to noise levels. Occasionally it was possible to observe axonal processes close to the surface of the organotypic slice, however this was inconsistent and produced poor quality images. As an alternative to imaging the transport of small motile particles, we instead decided to image the dynamics of large synaptic

Figure 4.2

Ai — Syp-GFP (raw) — A.U. 85.0 / 0.0 — 5µm

Aii — deconvolved — A.U. 85.0 / 0.0 — 5µm

B — control — 20µM gbz

0hr   1hr   2hr   3hr   4hr   5hr   6hr   2µm

Ci — volume (µm³) — Control / Gbz — Gbz — n.s. — Time (hrs)

Cii — relative volume — Control / Gbz — Gbz — n.s. — Time (hrs)
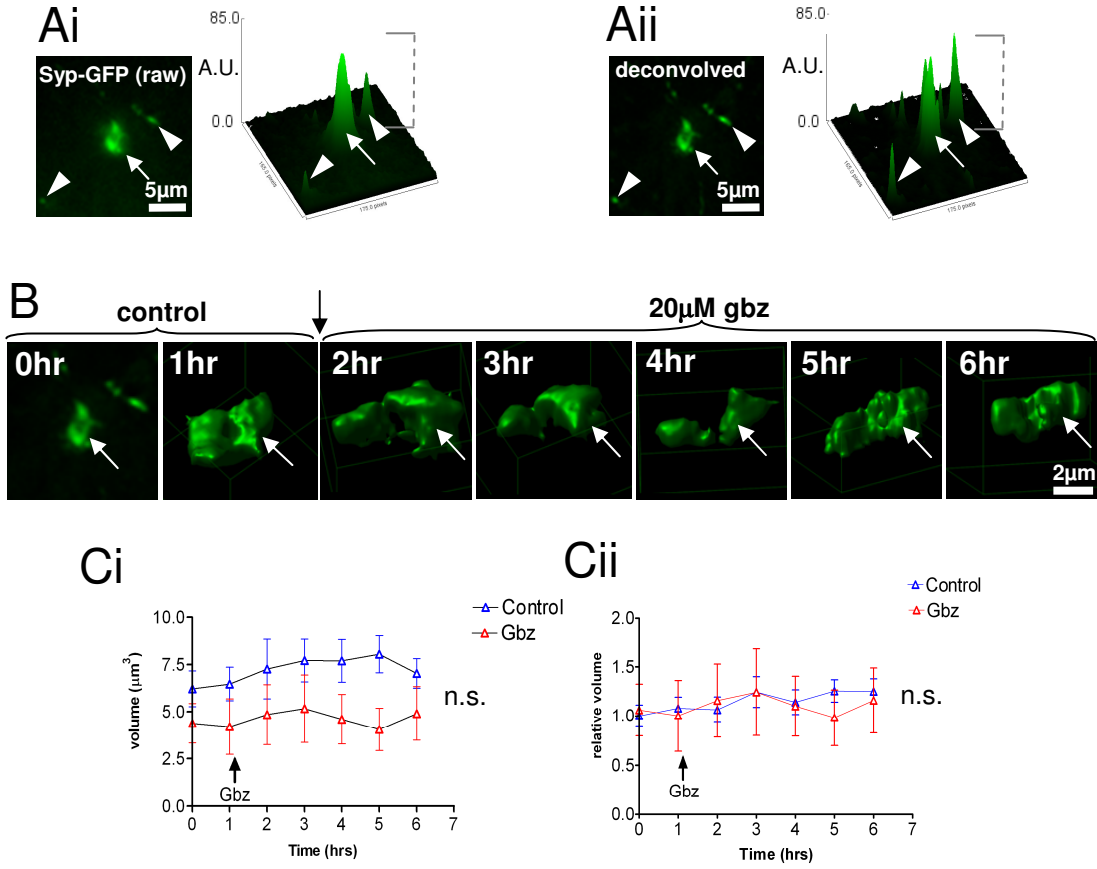
Figure 4.2 – No detectable change in vesicle cluster volume was observed following treatment with the GABA$_A$ receptor antagonist gabazine.

To investigate the effects of epileptiform activity on mossy fiber vesicle cluster dynamics, syp-GFP positive mossy fibers were imaged repeatedly (every hour) in the presence or absence of the GABA$_A$ receptor anatagonist gabazine (20µM). Individual vesicle clusters, identified along the stratum lucidum, were individually deconvolved to improve signal to noise levels. **Ai)** Left: an image of a typical non-deconvolved vesicle cluster. Right: a surface map showing the grey scale intensity of the vesicle cluster (measured in arbitrary units (A.U.). **Aii)** Left: a micrograph showing the same vesicle cluster from Ai), following deconvolution. Right: an intensity surface map of the deconvolved vesicle cluster. Large arrow heads indicate small vesicle clusters that now have improved signal to noise. Background noise is also improved following deconvolution. In the deconvolved surface map in Aii), the background is darker and closer to zero when compared to the surface map in Ai). **B)** A typical time course experiment showing an individual vesicle cluster over 6hrs (rendered in 3D). gbz was perfused onto the slice only after 1hr, this was done to initially establish a baseline measure of vesicle cluster volume. **Ci)** A scatter plot showing average vesicle cluster volume over time. Vesicle cluster volume from control slices is shown in blue. Vesicle cluster volume from gbz treated slices is shown in red. The time of gbz application is marked by a black arrow. In both control and treated slices there was no detectable deviation in the volume of vesicle clusters over time. **Cii)** A scatter plot of normalised volume over time. Cluster volumes were normalised against time zero. There was no detectable change in vesicle cluster volume in either control or treated cultures over time; p=0.19. Control and treated cultures, were also not significantly different from each other, p=0.70; two-way ANOVA.

vesicle clusters. These clusters were larger and brighter than motile particles and were more amenable to imaging.

To study the effects of epileptiform activity on vesicle cluster dynamics we imaged syp-GFP positive synaptic vesicle clusters for 5hrs in the presence or absence of the $GABA_A$ antagonist gabazine (gbz) (gabazine like bicuculline reliably induces epileptiform activity in slice cultures). Optical sectioning (0.3μm z-step) was used to capture the entire structure of individual vesicle clusters at one hour intervals for six hours (one hour baseline / five hours treatment). Vesicle clusters were then individually deconvolved (Huygens, U.S.A.) before being rendered into 3D and manually measured for changes in volume.

In both control and gbz treated cultures there was no detectable change in vesicle cluster volume over a period of five hours (Fig. 4.2 C). In control cultures the average vesicle cluster volume at baseline was $6.6±1.7μm^3$, after six hours imaging this did not significantly change, remaining at $7.1±0.79μm^3$, n=25 clusters, 4 experiments, p>0.05. In gbz treated cultures the average vesicle cluster volume at control baseline was $4.4±1.04μm^3$, whilst following 5hrs treatment with gbz, vesicle cluster volume was $4.9±1.43μm^3$, n=7, 3 experiments, p>0.05. No obvious change in vesicle cluster localisation could be observed over 6 hours, summarised in Figure 4 Cii. In neither control or treated cultures was there any apparent change in vesicle cluster volume.

Aside from changes in vesicle cluster size there was also no evidence of vesicle cluster rearrangement during the imaging period. However, because so few vesicle clusters were accessible for live imaging with the wide field microscope it cannot not be ruled our. For example, in gbz treated experiments it was only possible to image a total of 7 vesicle clusters from 3 experiments. This was significantly less than could be imaged by confocal imaging, using a confocal microscope at the same magnification we observed approximately 180±40 vesicle clusters in a single experiment, which was a dramatic improvement to widefield imaging. This increase in yield prompted us to use confocal imaging to assess potential changes in vesicle cluster size and dynamics.

Figure 4.3

A

Increasing threshold (δ = 10) ⟶

stable count

Bi

Bii
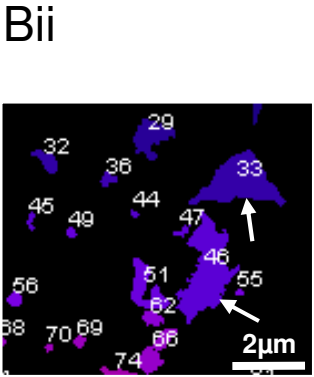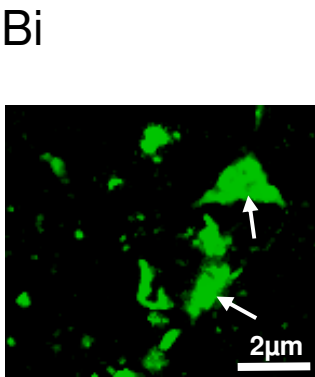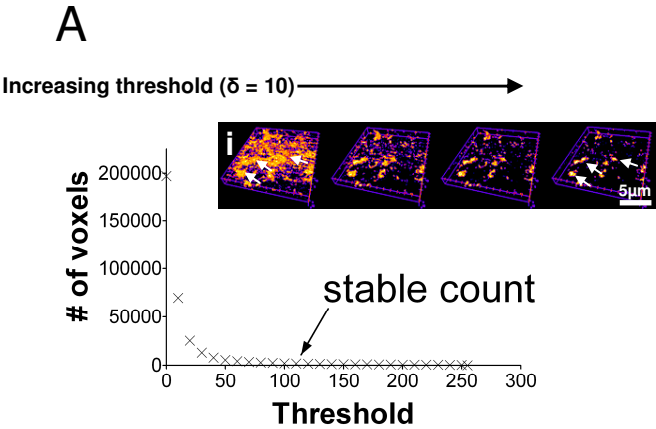
Figure 4.3 – The individual volumes of large numbers of vesicle clusters can be automatically quantified in fixed tissue.

To quantify the volume of large numbers of syp-GFP positive vesicle clusters (in fixed tissue) it was necessary to automate the process of image analysis. We used a segmentation algorthim developed by Russell et al. 2009, to deterministically identify individual vesicle clusters from background noise; In conjunction with this we also used '3D object counter' (a widely used plugin for NIH software: image j) developed by Bolte & Cordelières, 2006, to measure the volume of objects in 3D. **A)** A scatter plot showing how the number of voxels counted in the confocal stack decreases as the threshold value is increased. A 'stable count' is determined when there is no significant decrease in pixels between subsequent and defined (δ) increases in threshold. The algorithm then assumes (at this point) that objects of interest have been adequatly identified from the background. The image seen in Ai) demonstrates that as threshold is increased, indvidual vesicle clusters (white arrows) can be identified from background noise. **Bi)** A micrograph showing raw and unsegmented syp-GFP positive vesicle clusters. **Bii)** An image showing the same region following segmentation and identification by object counter 3D. Individual vesicle clusters can be automatically measured and numbered. This meathod of automation provides a rapid and unbiased way of identifying the volume of large numbers of vesicle clusters.

4.3 Vesicle clusters can be automatically quantified in 3D

To improve image quality following difficulties with wide field imaging we switched to using a confocal microscope in order to study the effects of epileptiform activity on the size and distribution of vesicle clusters. However, to measure volume changes in large numbers of vesicle clusters it was necessary to develop an analysis protocol that permitted the measurement of vesicle cluster volume automatically. The workflow for this protocol is described in Figure 2.1. In this workflow we combined an algorithm designed and validated by (Russell et al., 2009), which was capable of deterministically thresholding each confocal stack automatically and when used in conjunction with object counter 3D, a widely used plug-in for image J, permitted the measurement of vesicle cluster volume (Bolte and Cordelieres, 2006). By combining these complimentary analysis packages we were able to automatically and impartially measure the volume of thousands of vesicle clusters. An example is shown in Figure 4.3, which shows how vesicle clusters were accurately and deterministically thresholded from background noise. Following thresholding each object was automatically coloured and labelled so that it could be assessed for accurate segmentation.

4.4 Distribution of syp-GFP positive vesicle clusters following automatic volume analysis

Following automatic vesicle cluster analysis we observed a broad and non discreet distribution of vesicle cluster volumes in control slices. Vesicle clusters ranged in volume from 0.2-80μm^3. Small vesicle clusters were the most numerous, whilst larger vesicle clusters appeared less frequently. For the purpose of analysis we adopted terminology used by previous authors to categorise the size of vesicle clusters. Based on the analysis of mossy fiber terminals by (Bischofberger et al., 2006) we identified vesicle clusters >15μm^3 as belonging to large mossy fiber terminals. Clusters larger than 15μm^3 are significantly larger than typical hippocampal synapse and represent with a high degree of certainty, large mossy

Figure 4.4

Ai

5µm
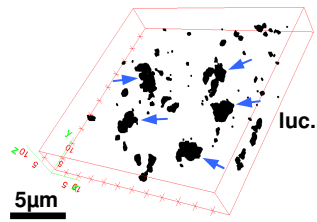
Aii
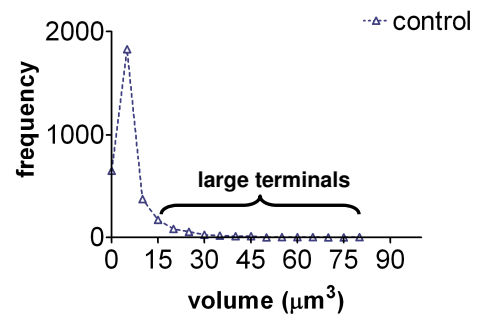
Aiii
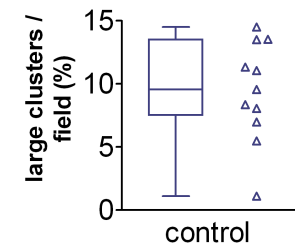
Figure 4.4 – The identification of large vesicle clusters belonging to large mossy fiber terminals.

To quantify the activity dependent rearrangement of vesicle clusters in large mossy fiber terminals, we identified large vesicle clusters based on their distinctive size, >15µm^3 (Bischofberger et al., 2006). **Ai)** A 3D reconstruction of vesicle clusters identified in the stratum lucidum. Large vesicle clusters are highlighted by blue arrows. **Aii)** A histogram showing the size distribution of vesicle clusters (11 regions from 5 experiments, >3000 vesicle clusters). Approximately 10% of all clusters analysed were considered to be large vesicle clusters. Objects <2µm^3 were ignored as these were likely to be individual particles rather than vesicle clusters (Paola et al, 2006). **Aiii)** A box and scatter plot describing the proportion of large vesicle clusters per field (control slices).

fiber vesicle clusters. In addition to identifying large vesicle cluster we ignored GFP positive structures that had volumes less 2μm^3. These were ignored to minimise the unintentional analysis of small motile particles that can be observed as they move along the axon. Based on this, any vesicle cluster >15μm^3 was classed as a large vesicle cluster, whilst any vesicle cluster with a volume between 2-15μm^3 was considered to be small a vesicle cluster. In control slices we found that large vesicle clusters represented approximately 9.4±1.21% of all vesicle clusters. A scatter plot showing the proportion of large clusters / field is shown in Fig 4.2 – Aiii) (n=11; 5 experiments). This suggests that small vesicle clusters out number large clusters 9:1. Previous estimates for this proportion suggest that small MF terminals out number large MF terminals 10:1 (Acsady et al., 1998), thus, our assignment of large vesicle clusters to large MF terminals and small vesicle clusters to small MF terminals fitted well with this estimate.

4.5 Epileptiform activity decreases the proportion of large vesicle clusters

To study the effects of prolonged epileptiform activity on the distribution and volume of mossy fiber vesicle clusters, organotypic hippocampal slices previously injected with lenti-syp-GFP into the DG cell body layer were treated with bic (20 μM) for 48hrs. The volume of individual vesicle clusters was then measured and the proportion of large vesicle clusters was compared between control and bic treated slices. Field recordings were used to detect electrical activity from the CA3 cell body layer. Bic treatment triggered epileptiform-like activity approximately 10 minutes following application (Fig 4.5 Aii). After 48hrs this led to a significant decrease in the proportion of large vesicle clusters. In figure 4.5 Ci, epileptiform activity reduced the proportion of large vesicle clusters to less than 50%. In control slices the proportion of large vesicle clusters was 9.4±1.21% (n=11, 5 experiments), however in cultures treated with bic for 48hrs this proportion dropped to just 3.3±0.73% (p=0.0002, unpaired student t-test n=12, 5 experiments). The same decrease can be observed in the distribution of individual

143

Figure 4.5

Ai   Aii

control

20μM bic

0.5mV
100ms

Bi   Bii

control

48hr (bic)

luc.

luc.

5μm   5μm

Ci

P=0.0002
***

large clusters / field (%)

15

10

5

0

n=11   n=12

control   48hr (bic)

large clusters / field (%)

15

10

5

0

control   48hr (bic)

Cii

volume (μm³)

90
75
60
45
30
15
0

$p < 0.0001$
***

large clusters

control   48Hr

D

bic

large clusters / field (%)

12.5

10.0

7.5

5.0

2.5

0.0

p=0.06   p=0.09
n.s.   n.s.   **   ***

Control (%)

n.s.

n=11   n=9   n=12   n=10   n=12

Control   4hrs (bic)   12hrs (bic)   24hrs (bic)   48hrs (bic)

144

Figure 4.5 – Epileptiform activity leads to a decrease in the proportion of large vesicle clusters running along the stratum lucidum.

Hippocampal organotypic slice cultures transduced specifically with lenti-syp-GFP in the DG cell body layer were treated with the $GABA_A$ receptor antagonist bicuculline (20µM) to induce repetitive epileptiform activity. Regions of interest were identified and imaged as outlined in figure 4.1. To measure spontaneous or induced electrical activity, an extracellular recording electrode was placed into the CA3 cell body layer. A control baseline was recorded for 30 mins prior to bic treatment. **Ai)** A representative trace taken from an untreated hippocampal organotypic slice. **Aii)** A representative trace taken from a hippocampal organotypic slice treated with 20µM. Epileptiform activity was induced in slices treated with 20µM bic following 10 minutes of application (a phenomenon that has been characterised previously, Samoilova et al, 2003). **Bi)** A 3D stack rendered from a control hippocampal organotypic slice culture containing large vesicle clusters (blue arrows). **Bii)** A 3D stack rendered from a hippocampal organotypic slice culture treated for 48hrs with bic. Epileptiform activity leads to a visible decrease in the proportion of large vesicle clusters. **Ci)** A bar chart (left) and scatter plot (right) showing the effect 48hr treatment with bic on the proportion of large vesicle clusters. **Cii)** A scatter plot showing the volume of all individual vesicle clusters identified in control (blue) and bic treated slices (red). There was a significant decrease in the median volume of large vesicle clusters, from 22.10µm3 to 18.53µm3 ($p<0.0001$, Mann-Whitney non parametric, n=35, 5 experiments). **D)** A time course summary plot showing the effect of increased activity on the proportion of large vesicle clusters. Following 24hrs treatment, bic induced activity caused a significant reduction in the proportion of large vesicle clusters. No significant reduction in large vesicle clusters was detectable at 4hrs or 12hrs post treatment. Slices were exposed to bic for: 48hrs (5 slices), 24hrs (4 slices), 12hrs (4 slices) and 4hrs (3 slices). All statistics were performed using an unpaired student t-test unless otherwise stated. p values and n numbers are as shown.

vesicle clusters (fig 4.5 Cii). There was a significant decrease in the median volume of large vesicle clusters, from $22.10\mu m^3$ to $18.53\mu m^3$ (p<0.0001, Mann-Whitney non-parametric, n=356, 5 experiments). In order to identify when this decrease occurred we fixed bicuculline treated slices at different time points following bic application and measured the proportion of large vesicle clusters. Slices were fixed and immunolabelled at: 0hrs, 4hrs, 12hrs, 24hrs and 48hrs. The proportion of large vesicle clusters was compared between treated and untreated slices. Only by 24 hours was there a significant decrease in the proportion of large vesicle clusters, by 24hrs the proportion of large vesicle clusters had decreased from 9.4±1.21%, n=11, 5 experiments; down to 4.84%±0.72%, n=10, 4 experiments, P<0.001, one-way ANOVA. At 4hrs and 12hrs we detected no significant change in the proportion of large clusters. There was a tendency for epileptiform activity to decrease the proportion of large vesicle clusters following 4hrs and 12hrs treatment but this failed to reach significance (fig 4.5 D). These results suggest that prolonged epileptiform activity can significantly alter the proportion of large vesicle clusters.

4.6 Slices deficient in MeCP2 show a more pronounced but reversible decrease in large vesicle clusters

To examine possible vesicle transport deficits in Mecp2$^{Stop/y}$ organotypic slices we injected slices lacking MeCP2 with lenti-syp-GFP specifically into the DG cell body layer. These slices were then treated with 20µM bic for 48hrs to induce epileptiform activity. As a consequence of bic treatment we observed a significant decrease in the proportion of large vesicle clusters, from 7.2% ±1.78% in control cultures (n=6, 2 experiments), down to 0.9% ±0.6% in 48hr bic treated cultures (n=8, 3 experiments, p<0.0001, one way ANOVA). To test whether this decrease was reversible slices treated with bic for 48hrs were washed with fresh media and allowed to recover for 5 days before being fixed and analysed. We found that "recovered slices" had a similar proportion of large vesicle clusters to control slices and had significantly more large clusters than slices treated for 48hrs with bic. The

Figure 4.6
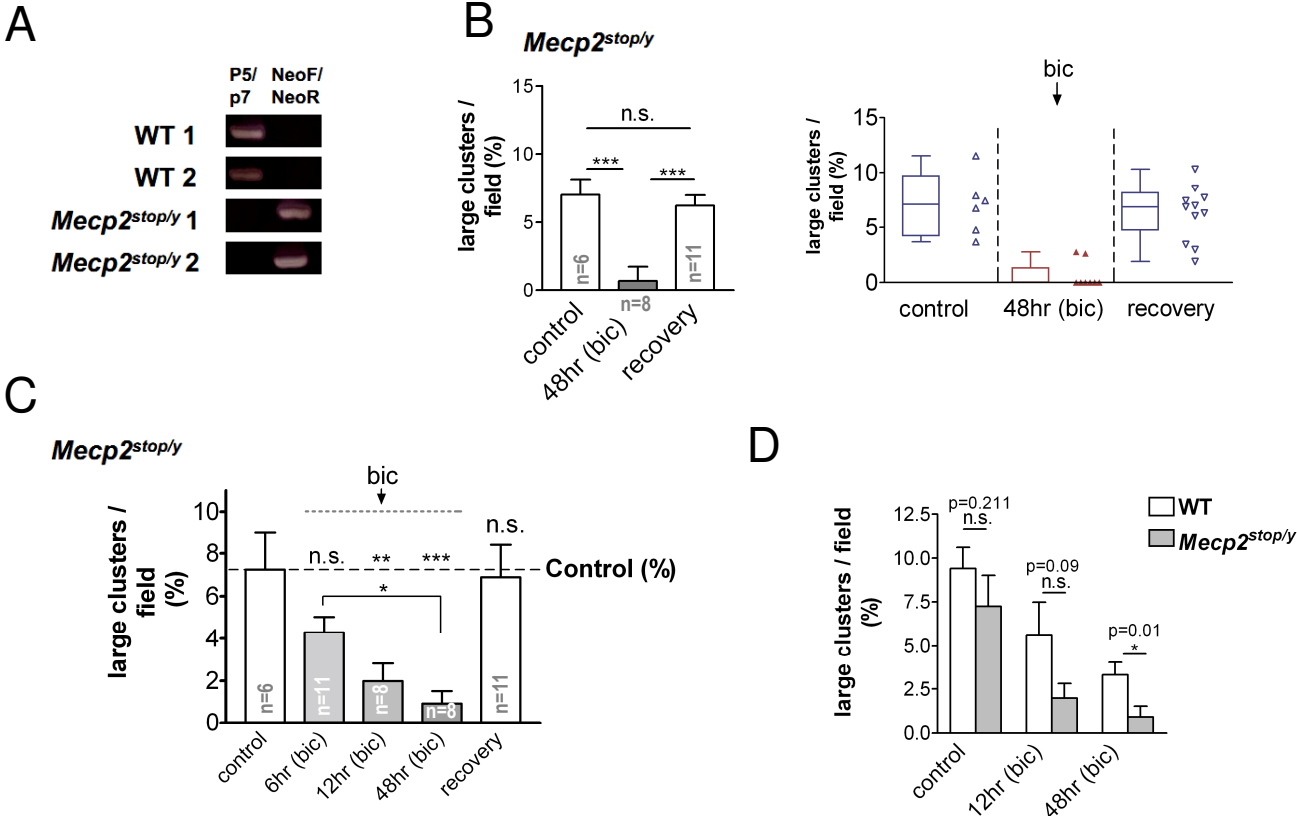
Figure 4.6 – Epileptiform activity leads to a pronounced but reversible decrease in the proportion of large vesicle clusters in slices lacking the essential nuclear protein Mecp2.

Vesicle cluster dynamics were investigated in slices lacking the essential nuclear protein Mecp2. Slices lacking Mecp2 were microinjected into the DG cell body layer with lenti-syp-GFP. Epileptiform activity was generated by application of the $GABA_A$ receptor antagonist bicuculline (bic) (20µM). **A)** An example of a genotyping experiment designed to identify the presence or absence of Mecp2 in transgenic mice; performed by Shih Ming Weng (Modified with permission from Weng, 2011). **B)** A bar chart summarising the effects of prolonged epileptiform activity on the proportion of large vesicle clusters in hippocampal organotypic slice cultures made from *Mecp2stop/y* mice In control cultures, we observed that the proportion of large vesicle clusters was 7.2% ±1.8%, (n=6, 2 experiments); this was significantly reduced to 0.9% ±0.6%, in 48hr bic treated cultures (p<0.0001, one-way ANOVA, n=8, 3 experiments). However, following recovery (5 days), the proportion of large vesicle clusters returned to a comparable level to what was observed in control slices; proportion of large vesicle clusters in recovered slices = 6.9% ±1.5% (n=11, 3 experiments). This suggests that epileptiform activity causes a reversible decrease in the proportion of large vesicle clusters. **C)** A bar chart summarising the temporal effects of epileptiform activity on the proportion of large vesicle clusters in organotypic hippocampal slices lacking Mecp2. Bic induced epileptiform activity leads to a significant decrease in the proportion of large vesicle clusters following 12hrs and 48hrs of treatment with bic. **D)** A bar chart comparing the temporal effects of epileptiform activity on the proportion of large vesicle clusters between wild type (WT) and *Mecp2stop/y* slices at 3 different times points (control, 12hrs and 48hrs). *Mecp2stop/y* slices show a greater decrease in the proportion of large vesicle clusters compared to WT slices following 48hrs of epileptiform activity. Statistics were calculated using a two-way ANOVA.

proportion of large vesicle clusters in 48hr bic treated culture was 0.9%±0.6% (n=8, 3 experiments), whilst in recovered slices the proportion of large vesicle clusters had returned to control levels, 6.9%±1.5% (p<0.0001, unpaired student t-test, n=11, 3 experiments). This apparent recovery suggests that a decrease in the proportion of large vesicle clusters was not a consequence of cell death or irreversible damage caused by epileptiform activity.

In Mecp2$^{Stop/y}$ slices we found that a decrease in the proportion of large vesicle clusters also took several hours to become apparent. Only by 12hrs did we detect a significant decrease in the proportion of large vesicle clusters. In control cultures the proportion of large vesicle clusters was 7.2%±1.78% (n=6, 2 experiments), whilst after 12hrs treatment with bic it was 1.98%±0.84% (n=8, 3 experiments). The decrease in the proportion of large vesicle clusters seemed to be more pronounced and occurred faster than in WT slices. To test this idea we compared the effects of bicuculline treatment on the proportion of vesicle clusters in both WT and Mecp2$^{stop/y}$ slices. We found that following 48hrs hours of treatment Mecp2$^{Stop/y}$ slices showed a more pronounced decrease in the proportion of large vesicle clusters. The proportion of large vesicle clusters in 48hr bic treated WT slices was 3.3%±0.73%, whilst in 48rs bic treated Mecp2$^{Stop/y}$ slices it was 0.9%±0.6% (p=0.01, two-way ANOVA). This difference was not detectable in untreated cultures or following 12hrs of treatment. The proportion of large vesicle clusters in WT untreated cultures was 9.4±1.21%, n=12, 5 experiments; whilst in Mecp2$^{Stop/y}$ untreated cultures the proportion was 7.2%±1.78% (p=0.2, two-way ANOVA n=6, 2 experiments). In WT culture treated for 12hrs the proportion of large vesicle clusters was 5.66±1.88%, n=12, 4 experiments; whilst in Mecp2$^{Stop/y}$ 12hr treated culture the proportion was, 1.98±0.84% (p=0.09, two-way ANOVA, n=8, 3 experiments). These observations suggest that WT and Mecp2$^{Stop/y}$ slices are only detectably different following 48hr treatment with bicuculline.

4.7 Discussion

In this chapter we set out to build on vesicle trafficking data described in chapter 3 by studying vesicle transport in a specific axonal subtype with known synaptic connections. We also explored the possibility that epileptiform activity might alter vesicle transport in large MF terminals. To do this we developed an assay for selectively visualising vesicle transport in mossy fiber terminals. We utilized a microinjection technique described by (Ehrengruber et al., 2001) to transduce specifically the DG cell body layer of hippocampal organotypic slices with lenti-synaptophysin-GFP. Following this, we could effectively visualise large vesicle clusters running along the stratum lucidum. Although we could not repeatedly image vesicle transport, we did image the effects of epileptiform activity on the size and dynamics of large vesicle clusters. We then used this assay to probe for possible early deficits in a mouse model of Rett syndrome.

Live imaging of wild type slices for up to 5hrs revealed no detectable change in either vesicle cluster size or vesicle cluster dynamics in response to epileptiform activity. In fixed tissue, we only detected a change in the proportion of large to small vesicle clusters following 24-48hrs of bicuculline treatment. This suggests that vesicle clusters are affected by epileptiform activity, but only after a significant delay. In slices lacking MeCP2, we detected a more pronounced decrease in the proportion of large vesicle clusters, but only following 48hrs treatment with bicuculline. This suggests that there may exist some small underlying differences between Mecp2$^{Stop/y}$ slices and WT slices, but that these differences are not immediately obvious under basal levels of activity.

Developing an assay for studying vesicle transport in a specific axonal subtype

In order to investigate vesicle transport in a specific axonal subtype we adopted a similar strategy to (Ehrengruber et al., 2001); who have previously demonstrated that it is possible to transduce specific cell types in different areas of the hippocampus, by microinjecting lentivirus. We achieved the focal transduction of MFs by embedding a micropipette into the DG cell body layer and pressure injecting a small amount of virus (<1μm / $1x10^7$ infectious units (I.U.s)) along the cell body layer. We confirmed that syp-GFP was correctly labelling MFs, by immunolabelling organotypic slices for NeuN and observing the location of vesicle clusters in relation to the CA3 cell body layer. Vesicle clusters could be clearly observed running along the stratum lucidum, in close proximity to the CA3 cell body layer (see supplementary video 3). These vesicle clusters are likely to be located within large mossy fiber terminals, both because of their location and because of their distinct size (Henze et al., 2002a). Some vesicle clusters were seen deep within the CA3 cell body layer; this can be attributed to mild synaptic rearrangements that often occur in organotypic slice culture (Coltman et al., 1995). Overall, we find that the tight arrangement of vesicle clusters to the stratum lucidum mimics the anatomical location of MFs (Galimberti et al., 2006). We conclude that pressure injection of lenti-syp-GFP into the DG cell body layer, results in the expression of syp-GFP within both MFs and large MF terminals.

A delayed decrease in the proportion of large vesicle clusters

To assess the effects of epileptiform activity on the size and distribution of large vesicle clusters, we treated organotypic slice cultures with the $GABA_A$ receptor antagonist bicuculline. As described in section 3.13, we used bicuculline, a known pro-epileptic to induce epileptiform activity. We confirmed the induction epileptiform activity by recording excitatory field potentials in the CA3 cell body layer (fig 4.5 A). We observed as a consequence of bicuculline treatment, a delayed but significant decrease in the proportion of large vesicle clusters. Live

imaging revealed no early changes in the size or dynamics of vesicle clusters (<5hrs), but analysis of fixed tissue at later time points (>24hrs) highlighted a decrease in the proportion of large vesicle clusters (fig 4.5 D). This decrease, probably reflects a decrease in the size of vesicle clusters, rather than just an increase in smaller vesicle clusters, given that in micrographs containing syp-GFP positive vesicle clusters, these vesicle clusters appear visibly smaller following treatment (see fig 4.5 B). A decrease in size of vesicle clusters was a consistent finding, in both organotypic and dissociated vesicle clusters. Vesicle clusters in the dissociated culture decreased in size by around 20% following 10hrs bic treatment (see fig 3.9); whilst in organotypic slices the proportion of large vesicle clusters treated with bic, decreased by around 50% following 48hrs treatment (see fig 4,5 Ci). Vesicle clusters in organotypic slices lacking Mecp2, showed an even more pronounced decrease in the proportion of large vesicle clusters, decreasing by around 90% following 48hrs bic treatment (fig 4.6). Taken together, these changes indicate that vesicle clusters decrease in size in response to increased activity. One thing that is still unclear, is whether these changes reflect an alteration in the transport of synaptic vesicles or whether synaptic vesicle specific proteins are somehow altered by epileptiform activity

As discussed earlier, one plausible explanation for why vesicle clusters appear to get smaller, is that the number of vesicles at the synapse are conserved, but synaptophysin-GFP diffuses away from the active zone (AZ). There is strong evidence that synaptobrevin, an integral SV membrane protein that closely associates with synaptophysin, is found to diffuse along the plasma membrane away from the synapse (Ahmari et al., 2000; Dittman and Kaplan, 2006; Bonanomi et al., 2007). It is possible that over time, low levels of syp-GFP protein may also diffuse away from the AZ. This would make it appear as if vesicle clusters were getting smaller. Supporting evidence for this comes from figure 3.4, where in addition to vesicle clusters and motile particles being fluorescent, there appears to be a diffuse GFP expression along the entire length of the axon. This could be an accumulation of individual synaptophysin-GFP positive molecules. To investigate this further, it would be necessary to look more closely at these clusters under the electron or STED microscope, correlating changes in live cluster dynamics with ultra high-resolution imaging.

An alternative explanation for the decrease seen in the size of vesicle clusters may come from a rearrangement of individual SVs. Although our analysis of motile particles (in the dissociated culture) detected no change in vesicle transport, it is unlikely that we were able to clearly distinguish the movement of individual SVs (Kopelman and Tan, 1993). Increased activity may produce a passive decrease in vesicles at the synapse. It is already known that individual synaptic vesicles can diffuse between neighbouring synapses (Staras et al., 2010; Herzog et al., 2011). During periods of increased activity, synapses may be unable to retain or capture diffuse SVs; vesicles would therefore move passively along the length of the axon, possibly making individual clusters appear smaller. Following a cessation of activity, as seen in the recovery of vesicle clusters in Mecp2 slices (see fig 4.6 B), it is possible that vesicle clusters reform and return to their original size. Studies on the synapsin-1 protein provide supporting evidence for this. Synapsin-1 is thought to function as a tether for SVs at the synapse, allowing SVs to cluster together (Chi et al., 2001; Menegon et al., 2006; Shupliakov et al., 2011). Following increased activity, synapsin-1 becomes phosphorylated and reversibly dissociates away from SVs (Chi et al., 2001; Menegon et al., 2006). As a consequence, vesicle tethering is decreased and may permit some SVs to diffuse away from the synapse and along the axon. If vesicles are diffusely spread along the length of the axon, they would then likely contribute to an increase in the extrasynaptic release of NT, which could act on extrasynaptic metabatrophic receptors, which play a role in neuromodulation and neuroprotection (Ambrosini et al., 1995; Faden et al., 2001; Movsesyan and Faden, 2006). A consequence of less vesicles at the synapse, would be a negative effect on synaptic transmission (Murthy et al., 1997). Fewer vesicles at the synapse might be an adaptation to a prolonged increase in activity (Manev et al., 1989). Glutamate is known to be toxic after chronic exposure (Eimerl and Schramm, 1991). Decreasing synaptic transmission in response to a prolonged increase in activity might aid in cell survival.

Supporting evidence for our observation that epileptiform activity leads to a decrease in the proportion of large vesicle clusters, comes from previous studies that have focused on imaging PSD95 in the postsynaptic domain. GFP-PSD95

positive dendritic spines, located on CA3 pyramidal neurons, retract following 48hrs treatment with gbz (Zha et al., 2005). Their treatment regime and time course of retraction fits closely with our observed presynaptic changes for bicuculline treatment. After 48hrs treatment, they found a 50% reduction in the number of PSD-95 positive spines. This decrease in spines has also been demonstrated *in-vivo,* through the live imaging of dendritic spines in response to bicuculline application (Mizrahi et al., 2004). Interestingly, the authors of this study conclude that bicuculline induced seizures also produce a delayed decrease in the number of dendritic spines. This suggests that in addition to our observed presynaptic changes, there are also concomitant postsynaptic changes occurring in parallel. This may represent real connectivity changes occurring as a result of prolonged epileptiform activity. In future investigations, it might be interesting to observe these changes further, imaging both the pre and post synaptic domains simultaneously. Each protein (either PSD95 or synaptophysin) can be tagged with a different fluorophore, emitting a different wavelength of light upon simulation. High resolution live imaging, such as multiphoton microscopy could be used to give an idea of the time course and sequence of individual structural changes.

A delayed but more pronounced decrease in the proportion of large vesicle clusters in Mecp2$^{Stop/y}$ slices treated with bicuculline

The main aims of this chapter were to study vesicle transport in a specific axonal subtype and to probe for potential vesicle trafficking deficits in different disease states. We chose to investigate vesicle transport deficits in a mouse model of Rett syndrome, at a time point that preceded symptom onset. Disrupted MeCP2 expression is known to cause Rett syndrome, a severe neurological disorder (Amir et al., 1999; Guy et al., 2001). Mecp2$^{Stop/y}$ mice lacking MeCP2 expression, recapitulate many of the overt symptoms seen in Rett Syndrome (Guy et al., 2007). Delayed symptom onset is a characteristic seen in both Mecp2$^{Stop/y}$ mice and patients with disrupted MeCP2 expression (Guy et al., 2001; Chahrour and Zoghbi, 2007). Scant evidence is available for functional deficits that occur prior to symptom onset, particularly with respect to vesicle transport. Because in other

disease states, such as: Alzheimers disease, Amylo-lateral sclerosis and Huntington's disease, vesicle transport deficits occur early in disease progression (Duncan and Goldstein, 2006), we hypothesised that this might also be the case for cells lacking MeCP2. By investigating the effects of epileptiform activity on the distribution of vesicle clusters in DIV 6-9 Mecp2$^{Stop/y}$ slices, we were able to detect significant differences between WT and Mecp2$^{Stop/y}$ slices following 48hrs treatment with bicuculline (see fig 4.6 D). Interestingly, we observed that epileptiform activity had a more pronounced effect on the proportion of large vesicle clusters in Mecp2$^{Stop/y}$ slices that in WT slices, which suggests that there may exist subtle deficits in Mecp2$^{Stop/y}$ slices even prior to symptom onset. However, these deficits are not evident under control conditions, which suggests that a physical stress (epileptiform activity) may be required to highlight differences between WT and Mecp2$^{Stop/y}$ slices (fig 4.6).

One possible explanation for this observed difference, is that Mecp2$^{Stop/y}$ slices are more sensitive to bicuculline induced seizures. Seizures are common in patients suffering from Rett syndrome (Chahrour and Zoghbi, 2007; Jian et al., 2007) and may be more severe in slices lacking MeCP2. There is already evidence to support the idea that slices lacking MeCP2 are more excitable than WT slices (Kline et al., 2010); for example, elevated potassium produces a more pronounced increase in spike frequency in slices lacking MeCP2 (Calfa et al., 2011). Although, we did not measure the progression of seizure severity here, it would interesting for future studies to correlate transport changes with changes in activity. Aside from hyper excitability, there are also a number of synaptic deficits known to be caused by MeCP2 deficiency; for example, reduced dendritic spine density is a commonly observed consequence of MeCP2 deficiency (Armstrong et al., 1995; Armstrong et al., 1998; Chapleau et al., 2012). As is reduced levels of brain derived neurotrophic factor (BDNF) (Wang et al., 2006; Abuhatzira et al., 2007). BDNF is an important growth factor, which promotes cell differentiation, neuronal development, neuronal survival and synapse formation; BDNF deficiency could make neurons more sensitive to activity induced toxicity, potentially amplifying the effects of epileptiform activity (Almeida et al., 2005).

Mechanistically, it is still unclear why vesicle clusters seem to decrease in size. nevertheless, we have still been able to observe a significant difference between

WT and Mecp2$^{Stop/y}$ slices prior to overt symptom onset. This is an interesting observation, given that the earlier deficits are detected, the more amenable they might be to therapy. In addition, identifying the order in which deficits become apparent, may help us to better understand the progression of the disease. Our observations should therefore be useful for future studies investigating the role of vesicle transport in the progression of Rett syndrome.

4.8 Conclusions

I conclude that in both WT and Mecp2$^{Stop/y}$ hippocampal organotypic slices, vesicle clusters located within mossy fiber terminals are sensitive to bicuculline induced epileptiform activity. I conclude that bicuculline treatment leads to a delayed but significant decrease in the proportion of large vesicle clusters, and that this is recoverable, at least in Mecp2$^{Stop/y}$ slices. In addition, I also conclude that presymptomatic Mecp2$^{Stop/y}$ slices, following 48hrs bicuculline treatment, show a more pronounced decrease in the proportion of large vesicle clusters. An observation that supports the idea of subtle, but possibly important deficits existing within these slices prior to symptom onset.

Chapter 5:

A novel dissociated cell culture assay for conserving hippocampal architecture and for studying vesicle transport in a specific cell type

5.0 Introduction

Hippocampal tissue can be maintained *in vitro* for several weeks by producing either dissociated cell cultures or organotypic slice cultures. The primary application of each of these culture assays is to permit the long-term study of biological processes *in vitro* (Simoni and Yu, 2006; Kaech and Banker, 2007). Thanks to lentiviral transduction various proteins tagged with fluorescent probes can be expressed in living neurons and cultured for long periods (Fernández-Suárez and Ting, 2008). Using high-resolution microscopy these proteins can be repeatedly imaged from hours to days or from days to weeks (De Paola et al., 2006; Galimberti et al., 2006).

Depending on the application each cell culture system offers specific advantages and disadvantages over the other. Dissociated cultures are optically accessible, but lack a conserved network architecture, which makes them more suitable for studying intracellular processes (Nakajima et al., 1985). Organotypic cultures on the other hand, are used in applications where connectivity is important, because they reliably maintain the gross architecture of the tissue (Yudowski et al., 2007; (Stoppini et al., 1991). However, to faithfully maintain tissue architecture organotypic tissue must be sliced at a thickness of between 300-400µm, which significantly hinders it's optical accessibility (Dhingra et al., 2001). This complicates both live imaging and the transduction of lentivirus, which is why dissociated cultures are still extensively used as a reduced and simplified cell culture system.

Over the years dissociated cultures have been created from almost every conceivable cell type and have been developed into a huge variety of assays. Many of these assays were designed to mimic important biological processes that occur within the body, but which are difficult to study *in vivo*. These include: wound healing (Rodriguez et al., 2005; Liang et al., 2007), glial infiltration following injury (Fitch et al., 1999) and the proliferation of malignant cancerous cell types (Nakamura et al., 2007). To study these processes in vitro it is often necessary to engineer a cell culture system that has a precise cellular arrangement. One

important example of this is the opposition culture. In this culture system specific cell populations are grown separately but in a close proximity, making it possible to study the movement of cells between two defined cellular layers. This has been used to investigate the efficiency of epithelial cells to achieve wound healing and has also been used to investigate factors that hinder or enhance the infiltration or migration of glia into damaged regions (Oberringer et al., 2007).

Although the opposition method has been used extensively with proliferating cell types we wanted to further investigate its potential for use with primary neurons. In particular, we wanted to use the opposition method to grow specific neuronal cell types that are naturally found to be in opposition in the brain, ie cells that synapse together. One particularly interesting synapse, which is found in the hippocampus, is the MF-CA3 synapse (Toth et al., 2000). The MF-CA3 synapse has been a constant interest to neuroscientists for decades, not least because of it's distinctively large size but also because MFs appear to express a potentially unique form of LTP and because MFs may also play a significant role in the pathogenesis of epilepsy (Babb et al., 1991; Toth et al., 2000; Kwon and Castillo, 2008). This makes investigating the MF-CA3 synapse an important research challenge. Previous literature describes attempts by labs to study the MF-CA3 synapse in the dissociated culture (Baranes et al., 1996; Kavalali et al., 1999). These labs set out to study the interactions of DG granule cells and CA3 pyramidal neurons as an isolated population, which they achieved by producing mixed cultures made from only DG and CA3 cells. Although this methodology provided an isolated environment for DG granule cells and CA3 pyramidal neurons to interact, it complicated the identification of specific cell types within the cell population. For example, the authors wanted to target specific cells for electrophsiological recordings, however, because each cell type was mixed together it was only possible to identify specific cells based on morphological criteria, ie through the shape and size of the soma and dendrites. Even though pyramidal neurons and granule cells tend to differ by both shape and size there still remains a significant level of ambiguity and error with morphological identification, which can be minimised by culturing cells in a specific and separate arrangement.

Our aim therefore was to improve the functionality of our primary dissociated cultures by engineering a similar cell culture assay to that of the opposition method, but with additional modifications. Using hippocampal architecture as an inspiration we aimed to re-create the MF-CA3 synapse by culturing DG granule cells and CA3 pyramidal neurons separately, but in close proximity. We hoped that this would simplify the identification of discreet cells types, whilst still permitting the study of specific cellular interactions. Our aim was to study network connections that naturally occur in the brain, whilst maintaining cells in a reduced and simplified environment. We aimed to use this assay to study both synapse formation and vesicle trafficking specifically in mossy fibers. Although the design of this assay is in tune with our desire to study vesicle transport in a known cell type, it is likely to have many other useful applications.

Aims

The specific aims of this chapter were: (1) To develop an assay for studying vesicle transport in known cell types, in the dissociated culture. (2) To mimic the cellular architecture of the hippocampus, by culturing pure populations of DG granule cells and CA3 pyramidal neurons in close proximity. (3) To characterise the suitability of the assay for studying vesicle transport.

Figure 5.1

Ai

Aii

Bi

magnetic wall   base magnet

Bii

C

"CBL 1"   "gap"   "CBL 2"

100μm
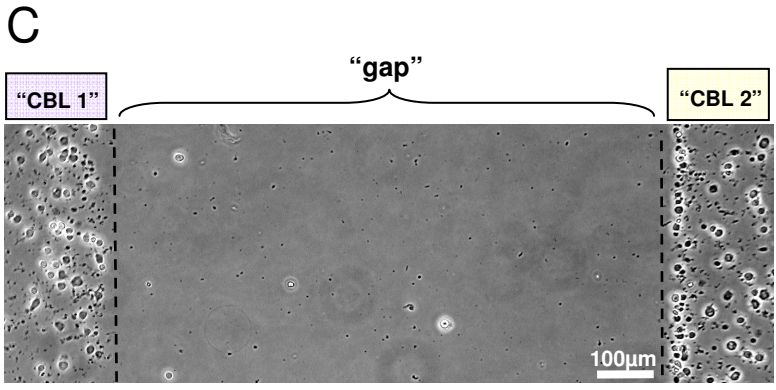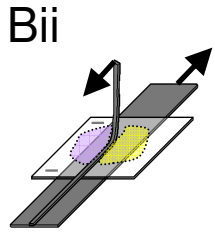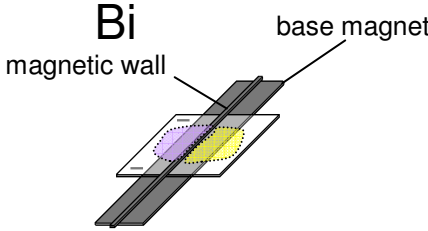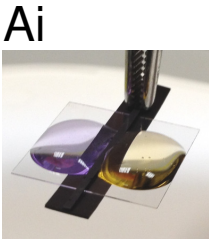
Figure 5.1 – Establishing a simple method for culturing separate and defined cell populations in close proximity.

Ai) An image of a working prototype magnetic wall (sandwich) used to separate two cell populations. Two stained solutions were used to test the functionality of the separation. **Aii)** An image showing how the device sits inside a petri dish in preparation for cell culture. **Bi)** A schematic of the magnetic wall (sandwich). Each magnet is a Halbach array, in which the magnetic field is directed strongly in one direction. The magnetic field of the base maget is directed upwards, whilst the magnetic field of the wall is directed downwards. A 1mm wide magnet is strong enough to overcome the surface tension of the media. **Bii)** A schematic of how the magnetic wall (sandwich) is removed from the primary disscoiated hippocampal culture (PDHC) following adherance of dissociated neurons to the cover slip. The cover slip was marked on two adjacent corners using a fine tip diamond cutter (shown by 2 lines on the left side of the cover slip seen in Bi and Bii); this was done to aid in the orientation and identification of the specific cell body layers during culture. **C)** A micrograph of a PDHC culture that was separated by a magnetic wall, 1mm wide (at T=1hr). The wall was removed to reveal a clear space (gap) between two separate cell body layers (CBL).

5.1 A novel magnetic "wall" for culturing separate cell populations in close proximity

Culturing cell populations separately was the first step in defining the architecture and arrangement of specific cell populations. For a defined architecture cells need to be spatially separate but capable of interacting. To achieve this, a number of strategies were attempted. The first attempt consisted of plating two small drops of cell suspension in close proximity on the cover slip. A volume of 20 - 50µl was used for each droplet. The water tension created by the small volume stopped the media from moving around and allowed each droplet to be plated in close proximity without mixing. Although this produced separate populations, the distance between the populations was often inconsistent. To overcome this problem, a thin "wall" of polydimethylsiloxane (PDMS is a polymer that is used regularly in cell culture) was used to separate the cell populations at a consistent distance. Thin strips of PDMS (0.5mm – 1mm thick) were placed across the cover slip and cells were plated on either side. PDMS allowed for the effective separation of the cell populations but often left trace material on the cover slip that interfered with axon growth. In response to this, PDMS was replaced with Teflon, a material that does not react with other materials or solutions readily. Unfortunately, Teflon was not heavy enough to overcome the water tension created by the two drops of cell suspensions. When the media was plated, the Teflon bar floated away and the cell populations mixed. It was realised that extra force was needed to overcome the force generated by the water tension. In light of this, two thin strips of halbach array magnets were cut and placed either side of the cover slip. Halbach array magnets were chosen because they have a strong magnetic field that faces in one direction. 1 x 15mm thick magnetic strips were strong enough to overcome the water tension generated by the cell suspensions. This magnetic wall was able to separate two droplets of media for at least one hour. To test this, two coloured dyes were placed either side of the wall and left for one hour. Dyes were checked every 15 minutes for evidence of mixing. There was no evidence of any mixing after >1hr. Separation of the two solutions is beneficial because it allows individual cell populations to be selectively treated with lentivirus.

Figure 5.2
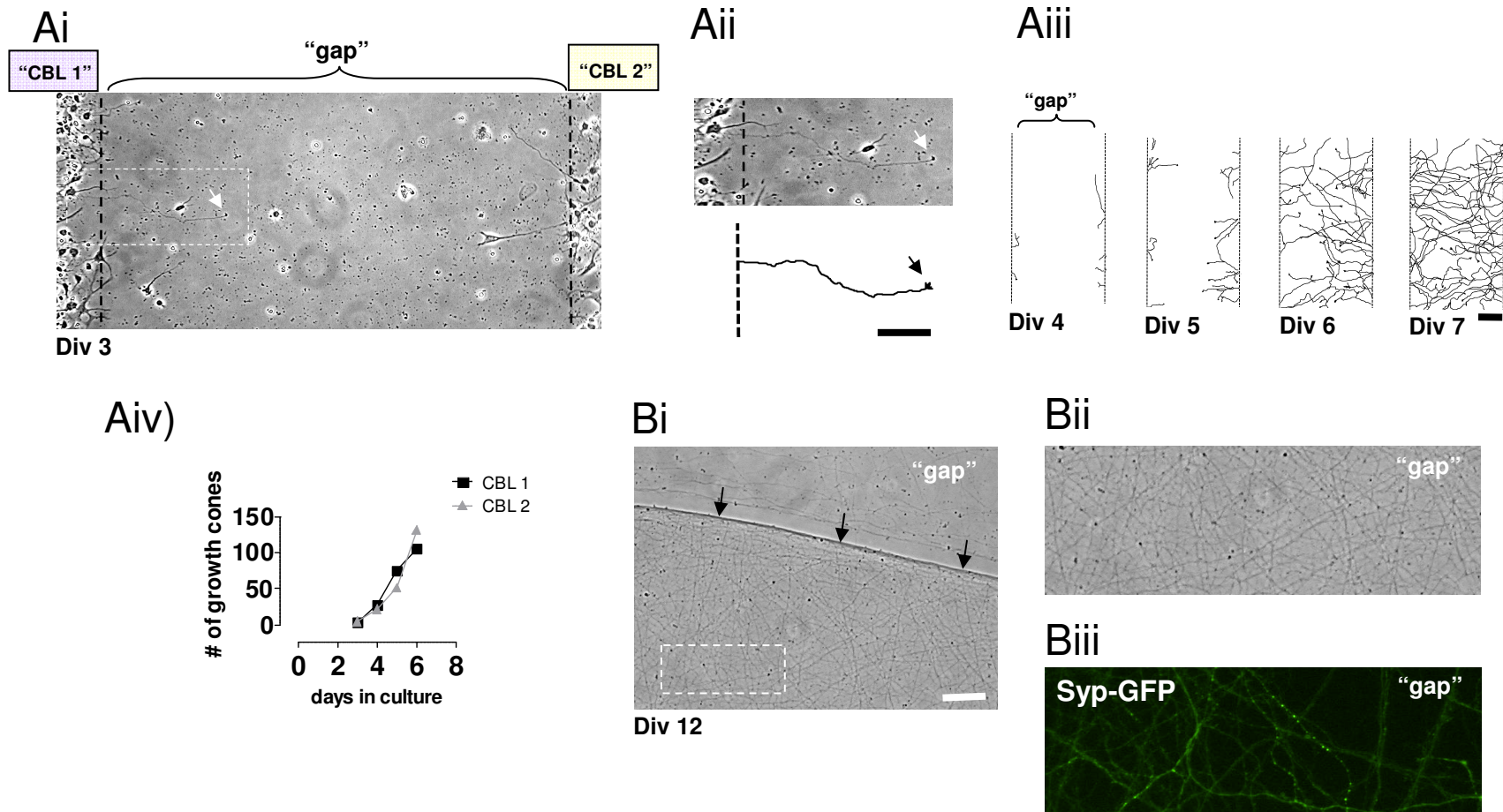
Figure 5.2 – Cell body layers become densely interconnected by axon like processes crossing the gap.

Ai) A micrograph of a DIV3 primary dissociated hippocampal culture (PDHC) that was separated by a 1mm wide magnetic wall. The white checker boxed region highlights the location of a putative axon and grow cone emerging from "CBL1". **Aii)** An enlarged image of the checker boxed region shown in (Ai). Top: an axon like projection (with growth cone) is marked by a white arrow. Bottom: a re-construction of the same putative axon and growth cone, marked by a black arrow. Individual axon like processes can be manually tracked as they cross over the gap and travel towards the opposite cell body layer. **Aiii)** Four sequential reconstructions (24 hours apart) of axon like processes crossing over the same portion of the gap. Growth cones and processes can be seen to emerge from each cell body layer, which traverse the gap over 96hours. **(Aiv)** A scatter plot summarising the amount of growth (# of emergent growth cones) occurring between the cell body layers. The growth cones of individual processes were tracked as they emerged from each cell body layer. It was possible to track single processes between DIV3 and DIV7 (before the density of axons was too great). **Bi)** A micrograph taken from the "gap" at DIV12 showing a dense layer of axon like processes. Numerous putative axons and axon bundles (black arrows) can be observed between the cell body layers. **Bii)** An enlarged image of the checker boxed region in Bi, which shows numerous thin axon like projections. **Biii)** A fluorescent micrograph showing a region of the gap from a PDHC transduced with lenti-syp-GFP. Syp-GFP positive axons can be seen criss-crossing the gap and appear more amenable to live imaging.

After successfully separating two coloured dyes, we then used the magnetic wall to separate two cell populations (Fig. 5.1 C). Following the removal of the magnetic wall, a clear "gap" remained between two distinct cell populations. These cell populations had obvious borders due to their interaction with the wall. Each cell population could be clearly defined thanks to marks on the glass cover slip (Fig 5.1 – B). Each cover slip was marked in two adjacent corners by a 1mm line, which allowed orientation of the cover slip and identification of specific cell body layers. This was done using a sterile diamond cutter prior to culture. The gap that was created upon removal of the magnetic wall was free from dirt, debris and other cells. A clear gap was achieved by allowing cells to incubate for at least one hour before the wall was removed. The magnetic wall was used to reliably separate two cell populations and was removed to allow the cell populations to interact. Each magnetic wall was reusable following sterilisation with virkon and 70% ethanol.

5.2 Separated cell body layers become densely interconnected with axons

To observe how each cell body layer interacted over time, mixed dissociated neurons were plated either side of the magnetic wall and were allowed to adhere for 1hr, the magnetic wall was then removed and cells were cultured normally. To follow axonal growth overlapping images were captured along the gap, under x40 magnification, every 24hrs for 12 days. By DIV3, axonal growth cones could be seen emerging from each cell body layer (Fig. 5.2 – Ai/Aii). These growth cones were seen over the next few days to migrate to the contralateral cell body layer (Fig 5.2 – Aiii-Aiv). In a single field we observed a high density of axons crossing between the cell body layer. The movement of axons was easy to track because the gap was clear and contained only thin axon like projections (Fig 5.2 – Aiv). By DIV7, each cell body layer had become densely interconnected and the gap was filled with axonal projections. At this time point it became difficult to track individual growth cones.

Figure 5.3

A

"CBL 1"   "gap"   Lenti-GFP   "CBL 2"

50μm

Bi   **Bii**   **Biii**   **C**

"CBL 1"   "CBL 2"   "gap"

GFP   GFP   GFP

MAP2   MAP2   MAP2

20μm   20μm   5μm

△ CBL 1
▲ CBL 2

Transfected cells (%)

100

75

50

25

0

Figure 5.3 – Efficient separation enables the differential manipulation of cell body layers, which reveals the origin of axons crossing the gap.

To identify the origin of axons crossing the gap, we transduced only a single cell body layer with lenti-GFP. Only primary dissociated hippocampal cells (PDHC) in "CBL2" were exposed to lenti-GFP before plating. **A)** A series of fluorescent micrographs were collated together to produce a cross section of the "gap". The PDHC was co-immunolabelled for MAP2, to reveal neuronal cell bodies and dendrites (red), as well as DAPI to label the nuclei of all cells (blue). This labelling revealed that the "gap" was mostly devoid of cell bodies and dendrites. **Bi)** A representative micrograph captured from "CBL1" containing a MAP2 positive neuron negative for GFP (white arrow). **Bii)** A representative micrograph captured from "CBL2" containing MAP2 positive neurons that are positive GFP (white arrows). **Biii)** A scatter plot describing the percentage of GFP positive cells / region. Ten regions were randomly selected from each cell body layer and the proportion of GFP positive cells was quantified as a percentage. Samples taken from the untransduced cell body layer (CBL1) are shown in red. Samples taken from the transduced cell body layer (CBL2) are shown in green. A low proportion of cells in CBL1 became transduced (by non-selective transduction) with GFP. This suggests that the vast majority of axons imaged in the gap should originate from CBL2. **C)** A representative micrograph captured from the checker boxed region shown in A. This micrograph shows a number of GFP positive and MAP2 negative axons crossing over the gap (white arrow). Given that only CBL2 was transduced with lenti-syp-GFP is it now easier to assign an origin to the GFP positive axon.

Following removal of the wall, the gap becomes an ideal place to view vesicle transport, because it is mostly free from cell bodies and dendrites, which can obstruct fluorescence signal. To view vesicle transport at DIV10-12 cultures were transduced with lenti-syp-GFP at DIV0. Following lenti-syp-GFP transduction, many syp-GFP positive processes could be clearly seen crossing between the cell body layers (fig 5.2 Biii).

5.3 A single cell body layer can be specifically transduced with lentivirus.

Although vesicle transport could be clearly observed in these axons, it was still difficult to assign direction to vesicle transport. This is because axons from both sides of the gap were transduced with lentivirus, thus, the origin of the axon could not be easily identified. To remedy this, we decided to transduce only a single population of cells (single cell body layer) with lentivirus. To achieve this, it was necessary to split a mixed population of dissociated neurons into two equal populations, prior to plating and to only expose one population to lentivirus. In initial experiments we used lenti-GFP as a control marker, to test both the effectiveness of the separation and the efficiency of specific transduction. Cells transduced with lenti-GFP were plated into cell body layer 2 (CBL2), whilst un-transduced cells were plated into CBL1. Following specific transduction, cell cultures were stained with DAPI and immunolabelled for anti-GFP, which permitted the quantification of transduced GFP positive cells in each cell body layer. Ten random fields were chosen per cover slip and the number of GFP positive cells and DAPI positive nuclei was quantified. As expected, CBL2 had significantly more transduced cells than CBL1 (CBL2, 38% ±3% of cells transduced; CBL1, 3% ±0.5% of cells transduced (p<0.0001, unpaired student t-test, n=27, 3 experiments). We observed very few cells in CBL1 that were positive for GFP, which suggests a high specificity of transduction for the desired cell body layer, thus, fluorescent axons seen crossing over the gap are likely to originate

Figure 5.4
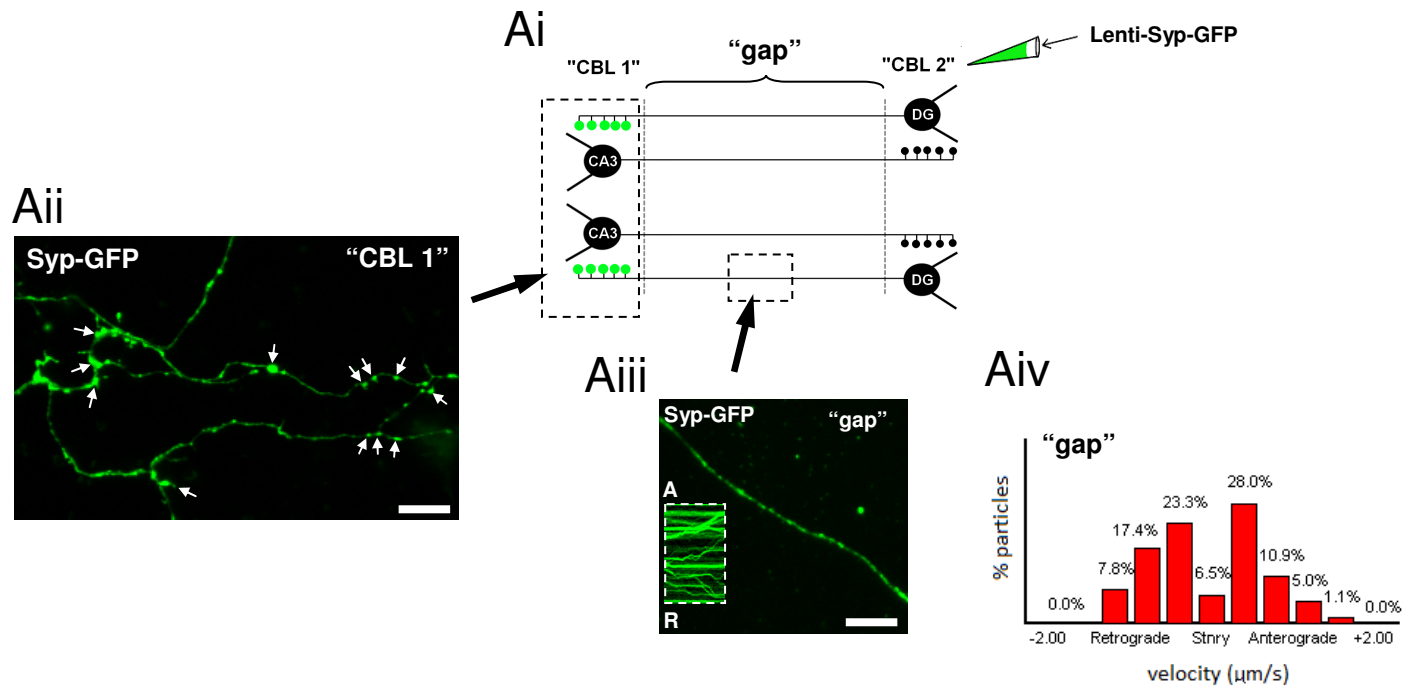
Figure 5.4 – Cell body layers can be constructed through the seeding of specific cell types.

In order to recreate the mossy fiber-to-CA3 synapse in the setting of a dissociated culture, the DG cell body layer and CA3 cell body layer were separately dissociated and then seeded onto opposite sides of the magnetic wall (described in fig. 5.1 and fig. 5.2). Only DG granule cells were incubated with lenti-syp-GFP prior to plating. This increased the chance that vesicle transport could be observed moving along mossy fibers. **Ai)** A cartoon schematic showing the arrangement of DG and CA3 cells in relation to the gap. **Aii)** A micrograph of a syp-GFP positive axon and containging vesicle clusters located in CBL1 (containing predominately CA3 pyramidal neurons). Vesicle clusters are denoted by white arrows. **Aiii)** A micrograph of a syp-GFP positive axon seen under high magnification traversing the gap. Inset shows a sample of vesicle movement in the form of a kymograph. Anterograde (A) and retrograde (R) directions are marked by the corresponding letters. **Aiv)** An example histogram summarising the direction and speed of syp-GFP particles in a putative mossy fiber axon in dissociated culture. Assigning a direction to vesicle transport is made easier because only one cell body layer has been transduced.

from the transduced cell body layer, making identification of their origin much more simple.

After specifically transducing a single cell body layer (Fig 5.3 – A), cell cultures were then immunolabelled for MAP2 to confirm that neuronal processes in the gap were axonal. A lack of MAP2 staining revealed that the gap was almost completely free of dendrites. This supports the idea that GFP positive processes crossing the gap, as seen in figure 5.3 C, are likely to represent axonal projections originating from CBL2. These were identified as axons, because they were GFP positive and MAP2 negative.

5.4 Specific synapses can be reconstructed in dissociated culture

To define specific synapses in the dissociated culture, both the CA3 and DG cell body layers were separately dissected out of acute slices prior to cell culture. Each cell population was dissociated separately and only DG granule cells were transduced with lenti-syp-GFP. Following this, each cell population was then plated onto opposite sides of the magnetic wall. Each cell population was grown in close proximity and allowed to interconnect. In this configuration any axons positive for syp-GFP are likely to originate from the DG cell body layer. At DIV10-12 (post transduction) we observed syp-GFP positive vesicle clusters located inside the CA3 cell body layer (CBL1) (fig 5.4 Aii). These axons likely originate from the DG cell body layer (CBL2) and are likely to be making contact onto CA3 pyramidal neurons. In this configuration we were able to image vesicle transport in these axonal projections (supplementary video 5). Image quality and stability were far superior to that of imaging in organotypic slices using the same microscope.

In addition to observing vesicle transport in syp-GFP positive axons in the CA3 cell body layer, it was also possible to observe vesicle transport in axons crossing over the gap. Particle transport observed in the gap appeared to be clearer than particle

Figure 5.5

A

NeuN

Calbindin

CA1
DG
CA3

Bi "CBL1"

N   C
*   *
*   *

Bii "CBL2"

N   C

Biii

calbindin positive neurons (%)

"CBL 1"   "CBL 2"

Ci

TSQ   CA1
DG
CA3

Cii

Syp-GFP

TSQ

Ciii

"CBL 1"   "GAP"   "CBL 2"

CA3   DG

CA3   DG
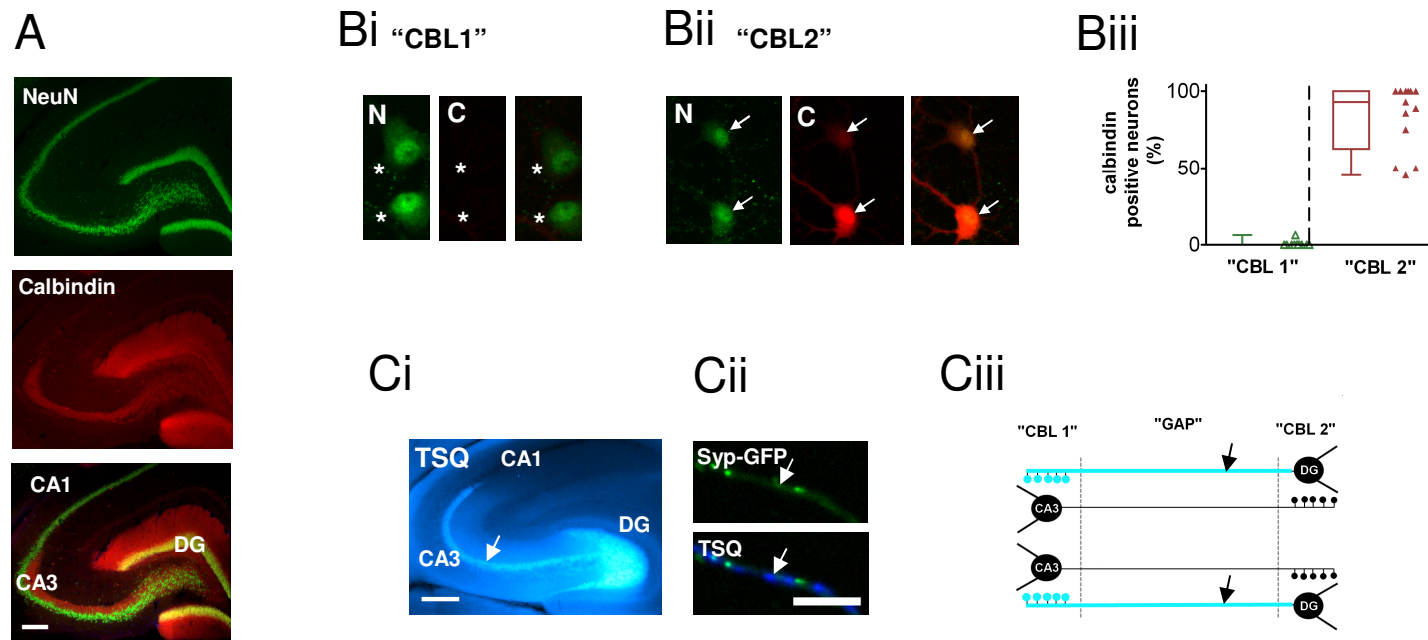
Figure 5.5 – Validation of cell separation and *post hoc* confirmation of mossy fiber identity.

A) Fluorescent micrographs of acute hippocampal slices immunolabelled for NeuN (green) and calbindin (Red). DG granule cells are strongly immuno-reactive for calbindin whilst CA3 pyramidal neurons are immuno-negative. In the bottom merged image, DG granule cells appear yellow due to the strong overlap of both NeuN and calbindin immuno-labeling, whilst the CA3 cell body layer appears green. **Bi)** A representative micrograph showing dissociated neurons from CBL1, which are NeuN positive (green) but calbindin negative. **Bii)** A representative micrograph from CBL2 showing dissociated neurons that are both NeuN (green) and calbindin positive (red). **Biii)** A scatter plot describing the percentage of calbindin positive neurons / region. Samples taken from the CA3 cell body layer (CBL1) are shown in green. Samples taken from the DG cell body layer (CBL2) are shown in red. In the DG cell body layer there is a high proportion of neurons co-expressing high levels of calbindin. In the CA3 cell body layer there was only trace calbindin labelling. Twelve regions from each cell body layer were chosen at random. **Ci)** Acute slice cultures were stained for 6-Methoxy-(8-*p*-toluenesulfonamido)quinoline (TSQ), which strongly and selectively stains zinc rich mossy fibers blue (white arrow). **Cii)** TSQ staining in the putative axon of a granule cell in a separated primary dissociated hippocampal culture (PDHC) selectively transduced with lenti-syp-GFP. **Ciii)** A cartoon schematic of TSQ staining in a separated PDHC. TSQ can be used for the *post hoc* identification of mossy fibers following live imaging of vesicle transport.

transport in the cell body layer, which likely comes as a result of the homogenous axonal population observed crossing over the gap. Importantly, by analysing vesicle transport in axons crossing the gap, we were able to assign direction to the movement of syp-GFP positive particles. An example is shown in figure 5.4 iv, where kymograph analysis was used to estimate the velocity and proportion of motile particles moving in both the anterograde and retrograde direction.

5.5 Validation of DG-CA3 culture and post hoc identification of mossy fibers

In order to validate the purity and viability of DG and CA3 cell body layers, we immunolabelled dissociated cultures for NeuN and calbindin. Calbindin is a calcium binding protein found in abundance in DG granule cells and is not detectable in CA3 pyramidal neurons, whilst NeuN is a widely used neuronal marker, their expression patterns can be observed in acute slices, immunlabelled for both calbindin and NeuN (figure 5.5 A). Calbindin is seen to label the DG granule cell body layer, as well as mosssy fiber axons running along the stratum lucidum. Co-localisation of NeuN and calbindin can be observed in the DG cell body (yellow) but not in the CA3 cell body layer (green).

After checking calbindin expression in acute slices, we then immunolabelled DG-CA3 specific cell cultures, to assess the purity of each cell body layer. Twelve random regions were imaged at x20 magnification from each cell body layer. In the DG cell body layer (CBL2) the vast majority of neurons co-localised with calbindin (84% ±5.3%, n=12, one experiment, ≈7 out of 9 calbindin positive neurons / field). However, in the CA3 cell body layer there was almost no co-localisation between NeuN and calbindin (0.5% ±0.57%, n=12, one experiment, <1 out of 6 calbindin

positive neurons / field). These data suggest that each cell body layer contained a relatively pure population of cell types.

Although this novel cell culture arrangement improves the likelihood of imaging vesicle transport specifically in MFs, it is still necessary to perform post-hoc analysis on imaged axons, to determine axonal identity. We used the vital dye N-(6-Methoxy-8-quinolyl)-p-toluenesulfonamide (TSQ) to confirm mossy fiber identity. Mossy fibers fluoresce brightly upon TSQ staining, due to their unusually high zinc content. TSQ strongly labels zinc rich mossy fiber terminals in acute slices (figure 5.5 Ci) and also zinc rich axons in dissociated culture (figure 5.5 Cii). The dye can be used immediately following live imaging to confirm mossy fiber identity. Post hoc TSQ staining has advantages when compared to immunocytochemistry, because it can be used immediately, even in tissue that is not fixed.

5.6 Discussion

Commonly used dissociated cell cultures lack the defined architecture of the tissue they were produced from. Once dissociated neurons fall at random onto the cover slip and produce a mishmash of synaptic connections, which makes studying specific cell types very difficult. This stands in stark contrast to the organised cellular arrangements observed in the hippocampus. Engineering dissociated cultures to preserve cellular arrangement is a common goal of a number of laboratories and would represent a significant improvement to current methods (Scholl et al., 2000; Taylor et al., 2005; Taylor et al., 2010). Our strategy for achieving this was to develop a simple method for culturing two defined cell populations in close proximity. We used a magnetic wall to temporarily separate each cell population and then removed the magnet so that each population could interact. After establishing that each cell body layer became densely interconnected with axons we then replaced each cell body layer with a defined cell type. We chose DG granule cells and CA3 pyramidal neurons, in order to recreate the MF-CA3 synaptic pathway. In this arrangement we transduced only DG granule cells with lenti-syp-GFP in order to study vesicle transport specifically in MFs. To demonstrate the viability of the method we successfully imaged vesicle transport specifically in MFs (supplementary video 5). We also observed that syp-GFP positive axons grew from the DG cell body layer into the CA3 cell body layer where they formed putative synaptic connections. The simplicity of this system and the improved accessibility it grants make it an attractive assay for studying the interaction of specific cell types in the dissociated culture.

Reconstructing the DG-CA3 synapse

In chapter 4 we set out to investigate the effects of epileptiform activity on the transport and distribution of synaptic vesicles within hippocampal mossy fibers. Unfortunately, due to the technical limits of our fluorescent microscope we were unable to reliably and repeatedly image the transport of syp-GFP positive vesicles in organotypic slices. We concluded that our wide field microscope was unsuitable for the live imaging of small fluorescent structures such as synaptic vesicles, a problem that has been described previously (Dumas et al., 2003; Murray, 2011). Rather than be deterred, we instead decided to modify our dissociated culture assay to continue studying vesicle transport specifically in MFs. We did this by designing a separate cell culture system with targeted lentiviral gene delivery, which not only improved optical accessibility, but also permitted specific populations of cells to be quickly and reliably identified and imaged.

The first step in developing our modified cell culture system was to develop a device that could reliably and controllably separate specific cell populations, whilst eventually allowing cell populations to interact. After testing several materials we eventually chose halbach array magnets as a suitable material for separating the cell populations. Initial testing of PDMS and teflon produced undesirable results, with PDMS leaving trace material on the cover slip and teflon being unable to overcome the surface tension of the cell culture media. To over come these issues we instead decided to use magnetic strips to separate the cell populations and to over come the surface tension of the media. We decided to use halbach array magnets, which have a unidirectional magnetic field that produces strong attractive forces. We found that by placing two 500µm thick magnetic strips in opposition over a glass cover slip that it was possible over come the surface tension of the media, without leaving trace material on the cover slip (Fig 5.1), the magnets could then be removed to allow each cell population to interact (Fig 5.2). The growth of axons crossing the gap could then be studied and exploited for living imaging.

To image vesicle transport in a specific cell type, a specific cell body layer was transduced prior plating and allowed to incubate with the virus for 1hr. After 7-10 days the specificity of the transduction process was assessed, which was done by checking for non-specific labelling in the un-transduced cell body layer. Less than 3 ±0.5% of the un-transduced cell body layer was seen to be positive for lenti-GFP, whilst 38% ±3% of cells in the transduced cell body layer were labelled. This a high specificity of transduction means that the vast majority of fluorescent axons observed within the culture will originate from the intended and trasduced cell body layer. There are modifications to the current methods that may increase the specificity of transduction. For example, decreasing the virus concentration would minimise non-specific transduction. Also, repeatedly washing the un-transduced cell body layer with virus free media may also help to reduce non-specific transduction.

With the possibility that a small proportion of axons may still originate from the un-transduced cell body layer we decided that post-hoc confirmation of axon identity would be necessary. We decided to use the mossy fiber specific marker N-(6-Methoxy-8-quinolyl)-p-toluenesulfonamide (TSQ). TSQ strongly and specifically labels mossy fiber axons in the hippocampus (Fig 5.5 Ci) as well as the dissociated culture (Kavalali et al., 1999). We used TSQ to successfully identify MFs in both hippocampal slices and putative MFs in dissociated cultures (Fig 5.5 C). Although TSQ appeared to correctly label MFs in both the slice and cell culture, there are still questions over whether TSQ is a suitable stain for identifying mossy fibers. For example, TSQ fluoresces only when bound to zinc and zinc is enriched in MFs (Coulter, 2000); however, zinc can be depleted in MFs following periods of epileptiform activity (Mitsuya et al., 2009). Although total depletion has a long time course (56 days) it may still be necessary to test the reliability of TSQ as a MF marker in future studies.

The benefits and advantages of developing a separate cell culture system

A key benefit of this assay derive from the fact that cells can be cultured in a monolayer. In thick tissue light is scattered and diffracted by cells and neuronal processes (Murray, 2011), which makes imaging small objects much more difficult. There do exist specialist microscopes that improve image quality, but the cost of these systems is far higher than commonly available wide-field systems and requires significantly more technical experience (Dumas et al., 2003). Fortunately, imaging dissociated neurons does help to alleviate this problem, because imaging cells in a mono layer significantly improves signal to noise and provides better image quality (Teschemacher et al., 2005). Another clear benefit of working with dissociated neurons is that cells can be easily transduced with lentivirus. To do this in organotypic slices requires transducing specific cell types with the focal injection of lentvirus, which is technically more challenging and takes a considerable amount of time. Transducing the dissociated culture with lentivirus required only that the virus was pipetted into the cell suspension prior to plating and washed off just prior to culture. This was far more simple.

Another benefit of developing this separate cell culture system is that cells are arranged to make physiologically relevant synaptic connections. Past criticisms of studies performed in the dissociated culture have focused on the fact that dissociated neurons lack the cellular arrangement and connectivity seen in hippocampal slices (Kleinfeld et al., 1988) and that dissociated neurons can often express morphological or biochemical artefacts (Baranes et al., 1996). We predict that arranging cells as they appear in the hippocampus may go some way to alleviating these artefacts, because cells would be able to form physiological connections. From a practical point of view arranging cells as they appear in the hippocampus is also beneficial, especially for navigating the cell culture system. Dissociated cell cultures unlike organotypic hippocampal slice cultures have no land marks for aiding with navigation. However, when cells are grouped together in specific cell body layers they can be easily identified on the cover slip. We used a diamond cutter to etch marks on 2 adjacent corners on the cover slip to help us

orientate the different cell body layers. This simple step was very useful for helping to navigate the culture.

Transducing only a single cell body layer with lentivirus is advantageous for the live imaging of vesicle transport. In our original experiments we often had difficulty identifying the direction of the cell body of the axon being imaging, because Syp-GFP assumed a punctate distribution. Also, when several axons are overlapping it became almost impossible to assign direction to vesicle transport. However, after transducing only a single cell body layer with lenti-syp-GFP the origin of vesicle transport was immediately clear. Even without secondary fluorescent markers such as RFP, it is still possible to assign direction to vesicle transport using this method.

In addition to benefitting the study of vesicle transport we also identified another potential application for this cell culture system, as described in Fig 5.2 Aiii it was also possible to track and follow the growth of axons emerging from each cell body layer over several days. It was possible days to follow the growth of individual axons by simply capturing overlapping images of the gap. This assay if used in conjunction with the selective tranduction of a single cell body layer may represent a powerful tool for studying the contribution of pre and postsynaptic mechanisms to axonal growth and targeting.

The are many advantages to organising dissociated neurons to have a defined arrangement. This is why several laboratories are also endeavouring to improve the organisation of their neuronal dissociated cultures (Scholl et al., 2000; Tooker et al., 2004; Taylor et al., 2005; Taylor et al., 2010). However, many labs often employ complex strategies for achieving their particular cell or synaptic arrangements, which can include microfluidic devices, printed patterned surfaces or the fabrication of nano structures directly onto the cell culture surface (Scholl et al., 2000; Tooker et al., 2004; Taylor et al., 2005; Taylor et al., 2010). Although some of these strategies are showing great promise many are not commercially available, take a considerable amount time to develop and require significant in-

house expertise. In addition, a disadvantage of developing complex structures is that it is often only possible to develop one or two prototype devices and limits the opportunity of other labs to test and use this technology for their own purposes. The separate culture system described in this chapter circumvents the need for complex structures and only requires the purchase of low-cost and commercially available magnetic strips, which can be cut to a desired thickness and used to separate the different cell populations. The simplicity of this method makes it attractive for future studies.

To the best of our knowledge this is the first time DG granule cells and CA3 pyramidal neurons have been grown in this configuration. Although there have been past instances of labs specifically culturing CA3 and DG granule cells, in particular (Baranes et al., 1996), the cells in this culture system were never grown as separate populations but only as a mixed population. This arrangement brought difficulties in terms of cell identification and meant that single cell transduction was not possible. In contrast to their method our method permits rapid cell identification, due to both the cell arrangement and specific lentiviral transduction. This is a significant improvement that should prove useful for future studies.

5.6 Conclusions

Overall I conclude that this novel method for culturing specific cell populations provides many practical benefits over imaging vesicle transport in organotypic slices, whilst still allowing specific cell types to be repeatedly identified. Although improved accessibility is a clear benefit future experiments will also likely to benefit from the controlled cell arrangement. Overall this simple method for culturing neurons in a defined arrangement confers *ex-vivo* qualities to an *in vitro* system.

Chapter 6:

General discussion

6.1 Major Findings and developments

In chapter 3 we found that prolonged increased neuronal activity, produced by a blockade of $GABA_A$ receptors, selectively altered the dynamics of synaptic vesicle clusters without altering the rate of vesicle transport. Although vesicle clusters decreased in size and balanced turnover was promoted by increased neuronal activity there was no concomitant change in vesicle transport. An observation that might suggest vesicles at the synapse and vesicles transported along the axon are somehow differentially regulated by increased activity.

In chapter 4, to build on these findings we developed an assay for studying vesicle transport in a specific axonal subtype. We used focal lentiviral injection selectively into the DG cell body layer with the aim of studying vesicle transport specifically in mossy fibers (MFs). We found that persistent epileptiform activity led to a delayed (>12hrs) decrease in the proportion of large vesicle clusters running along the stratum lucidum. We recapitulated this finding in $Mecp2^{Stop/y}$ slices, but observed a more pronounced decrease in the proportion of large vesicle clusters by 48hrs, which was also recoverable.

In chapter 5 we developed a novel method for maintaining hippocampal architecture in the dissociated culture. Using a magnetic separation device we were able to culture a pure population of DG granule cells and a pure population of CA3 pyramidal neurons in close proximity. We then transduced only DG granule cells with lenti-syp-GFP, which allowed us to image vesicle transport specifically in MFs emerging from the DG cell body layer, as confirmed by TSQ staining. We find that this method improves the current dissociated cell culture protocol because cells are arranged to form physiological synaptic connections, which simplifies the identification and imaging of specific cell types.

6.2 General discussion

As discussed in chapter 3, our results suggest that increased neuronal activity can selectively modulate vesicle cluster size and turnover, without detectably altering the rate or quantity of vesicle transport along the axon. This observation supports the possibility that synaptic vesicles and transport vesicles are functionally different. Synaptic vesicles, which cluster at the synapse, are known to be sensitive to increased neuronal activity, through calcium sensitive proteins in their membrane (Quetglas et al., 2002). This allows them to respond to increased activity by participating in neurotransmitter release. Transport vesicles may lack this sensitivity, which would allow them to deliver protein and cargo without being interrupted by increased activity. There is structural evidence to support the idea that the two vesicle populations are different (Bodian, 1970; Tsukita and Ishikawa, 1980; Nirenberg et al., 1995; Hirokawa, 1998), but ours is the first study to detect through vesicle trafficking experiments that each population might be differentially modulated by increased activity. Although we could not confirm this finding in organotypic slices, due to technical limitations, we did go on to develop a new cell culture assay that would allow these changes to be investigated further, but in the dissociated cell culture. Future studies should benefit from a dissociated culture that has a conserved cellular architecture.

As discussed in chapter 4, we observed a delayed, but significant, decrease in the proportion of large vesicle clusters located within large MF terminals following prolonged epilepsy. This finding was recapitulated in Mecp2$^{Stop/y}$ slices, but was more pronounced and could be recovered. Observing a decrease in the proportion of large vesicle clusters supports the idea that vesicle clusters are modulated by increased activity (Fatt and Katz, 1952; Brose et al., 1992; Augustine and Kasai, 2007; Neher and Sakaba, 2008). Observing a more pronounced decrease in Mecp2$^{Stop/y}$ slices supports the idea that underlying deficits exist in Mecp2$^{Stop/y}$ slices prior to overt symptom onset (Asaka et al., 2006; Smrt et al., 2007; Kline et al., 2010; Weng et al., 2011). In Mecp2$^{Stop/y}$ mice, symptom onset occurs at 8 week
s and accompanied by numerous synaptic alterations (Guy et al., 2001), as well as deficits in synaptic plasticity (Weng et al., 2011). There is scare evidence for pre-

symptomatic deficits in these mice, but see (Guy et al., 2011); our results represent a potentially interesting observation of early functional deficits related to the localisation of synaptophysin positive vesicles.

In organotypic slices, technical limitations precluded the analysis of vesicle transport. To overcome this, we reverted to studying vesicle transport in dissociated cultures. However, instead of mixed cultures, we organised cells into discreet cell body layers. We configured each cell body layer with either pure DG granule cells or pure CA3 pyramidal neurons. This allowed us to reconstruct an artificial MF-CA3 pathway on a single glass cover slip. By transducing only granule cells with lenti-syp-GFP it was then possible to monitor vesicle trafficking specifically in mossy fibers. This simple cell culture method permits the study of physiologically relevant synaptic connections in a culture environment that is both optically and experimentally accessible.

6.3 Summary and conclusions.

Based on these data, it is possible to conclude that motile particle transport does not detectably alter in response to an increase in network activity; at least not in dissociated cultures treated with bicuculline. There are several detectable changes occurring at the synapse, with the modification of vesicle cluster size and turnover; however, these changes do not correlate with changes in vesicle transport. This suggests that vesicle transport is independent of changes occurring at the synapse and that vesicle transport maintains a consistent rate even during periods of increased activity. However, because we did not successfully record vesicle transport in organotypic slices, we cannot conclude vesicle transport in mossy fibers remains unchanged following increased activity. However, with the development of a new method for culturing specific cell types in close proximity, it is now possible to investigate this using a commonly available widefield fluorescence microscope. This new system emulates hippocampal connectivity, but in the setting of a dissociated culture, which is likely to be very useful for studying many other experimental paradigms, not only vesicle transport.

6.4 Limitations.

It is important to acknowledge a number of limitations inherent within this study.

1. Length of live imaging.

A common problem when imaging endogenously expressed fluorescent probes is fluorescent fading, which in our experiments was a significant problem. Due to the rapid fading of the syp-GFP signal we were forced to reduce our imaging times drastically. We found that continuous fluorescence exposure, greater than 60s, resulted in a loss of GFP signal, which forced us into performing shorter experimental protocols. Ideally, continuous live imaging would be used to observe all vesicle dynamics over time. However, this was not possible with syp-GFP. Instead, we were forced into imaging at shorter and more infrequent time intervals.

2. Continuously recording electrical activity.

Unfortunately, it was not possible to repeatedly record electrical activity from our imaging setup. This was due to the fact that we used a closed imaging chamber to record vesicle trafficking data. The closed imaging chamber was useful for maintaining cell survival and temperature, whilst allowing us to image the same axon over 10 hours. However, the chamber was not accessible to electrodes or micromanipulation. As a compromise, we opted to estimate neuronal activity through the use of calcium sensitive dyes. Unfortunately, these dyes too have their limitations and are only suitable for short sampling experiments. The toxic nature of the dyes prevents the long-term sampling of neuronal activity. Novel endogenously expressed calcium probes may be useful in alleviating this problem.

3. Assigning direction to vesicle trafficking experiments.

In the dissociated culture cell arrangements are highly erratic and there can be tens of thousands of axonal connections criss-crossing the surface of the cover slip. Using syp-GFP as a fluorescent probe made it very difficult to identify the origin of axons that were suitable for live imaging. Therefore, in many experiments we could simply not assign direction to vesicle movement. Although this is a significant problem, it is greatly reduced by our separate culture method described in chapter 5, due to the fact that only one cell body layer is labelled with lenti-syp-GFP, thus, it becomes much easier to assign direction to the transport of vesicles.

4. Live imaging in the hippocampal organotypic slice culture.

A significant limitation of this study was our inability to reliably image vesicle transport in organotypic slices; because of this, we only achieved a handful of imaging experiments that showed clear vesicle transport (example: supplementary video 3). Following exhaustive attempts to gather high quality videos, we decided instead to use immunocytochemistry and confocal microscopy to the study the distribution of vesicle clusters. However, we did develop the separate cell culture method (described in chapter 5) as an answer to the poor image quality observed in organotypic slices. This method overcame the issue of poor imaging quality and allowed us to continue to study the transport of vesicles specifically in mossy fibers.

5. Measuring the proportion of large vesicle clusters in organotypic slice culture.

One limitation observed in this study was our ability to quantify the number of large syp-GFP positive vesicle clusters observed in organotypic slices. Despite every effort to produce slices that were consistently transduced with lentivirus, we were unable to control the precise number of infected cells. This made measuring the total number of large vesicle clusters irrelevant, as the amount of transduced cells

would vary between slices, so we settled instead on measuring the proportion of large vesicle clusters. We based this idea on preliminary measurements made by our collaborators (Kumlesh K. Dev; Trinity College Dublin; unpublished observations). Unfortunately, a change in the proportion of large vesicle clusters only gives an indication about what is happening to the vesicle population; ultra high resolution microscopy is still required to confirm the fate of vesicle clusters, as a result of epileptiform activity.

6.5 Future studies

From our experience we suggest a number of directions for future research:

Due to the labour intensive nature of viral production and viral injection, experimenters wishing to investigate vesicle transport using a fluorescent reporter, may benefit from investing into the development or purchase of a transgenic mouse line. Specifically the Thy1 reporter line, described by (De Paola et al., 2003), which can be used to endogenously express synaptophysin-GFP in a sparse distribution of cells.

Those wishing to study the transport of synaptophysin positive vesicles in future experiments, are directed to: (Ratnayaka et al., 2011), who describe the use of a novel synaptophysin-GFP construct that shows minimal fluorescence fading. This construct can also be photo-switched to emit light at a different wavelength, which permits the study of individual vesicles. This construct should permit the continuous image capture of vesicle dynamics.

After developing the separate cell culture method described in chapter 5, we showed that the gap primarily contained axons. These axons were grown in a region that was free from: cell bodies, dendrites and glia. To test whether external influences, such as glial and synaptic contacts affect vesicle transport, it may be possible to compare vesicle trafficking in the gap to vesicle trafficking in the cell body layers. This would be an interesting future experiment made possible by the

development of this particular culture method. Another interesting future use for the separate cell culture system would be to investigate how different cell body layers interact. One might imagine replacing each cell body layer with any combination of the: CA3, CA1 or DG cell populations and assessing axon growth, synaptic connectivity and network activity. This would provide a novel assay for investigating network formation. Using this method, it would also be interesting to image vesicle transport in different cell types, because different cell types possess varied morphologies and connectivity patterns, it would be interesting to see if they possess different vesicle transport dynamics.

Specific Acknowledgements

References:

Abuhatzira L, Makedonski K, Kaufman Y, Razin A, Shemer R (2007) MeCP2 deficiency in the brain decreases BDNF levels by REST/CoREST-mediated repression and increases TRKB production. Epigenetics : official journal of the DNA Methylation Society 2:214-222.

Acsady L, Kamondi A, Sik A, Freund T, Buzsaki G (1998) GABAergic cells are the major postsynaptic targets of mossy fibers in the rat hippocampus. The Journal of neuroscience : the official journal of the Society for Neuroscience 18:3386-3403.

Ahmari SE, Buchanan J, Smith SJ (2000) Assembly of presynaptic active zones from cytoplasmic transport packets. Nature neuroscience 3:445-451.

Akhmanova A, Hoogenraad CC (2005) Microtubule plus-end-tracking proteins: mechanisms and functions. Current opinion in cell biology 17:47-54.

Al-Bassam S, Xu M, Wandless TJ, Arnold DB (2012) Differential trafficking of transport vesicles contributes to the localization of dendritic proteins. Cell reports 2:89-100.

Ally S, Jolly AL, Gelfand VI (2008) Motor-cargo release: CaMKII as a traffic cop. Nature cell biology 10:3-5.

Almeida RD, Manadas BJ, Melo CV, Gomes JR, Mendes CS, Graos MM, Carvalho RF, Carvalho AP, Duarte CB (2005) Neuroprotection by BDNF against glutamate-induced apoptotic cell death is mediated by ERK and PI3-kinase pathways. Cell death and differentiation 12:1329-1343.

Amado RG, Chen IS (1999) Lentiviral vectors--the promise of gene therapy within reach? Science 285:674-676.

Ambrosini A, Bresciani L, Fracchia S, Brunello N, Racagni G (1995) Metabotropic glutamate receptors negatively coupled to adenylate cyclase inhibit N-methyl-D-aspartate receptor activity and prevent neurotoxicity in mesencephalic neurons in vitro. Molecular pharmacology 47:1057-1064.

Amir RE, Van den Veyver IB, Wan M, Tran CQ, Francke U, Zoghbi HY (1999) Rett syndrome is caused by mutations in X-linked MECP2, encoding methyl-CpG-binding protein 2. Nature genetics 23:185-188.

Armstrong D, Dunn JK, Antalffy B, Trivedi R (1995) Selective dendritic alterations in the cortex of Rett syndrome. Journal of neuropathology and experimental neurology 54:195-201.

Armstrong DD, Dunn K, Antalffy B (1998) Decreased dendritic branching in frontal, motor and limbic cortex in Rett syndrome compared with trisomy 21. Journal of neuropathology and experimental neurology 57:1013-1017.

Armstrong R, Toews AD, Morell P (1987) Rapid axonal transport in focally demyelinated sciatic nerve. The Journal of neuroscience : the official journal of the Society for Neuroscience 7:4044-4053.

Arnold FJ, Hofmann F, Bengtson CP, Wittmann M, Vanhoutte P, Bading H (2005) Microelectrode array recordings of cultured hippocampal networks reveal a simple model for transcription and protein synthesis-dependent plasticity. The Journal of physiology 564:3-19.

Arthur CP, Stowell MH (2007) Structure of synaptophysin: a hexameric MARVEL-domain channel protein. Structure 15:707-714.

Asaka Y, Jugloff DG, Zhang L, Eubanks JH, Fitzsimonds RM (2006) Hippocampal synaptic plasticity is impaired in the Mecp2-null mouse model of Rett syndrome. Neurobiology of disease 21:217-227.

Augustine GJ, Kasai H (2007) Bernard Katz, quantal transmitter release and the foundations of presynaptic physiology. The Journal of physiology 578:623-625.

Baas PW, Deitch JS, Black MM, Banker GA (1988) Polarity orientation of microtubules in hippocampal neurons: uniformity in the axon and nonuniformity in the dendrite. Proceedings of the National Academy of Sciences of the United States of America 85:8335-8339.

Babb TL, Kupfer WR, Pretorius JK, Crandall PH, Levesque MF (1991) Synaptic reorganization by mossy fibers in human epileptic fascia dentata. Neuroscience 42:351-363.

Baranes D, Lopez-Garcia JC, Chen M, Bailey CH, Kandel ER (1996) Reconstitution of the hippocampal mossy fiber and associational-commissural pathways in a novel dissociated cell culture system. Proceedings of the National Academy of Sciences of the United States of America 93:4706-4711.

Bartos M, Vida I, Jonas P (2007) Synaptic mechanisms of synchronized gamma oscillations in inhibitory interneuron networks. Nature reviews Neuroscience 8:45-56.

Basarsky TA, Parpura V, Haydon PG (1994) Hippocampal synaptogenesis in cell culture: developmental time course of synapse formation, calcium influx, and synaptic protein distribution. The Journal of neuroscience : the official journal of the Society for Neuroscience 14:6402-6411.

Bats C, Groc L, Choquet D (2007) The interaction between Stargazin and PSD-95 regulates AMPA receptor surface trafficking. Neuron 53:719-734.

Becherer U, Rettig J (2006) Vesicle pools, docking, priming, and release. Cell and tissue research 326:393-407.

Bence M, Levelt CN (2005) Structural plasticity in the developing visual system. Progress in brain research 147:125-139.

Benes FM, Berretta S (2001) GABAergic interneurons: implications for understanding schizophrenia and bipolar disorder. Neuropsychopharmacology : official publication of the American College of Neuropsychopharmacology 25:1-27.

Bernhardt R, Matus A (1984) Light and electron microscopic studies of the distribution of microtubule-associated protein 2 in rat brain: a difference between dendritic and axonal cytoskeletons. The Journal of comparative neurology 226:203-221.

Betz WJ, Wu LG (1995) Synaptic transmission. Kinetics of synaptic-vesicle recycling. Current biology : CB 5:1098-1101.

Bischofberger J, Engel D, Frotscher M, Jonas P (2006) Timing and efficacy of transmitter release at mossy fiber synapses in the hippocampal network. Pflugers Archiv : European journal of physiology 453:361-372.

Bodian D (1970) An electron microscopic characterization of classes of synaptic vesicles by means of controlled aldehyde fixation. The Journal of cell biology 44:115-124.

Bolte S, Cordelieres FP (2006) A guided tour into subcellular colocalization analysis in light microscopy. Journal of microscopy 224:213-232.

Bonanomi D, Rusconi L, Colombo CA, Benfenati F, Valtorta F (2007) Synaptophysin I selectively specifies the exocytic pathway of synaptobrevin 2/VAMP2. The Biochemical journal 404:525-534.

Borisy GG, Taylor EW (1967) The mechanism of action of colchicine. Binding of colchincine-3H to cellular protein. The Journal of cell biology 34:525-533.

Bowery NG (1993) GABAB receptor pharmacology. Annual review of pharmacology and toxicology 33:109-147.

Brewer GJ, Torricelli JR (2007) Isolation and culture of adult neurons and neurospheres. Nature protocols 2:1490-1498.

Brittis PA, Lu Q, Flanagan JG (2002) Axonal protein synthesis provides a mechanism for localized regulation at an intermediate target. Cell 110:223-235.

Brose N, Petrenko AG, Sudhof TC, Jahn R (1992) Synaptotagmin: a calcium sensor on the synaptic vesicle surface. Science 256:1021-1025.

Bulinski JC, Gundersen GG (1991) Stabilization of post-translational modification of microtubules during cellular morphogenesis. BioEssays :

news and reviews in molecular, cellular and developmental biology 13:285-293.

Burns ME, Augustine GJ (1995) Synaptic structure and function: dynamic organization yields architectural precision. Cell 83:187-194.

Bury LA, Sabo SL (2011) Coordinated trafficking of synaptic vesicle and active zone proteins prior to synapse formation. Neural development 6:24.

Calfa G, Hablitz JJ, Pozzo-Miller L (2011) Network hyperexcitability in hippocampal slices from Mecp2 mutant mice revealed by voltage-sensitive dye imaging. Journal of neurophysiology 105:1768-1784.

Cavazos JE, Golarai G, Sutula TP (1991) Mossy fiber synaptic reorganization induced by kindling: time course of development, progression, and permanence. The Journal of neuroscience : the official journal of the Society for Neuroscience 11:2795-2803.

Chahrour M, Zoghbi HY (2007) The story of Rett syndrome: from clinic to neurobiology. Neuron 56:422-437.

Chalfie M, Tu Y, Euskirchen G, Ward WW, Prasher DC (1994) Green fluorescent protein as a marker for gene expression. Science 263:802-805.

Chapleau CA, Boggio EM, Calfa G, Percy AK, Giustetto M, Pozzo-Miller L (2012) Hippocampal CA1 Pyramidal Neurons of Mecp2 Mutant Mice Show a Dendritic Spine Phenotype Only in the Presymptomatic Stage. Neural plasticity 2012:976164.

Chi P, Greengard P, Ryan TA (2001) Synapsin dispersion and reclustering during synaptic activity. Nature neuroscience 4:1187-1193.

Chicurel ME, Harris KM (1992) Three-dimensional analysis of the structure and composition of CA3 branched dendritic spines and their synaptic relationships with mossy fiber boutons in the rat hippocampus. The Journal of comparative neurology 325:169-182.

Chu Y, Morfini GA, Langhamer LB, He Y, Brady ST, Kordower JH (2012) Alterations in axonal transport motor proteins in sporadic and experimental Parkinson's disease. Brain : a journal of neurology 135:2058-2073.

Claiborne BJ, Amaral DG, Cowan WM (1986) A light and electron microscopic analysis of the mossy fibers of the rat dentate gyrus. The Journal of comparative neurology 246:435-458.

Clayton EL, Evans GJ, Cousin MA (2008) Bulk synaptic vesicle endocytosis is rapidly triggered during strong stimulation. The Journal of neuroscience : the official journal of the Society for Neuroscience 28:6627-6632.

Cole KS, Curtis HJ (1939) Electric Impedance of the Squid Giant Axon during Activity. The Journal of general physiology 22:649-670.

Coltman BW, Earley EM, Shahar A, Dudek FE, Ide CF (1995) Factors influencing mossy fiber collateral sprouting in organotypic slice cultures of neonatal mouse hippocampus. The Journal of comparative neurology 362:209-222.

Conde C, Caceres A (2009) Microtubule assembly, organization and dynamics in axons and dendrites. Nature reviews Neuroscience 10:319-332.

Conn PJ, Pin JP (1997) Pharmacology and functions of metabotropic glutamate receptors. Annual review of pharmacology and toxicology 37:205-237.

Corbeel L, Freson K (2008) Rab proteins and Rab-associated proteins: major actors in the mechanism of protein-trafficking disorders. European journal of pediatrics 167:723-729.

Coulter DA (2000) Mossy fiber zinc and temporal lobe epilepsy: pathological association with altered "epileptic" gamma-aminobutyric acid A receptors in dentate granule cells. Epilepsia 41 Suppl 6:S96-99.

Curtis DR, Watkins JC (1960) The excitation and depression of spinal neurones by structurally related amino acids. Journal of neurochemistry 6:117-141.

Danzer SC, McNamara JO (2004) Localization of brain-derived neurotrophic factor to distinct terminals of mossy fiber axons implies regulation of both excitation and feedforward inhibition of CA3 pyramidal cells. The Journal of neuroscience : the official journal of the Society for Neuroscience 24:11346-11355.

De Gois S, Schafer MK, Defamie N, Chen C, Ricci A, Weihe E, Varoqui H, Erickson JD (2005) Homeostatic scaling of vesicular glutamate and GABA transporter expression in rat neocortical circuits. The Journal of neuroscience : the official journal of the Society for Neuroscience 25:7121-7133.

De Paola V, Arber S, Caroni P (2003) AMPA receptors regulate dynamic equilibrium of presynaptic terminals in mature hippocampal networks. Nature neuroscience 6:491-500.

De Paola V, Holtmaat A, Knott G, Song S, Wilbrecht L, Caroni P, Svoboda K (2006) Cell type-specific structural plasticity of axonal branches and boutons in the adult neocortex. Neuron 49:861-875.

de Wit J, Toonen RF, Verhaagen J, Verhage M (2006) Vesicular trafficking of semaphorin 3A is activity-dependent and differs between axons and dendrites. Traffic 7:1060-1077.

Del Castillo J, Katz B (1954) Quantal components of the end-plate potential. The Journal of physiology 124:560-573.

Del Castillo J, De Mello WC, Morales T (1964) Inhibitory action of gamma-aminobutyric acid (GABA) on Ascaris muscle. Experientia 20:141-143.

Dhingra NK, Reddy R, Govindaiah, Hemavathy U, Raju TR, Ramamohan Y (2001) Synaptic development in semi-dissociated cultures of rat retina. International journal of developmental neuroscience : the official journal of the International Society for Developmental Neuroscience 19:533-540.

Dingledine R, Borges K, Bowie D, Traynelis SF (1999) The glutamate receptor ion channels. Pharmacological reviews 51:7-61.

Dittman JS, Kaplan JM (2006) Factors regulating the abundance and localization of synaptobrevin in the plasma membrane. Proceedings of the National Academy of Sciences of the United States of America 103:11399-11404.

Dumas D, Grossin L, Cauchois G, Gentils M, Santus R, Stoltz JF (2003) Comparison of wide-field/deconvolution and confocal microscopy in bioengineering. Interest of multi-photon microscopy in the study of articular cartilage. Biorheology 40:253-259.

Duncan JE, Goldstein LS (2006) The genetics of axonal transport and axonal transport disorders. PLoS genetics 2:e124.

Dunn S, Morrison EE, Liverpool TB, Molina-Paris C, Cross RA, Alonso MC, Peckham M (2008) Differential trafficking of Kif5c on tyrosinated and detyrosinated microtubules in live cells. Journal of cell science 121:1085-1095.

Ehrengruber MU, Hennou S, Bueler H, Naim HY, Deglon N, Lundstrom K (2001) Gene transfer into neurons from hippocampal slices: comparison of recombinant Semliki Forest Virus, adenovirus, adeno-associated virus, lentivirus, and measles virus. Molecular and cellular neurosciences 17:855-871.

Eimerl S, Schramm M (1991) Acute glutamate toxicity in cultured cerebellar granule cells: agonist potency, effects of pH, Zn2+ and the potentiation by serum albumin. Brain research 560:282-290.

Eliasson L, Renstrom E, Ding WG, Proks P, Rorsman P (1997) Rapid ATP-dependent priming of secretory granules precedes Ca(2+)-induced exocytosis in mouse pancreatic B-cells. The Journal of physiology 503 (Pt 2):399-412.

Engert F, Bonhoeffer T (1999) Dendritic spine changes associated with hippocampal long-term synaptic plasticity. Nature 399:66-70.

Faden AI, O'Leary DM, Fan L, Bao W, Mullins PG, Movsesyan VA (2001) Selective blockade of the mGluR1 receptor reduces traumatic neuronal injury in vitro and improvesoOutcome after brain trauma. Experimental neurology 167:435-444.

Fatt P, Katz B (1952) Spontaneous subthreshold activity at motor nerve endings. The Journal of physiology 117:109-128.

Fernandez-Alfonso T, Ryan TA (2008) A heterogeneous "resting" pool of synaptic vesicles that is dynamically interchanged across boutons in mammalian CNS synapses. Brain cell biology 36:87-100.

Fitch MT, Doller C, Combs CK, Landreth GE, Silver J (1999) Cellular and molecular mechanisms of glial scarring and progressive cavitation: in vivo and in vitro analysis of inflammation-induced secondary injury after CNS trauma. The Journal of neuroscience : the official journal of the Society for Neuroscience 19:8182-8198.

Fletcher TL, Cameron P, De Camilli P, Banker G (1991) The distribution of synapsin I and synaptophysin in hippocampal neurons developing in culture. The Journal of neuroscience : the official journal of the Society for Neuroscience 11:1617-1626.

Fotin A, Kirchhausen T, Grigorieff N, Harrison SC, Walz T, Cheng Y (2006) Structure determination of clathrin coats to subnanometer resolution by single particle cryo-electron microscopy. Journal of structural biology 156:453-460.

Fotin A, Cheng Y, Sliz P, Grigorieff N, Harrison SC, Kirchhausen T, Walz T (2004) Molecular model for a complete clathrin lattice from electron cryomicroscopy. Nature 432:573-579.

Freund TF, Buzsaki G (1996) Interneurons of the hippocampus. Hippocampus 6:347-470.

Frotscher M (1985) Mossy fibres form synapses with identified pyramidal basket cells in the CA3 region of the guinea-pig hippocampus: a combined Golgi-electron microscope study. Journal of neurocytology 14:245-259.

Frotscher M, Jonas P, Sloviter RS (2006) Synapses formed by normal and abnormal hippocampal mossy fibers. Cell and tissue research 326:361-367.

Galimberti I, Gogolla N, Alberi S, Santos AF, Muller D, Caroni P (2006) Long-term rearrangements of hippocampal mossy fiber terminal connectivity in the adult regulated by experience. Neuron 50:749-763.

Galli T, Haucke V (2004) Cycling of synaptic vesicles: how far? How fast! Science's STKE : signal transduction knowledge environment 2004:re19.

Gan J, Greenwood SM, Cobb SR, Bushell TJ (2011) Indirect modulation of neuronal excitability and synaptic transmission in the hippocampus by activation of proteinase-activated receptor-2. British journal of pharmacology 163:984-994.

Gandhi SP, Stevens CF (2003) Three modes of synaptic vesicular recycling revealed by single-vesicle imaging. Nature 423:607-613.

Glover CP, Bienemann AS, Heywood DJ, Cosgrave AS, Uney JB (2002) Adenoviral-mediated, high-level, cell-specific transgene expression: a SYN1-WPRE cassette mediates increased transgene expression with no loss of neuron specificity. Molecular therapy : the journal of the American Society of Gene Therapy 5:509-516.

Gogolla N, Galimberti I, Caroni P (2007) Structural plasticity of axon terminals in the adult. Current opinion in neurobiology 17:516-524.

Granseth B, Odermatt B, Royle SJ, Lagnado L (2006) Clathrin-mediated endocytosis is the dominant mechanism of vesicle retrieval at hippocampal synapses. Neuron 51:773-786.

Grutzendler J, Kasthuri N, Gan WB (2002) Long-term dendritic spine stability in the adult cortex. Nature 420:812-816.

Guillaud L, Setou M, Hirokawa N (2003) KIF17 dynamics and regulation of NR2B trafficking in hippocampal neurons. The Journal of neuroscience : the official journal of the Society for Neuroscience 23:131-140.

Gunawardena S, Her LS, Brusch RG, Laymon RA, Niesman IR, Gordesky-Gold B, Sintasath L, Bonini NM, Goldstein LS (2003) Disruption of axonal transport by loss of huntingtin or expression of pathogenic polyQ proteins in Drosophila. Neuron 40:25-40.

Guy J, Cheval H, Selfridge J, Bird A (2011) The role of MeCP2 in the brain. Annual review of cell and developmental biology 27:631-652.

Guy J, Hendrich B, Holmes M, Martin JE, Bird A (2001) A mouse Mecp2-null mutation causes neurological symptoms that mimic Rett syndrome. Nature genetics 27:322-326.

Guy J, Gan J, Selfridge J, Cobb S, Bird A (2007) Reversal of neurological defects in a mouse model of Rett syndrome. Science 315:1143-1147.

Hales CM, Zeller-Townson R, Newman JP, Shoemaker JT, Killian NJ, Potter SM (2012) Stimulus-evoked high frequency oscillations are present in neuronal networks on microelectrode arrays. Frontiers in neural circuits 6:29.

Han ZS, Buhl EH, Lorinczi Z, Somogyi P (1993) A high degree of spatial selectivity in the axonal and dendritic domains of physiologically identified local-circuit neurons in the dentate gyrus of the rat hippocampus. The European journal of neuroscience 5:395-410.

Haucke V, Neher E, Sigrist SJ (2011) Protein scaffolds in the coupling of synaptic exocytosis and endocytosis. Nature reviews Neuroscience 12:127-138.

Hendricks AG, Perlson E, Ross JL, Schroeder HW, 3rd, Tokito M, Holzbaur EL (2010) Motor coordination via a tug-of-war mechanism drives bidirectional vesicle transport. Current biology : CB 20:697-702.

Henkel AW, Lubke J, Betz WJ (1996) FM1-43 dye ultrastructural localization in and release from frog motor nerve terminals. Proceedings of the National Academy of Sciences of the United States of America 93:1918-1923.

Henze DA, Wittner L, Buzsaki G (2002a) Single granule cells reliably discharge targets in the hippocampal CA3 network in vivo. Nature neuroscience 5:790-795.

Henze DA, McMahon DB, Harris KM, Barrionuevo G (2002b) Giant miniature EPSCs at the hippocampal mossy fiber to CA3 pyramidal cell synapse are monoquantal. Journal of neurophysiology 87:15-29.

Hertz L, Dringen R, Schousboe A, Robinson SR (1999) Astrocytes: glutamate producers for neurons. Journal of neuroscience research 57:417-428.

Herzog E, Takamori S, Jahn R, Brose N, Wojcik SM (2006) Synaptic and vesicular co-localization of the glutamate transporters VGLUT1 and VGLUT2 in the mouse hippocampus. Journal of neurochemistry 99:1011-1018.

Herzog E, Nadrigny F, Silm K, Biesemann C, Helling I, Bersot T, Steffens H, Schwartzmann R, Nagerl UV, El Mestikawy S, Rhee J, Kirchhoff F, Brose N (2011) In vivo imaging of intersynaptic vesicle exchange using VGLUT1 Venus knock-in mice. The Journal of neuroscience : the official journal of the Society for Neuroscience 31:15544-15559.

Heuser JE, Reese TS (1973) Evidence for recycling of synaptic vesicle membrane during transmitter release at the frog neuromuscular junction. The Journal of cell biology 57:315-344.

Heuser JE, Reese TS, Dennis MJ, Jan Y, Jan L, Evans L (1979) Synaptic vesicle exocytosis captured by quick freezing and correlated with quantal transmitter release. The Journal of cell biology 81:275-300.

Hirokawa N (1998) Kinesin and dynein superfamily proteins and the mechanism of organelle transport. Science 279:519-526.

Hirokawa N, Noda Y (2008) Intracellular transport and kinesin superfamily proteins, KIFs: structure, function, and dynamics. Physiological reviews 88:1089-1118.

Hirokawa N, Noda Y, Tanaka Y, Niwa S (2009) Kinesin superfamily motor proteins and intracellular transport. Nature reviews Molecular cell biology 10:682-696.

Hodgkin AL, Katz B (1949) The effect of sodium ions on the electrical activity of giant axon of the squid. The Journal of physiology 108:37-77.

Hodgkin AL, Huxley AF (1952) A quantitative description of membrane current and its application to conduction and excitation in nerve. The Journal of physiology 117:500-544.

Hokfelt T, Broberger C, Xu ZQ, Sergeyev V, Ubink R, Diez M (2000) Neuropeptides--an overview. Neuropharmacology 39:1337-1356.

Holmes GL (2009) The long-term effects of neonatal seizures. Clinics in perinatology 36:901-914, vii-viii.

Holmes GL, Sarkisian M, Ben-Ari Y, Chevassus-Au-Louis N (1999) Mossy fiber sprouting after recurrent seizures during early development in rats. The Journal of comparative neurology 404:537-553.

Holtmaat A, Svoboda K (2009) Experience-dependent structural synaptic plasticity in the mammalian brain. Nature reviews Neuroscience 10:647-658.

Holtmaat AJ, Trachtenberg JT, Wilbrecht L, Shepherd GM, Zhang X, Knott GW, Svoboda K (2005) Transient and persistent dendritic spines in the neocortex in vivo. Neuron 45:279-291.

Holzbaur EL (2004) Motor neurons rely on motor proteins. Trends in cell biology 14:233-240.

Horton AC, Ehlers MD (2003) Neuronal polarity and trafficking. Neuron 40:277-295.

Ikegami K, Setou M (2010) Unique post-translational modifications in specialized microtubule architecture. Cell structure and function 35:15-22.

Ikegami K, Heier RL, Taruishi M, Takagi H, Mukai M, Shimma S, Taira S, Hatanaka K, Morone N, Yao I, Campbell PK, Yuasa S, Janke C, Macgregor GR, Setou M (2007) Loss of alpha-tubulin polyglutamylation in ROSA22 mice is associated with abnormal targeting of KIF1A and modulated synaptic function. Proceedings of the National Academy of Sciences of the United States of America 104:3213-3218.

Ivenshitz M, Segal M (2010) Neuronal density determines network connectivity and spontaneous activity in cultured hippocampus. Journal of neurophysiology 104:1052-1060.

Janke C, Bulinski JC (2011) Post-translational regulation of the microtubule cytoskeleton: mechanisms and functions. Nature reviews Molecular cell biology 12:773-786.

Jessell TM, Kandel ER (1993) Synaptic transmission: a bidirectional and self-modifiable form of cell-cell communication. Cell 72 Suppl:1-30.

Jian L, Nagarajan L, de Klerk N, Ravine D, Christodoulou J, Leonard H (2007) Seizures in Rett syndrome: an overview from a one-year calendar study. European journal of paediatric neurology : EJPN : official journal of the European Paediatric Neurology Society 11:310-317.

Johansson BB, Belichenko PV (2002) Neuronal plasticity and dendritic spines: effect of environmental enrichment on intact and postischemic rat brain. Journal of cerebral blood flow and metabolism : official journal of the International Society of Cerebral Blood Flow and Metabolism 22:89-96.

Johnston PA, Jahn R, Sudhof TC (1989) Transmembrane topography and evolutionary conservation of synaptophysin. The Journal of biological chemistry 264:1268-1273.

Jordan BA, Fernholz BD, Boussac M, Xu C, Grigorean G, Ziff EB, Neubert TA (2004) Identification and verification of novel rodent postsynaptic density proteins. Molecular & cellular proteomics : MCP 3:857-871.

Kapitein LC, Schlager MA, Kuijpers M, Wulf PS, van Spronsen M, MacKintosh FC, Hoogenraad CC (2010) Mixed microtubules steer dynein-driven cargo transport into dendrites. Current biology : CB 20:290-299.

Karmarkar UR, Buonomano DV (2006) Different forms of homeostatic plasticity are engaged with distinct temporal profiles. The European journal of neuroscience 23:1575-1584.

Kasai H, Matsuzaki M, Noguchi J, Yasumatsu N, Nakahara H (2003) Structure-stability-function relationships of dendritic spines. Trends in neurosciences 26:360-368.

Kavalali ET, Klingauf J, Tsien RW (1999) Activity-dependent regulation of synaptic clustering in a hippocampal culture system. Proceedings of the National Academy of Sciences of the United States of America 96:12893-12900.

Kim E, Sheng M (2004) PDZ domain proteins of synapses. Nature reviews Neuroscience 5:771-781.

Kleinfeld D, Kahler KH, Hockberger PE (1988) Controlled outgrowth of dissociated neurons on patterned substrates. The Journal of neuroscience : the official journal of the Society for Neuroscience 8:4098-4120.

Kline DD, Ogier M, Kunze DL, Katz DM (2010) Exogenous brain-derived neurotrophic factor rescues synaptic dysfunction in Mecp2-null mice. The Journal of neuroscience : the official journal of the Society for Neuroscience 30:5303-5310.

Kondo S, Okabe S (2011) Turnover of synapse and dynamic nature of synaptic molecules in vitro and in vivo. Acta histochemica et cytochemica 44:9-15.

Kopelman R, Tan W (1993) Near-field optics: imaging single molecules. Science 262:1382-1384.

Kosik KS, Finch EA (1987) MAP2 and tau segregate into dendritic and axonal domains after the elaboration of morphologically distinct neurites: an immunocytochemical study of cultured rat cerebrum. The Journal of neuroscience : the official journal of the Society for Neuroscience 7:3142-3153.

Krueger SR, Kolar A, Fitzsimonds RM (2003) The presynaptic release apparatus is functional in the absence of dendritic contact and highly mobile within isolated axons. Neuron 40:945-957.

Kural C, Kim H, Syed S, Goshima G, Gelfand VI, Selvin PR (2005) Kinesin and dynein move a peroxisome in vivo: a tug-of-war or coordinated movement? Science 308:1469-1472.

Kushner SA, Elgersma Y, Murphy GG, Jaarsma D, van Woerden GM, Hojjati MR, Cui Y, LeBoutillier JC, Marrone DF, Choi ES, De Zeeuw CI, Petit TL, Pozzo-Miller L, Silva AJ (2005) Modulation of presynaptic plasticity and learning by the H-ras/extracellular signal-regulated kinase/synapsin I signaling pathway. The Journal of neuroscience : the official journal of the Society for Neuroscience 25:9721-9734.

Kwon HB, Castillo PE (2008) Long-term potentiation selectively expressed by NMDA receptors at hippocampal mossy fiber synapses. Neuron 57:108-120.

Kwon SE, Chapman ER (2011) Synaptophysin regulates the kinetics of synaptic vesicle endocytosis in central neurons. Neuron 70:847-854.

Lawrence JJ, McBain CJ (2003) Interneuron diversity series: containing the detonation--feedforward inhibition in the CA3 hippocampus. Trends in neurosciences 26:631-640.

Le Roy C, Wrana JL (2005) Clathrin- and non-clathrin-mediated endocytic regulation of cell signalling. Nature reviews Molecular cell biology 6:112-126.

Lee SH, Peng IF, Ng YG, Yanagisawa M, Bamji SX, Elia LP, Balsamo J, Lilien J, Anastasiadis PZ, Ullian EM, Reichardt LF (2008) Synapses are regulated by the cytoplasmic tyrosine kinase Fer in a pathway mediated by p120catenin, Fer, SHP-2, and beta-catenin. The Journal of cell biology 183:893-908.

Leenders AG, Lopes da Silva FH, Ghijsen WE, Verhage M (2001) Rab3a is involved in transport of synaptic vesicles to the active zone in mouse brain nerve terminals. Molecular biology of the cell 12:3095-3102.

Li L, Chin LS, Shupliakov O, Brodin L, Sihra TS, Hvalby O, Jensen V, Zheng D, McNamara JO, Greengard P, et al. (1995) Impairment of synaptic vesicle clustering and of synaptic transmission, and increased seizure propensity, in synapsin I-deficient mice. Proceedings of the National Academy of Sciences of the United States of America 92:9235-9239.

Li X, Zhou W, Zeng S, Liu M, Luo Q (2007) Long-term recording on multi-electrode array reveals degraded inhibitory connection in neuronal network development. Biosensors & bioelectronics 22:1538-1543.

Liang CC, Park AY, Guan JL (2007) In vitro scratch assay: a convenient and inexpensive method for analysis of cell migration in vitro. Nature protocols 2:329-333.

Lisman JE, Raghavachari S, Tsien RW (2007) The sequence of events that underlie quantal transmission at central glutamatergic synapses. Nature reviews Neuroscience 8:597-609.

Littleton JT, Bellen HJ (1995) Presynaptic proteins involved in exocytosis in Drosophila melanogaster: a genetic analysis. Invertebrate neuroscience : IN 1:3-13.

Lodge D (2009) The history of the pharmacology and cloning of ionotropic glutamate receptors and the development of idiosyncratic nomenclature. Neuropharmacology 56:6-21.

Lynd-Balta E, Pilcher WH, Joseph SA (2004) AMPA receptor alterations precede mossy fiber sprouting in young children with temporal lobe epilepsy. Neuroscience 126:105-114.

Ma H, Cai Q, Lu W, Sheng ZH, Mochida S (2009) KIF5B motor adaptor syntabulin maintains synaptic transmission in sympathetic neurons. The Journal of neuroscience : the official journal of the Society for Neuroscience 29:13019-13029.

MacGillavry HD, Kerr JM, Blanpied TA (2011) Lateral organization of the postsynaptic density. Molecular and cellular neurosciences 48:321-331.

Macosko JC, Newbern JM, Rockford J, Chisena EN, Brown CM, Holzwarth GM, Milligan CE (2008) Fewer active motors per vesicle may explain slowed vesicle transport in chick motoneurons after three days in vitro. Brain research 1211:6-12.

Majewska A, Tashiro A, Yuste R (2000) Regulation of spine calcium dynamics by rapid spine motility. The Journal of neuroscience : the official journal of the Society for Neuroscience 20:8262-8268.

Manev H, Favaron M, Guidotti A, Costa E (1989) Delayed increase of Ca2+ influx elicited by glutamate: role in neuronal death. Molecular pharmacology 36:106-112.

Markram H, Toledo-Rodriguez M, Wang Y, Gupta A, Silberberg G, Wu C (2004) Interneurons of the neocortical inhibitory system. Nature reviews Neuroscience 5:793-807.

Marsh M, McMahon HT (1999) The structural era of endocytosis. Science 285:215-220.

Mathews GC, Diamond JS (2003) Neuronal glutamate uptake Contributes to GABA synthesis and inhibitory synaptic strength. The Journal of neuroscience : the official journal of the Society for Neuroscience 23:2040-2048.

Matsuzaki F, Shirane M, Matsumoto M, Nakayama KI (2011) Protrudin serves as an adaptor molecule that connects KIF5 and its cargoes in vesicular transport during process formation. Molecular biology of the cell 22:4602-4620.

Maycox PR, Deckwerth T, Hell JW, Jahn R (1988) Glutamate uptake by brain synaptic vesicles. Energy dependence of transport and functional reconstitution in proteoliposomes. The Journal of biological chemistry 263:15423-15428.

Mayer ML (2005) Glutamate receptor ion channels. Current opinion in neurobiology 15:282-288.

McMahon HT, Bolshakov VY, Janz R, Hammer RE, Siegelbaum SA, Sudhof TC (1996) Synaptophysin, a major synaptic vesicle protein, is not essential for neurotransmitter release. Proceedings of the National Academy of Sciences of the United States of America 93:4760-4764.

McNamara JO (1994) Cellular and molecular basis of epilepsy. The Journal of neuroscience : the official journal of the Society for Neuroscience 14:3413-3425.

Menegon A, Bonanomi D, Albertinazzi C, Lotti F, Ferrari G, Kao HT, Benfenati F, Baldelli P, Valtorta F (2006) Protein kinase A-mediated synapsin I phosphorylation is a central modulator of Ca2+-dependent synaptic activity. The Journal of neuroscience : the official journal of the Society for Neuroscience 26:11670-11681.

Miki H, Okada Y, Hirokawa N (2005) Analysis of the kinesin superfamily: insights into structure and function. Trends in cell biology 15:467-476.

Minerbi A, Kahana R, Goldfeld L, Kaufman M, Marom S, Ziv NE (2009) Long-term relationships between synaptic tenacity, synaptic remodeling, and network activity. PLoS biology 7:e1000136.

Mitchison TJ, Kirschner MW (1987) Some thoughts on the partitioning of tubulin between monomer and polymer under conditions of dynamic instability. Cell biophysics 11:35-55.

Mitsuya K, Nitta N, Suzuki F (2009) Persistent zinc depletion in the mossy fiber terminals in the intrahippocampal kainate mouse model of mesial temporal lobe epilepsy. Epilepsia 50:1979-1990.

Mizrahi A, Crowley JC, Shtoyerman E, Katz LC (2004) High-resolution in vivo imaging of hippocampal dendrites and spines. The Journal of neuroscience : the official journal of the Society for Neuroscience 24:3147-3151.

Mizuno-Yamasaki E, Rivera-Molina F, Novick P (2012) GTPase networks in membrane traffic. Annual review of biochemistry 81:637-659.

Molnar P, Nadler JV (1999) Mossy fiber-granule cell synapses in the normal and epileptic rat dentate gyrus studied with minimal laser photostimulation. Journal of neurophysiology 82:1883-1894.

Morton AM, Cunningham AL, Diefenbach RJ (2010) Kinesin-1 plays a role in transport of SNAP-25 to the plasma membrane. Biochemical and biophysical research communications 391:388-393.

Movsesyan VA, Faden AI (2006) Neuroprotective effects of selective group II mGluR activation in brain trauma and traumatic neuronal injury. Journal of neurotrauma 23:117-127.

Mukherjee A, Jenkins B, Fang C, Radke RJ, Banker G, Roysam B (2011) Automated kymograph analysis for profiling axonal transport of secretory granules. Medical image analysis 15:354-367.

Murray JM (2011) Methods for imaging thick specimens: confocal microscopy, deconvolution, and structured illumination. Cold Spring Harbor protocols 2011:1399-1437.

Murthy VN, De Camilli P (2003) Cell biology of the presynaptic terminal. Annual review of neuroscience 26:701-728.

Murthy VN, Sejnowski TJ, Stevens CF (1997) Heterogeneous release properties of visualized individual hippocampal synapses. Neuron 18:599-612.

Nakajima Y, Nakajima S, Obata K, Carlson CG, Yamaguchi K (1985) Dissociated cell culture of cholinergic neurons from nucleus basalis of

Meynert and other basal forebrain nuclei. Proceedings of the National Academy of Sciences of the United States of America 82:6325-6329.

Nakamura JL, Haas-Kogan DA, Pieper RO (2007) Glioma invasiveness responds variably to irradiation in a co-culture model. International journal of radiation oncology, biology, physics 69:880-886.

Nakata T, Terada S, Hirokawa N (1998) Visualization of the dynamics of synaptic vesicle and plasma membrane proteins in living axons. The Journal of cell biology 140:659-674.

Nan X, Campoy FJ, Bird A (1997) MeCP2 is a transcriptional repressor with abundant binding sites in genomic chromatin. Cell 88:471-481.

Neher E, Sakmann B (1992) The patch clamp technique. Scientific American 266:44-51.

Neher E, Sakaba T (2008) Multiple roles of calcium ions in the regulation of neurotransmitter release. Neuron 59:861-872.

Neves G, Cooke SF, Bliss TV (2008) Synaptic plasticity, memory and the hippocampus: a neural network approach to causality. Nature reviews Neuroscience 9:65-75.

Nirenberg MJ, Liu Y, Peter D, Edwards RH, Pickel VM (1995) The vesicular monoamine transporter 2 is present in small synaptic vesicles and preferentially localizes to large dense core vesicles in rat solitary tract nuclei. Proceedings of the National Academy of Sciences of the United States of America 92:8773-8777.

Niwa S, Tanaka Y, Hirokawa N (2008) KIF1Bbeta- and KIF1A-mediated axonal transport of presynaptic regulator Rab3 occurs in a GTP-dependent manner through DENN/MADD. Nature cell biology 10:1269-1279.

Nogales E (2000) Structural insights into microtubule function. Annual review of biochemistry 69:277-302.

Oberringer M, Meins C, Bubel M, Pohlemann T (2007) A new in vitro wound model based on the co-culture of human dermal microvascular endothelial cells and human dermal fibroblasts. Biology of the cell / under the auspices of the European Cell Biology Organization 99:197-207.

Okabe S, Kim HD, Miwa A, Kuriu T, Okado H (1999) Continual remodeling of postsynaptic density and its regulation by synaptic activity. Nature neuroscience 2:804-811.

Packer AM, Yuste R (2011) Dense, unspecific connectivity of neocortical parvalbumin-positive interneurons: a canonical microcircuit for inhibition? The Journal of neuroscience : the official journal of the Society for Neuroscience 31:13260-13271.

Palay SL, Palade GE (1955) The fine structure of neurons. The Journal of biophysical and biochemical cytology 1:69-88.

Papa M, Bundman MC, Greenberger V, Segal M (1995) Morphological analysis of dendritic spine development in primary cultures of hippocampal neurons. The Journal of neuroscience : the official journal of the Society for Neuroscience 15:1-11.

Pennuto M, Bonanomi D, Benfenati F, Valtorta F (2003) Synaptophysin I controls the targeting of VAMP2/synaptobrevin II to synaptic vesicles. Molecular biology of the cell 14:4909-4919.

Pierce JP, Milner TA (2001) Parallel increases in the synaptic and surface areas of mossy fiber terminals following seizure induction. Synapse 39:249-256.

Pin JP, Duvoisin R (1995) The metabotropic glutamate receptors: structure and functions. Neuropharmacology 34:1-26.

Proper EA, Oestreicher AB, Jansen GH, Veelen CW, van Rijen PC, Gispen WH, de Graan PN (2000) Immunohistochemical characterization of mossy fibre sprouting in the hippocampus of patients with pharmaco-resistant temporal lobe epilepsy. Brain : a journal of neurology 123 (Pt 1):19-30.

Pun S, Santos AF, Saxena S, Xu L, Caroni P (2006) Selective vulnerability and pruning of phasic motoneuron axons in motoneuron disease alleviated by CNTF. Nature neuroscience 9:408-419.

Puthanveettil SV, Monje FJ, Miniaci MC, Choi YB, Karl KA, Khandros E, Gawinowicz MA, Sheetz MP, Kandel ER (2008) A new component in synaptic plasticity: upregulation of kinesin in the neurons of the gill-withdrawal reflex. Cell 135:960-973.

Qiu Z, Sylwestrak EL, Lieberman DN, Zhang Y, Liu XY, Ghosh A (2012) The Rett syndrome protein MeCP2 regulates synaptic scaling. The Journal of neuroscience : the official journal of the Society for Neuroscience 32:989-994.

Quetglas S, Iborra C, Sasakawa N, De Haro L, Kumakura K, Sato K, Leveque C, Seagar M (2002) Calmodulin and lipid binding to synaptobrevin regulates calcium-dependent exocytosis. The EMBO journal 21:3970-3979.

Rakowski RF, Gadsby DC, De Weer P (1989) Stoichiometry and voltage dependence of the sodium pump in voltage-clamped, internally dialyzed squid giant axon. The Journal of general physiology 93:903-941.

Ramirez-Amaya V, Balderas I, Sandoval J, Escobar ML, Bermudez-Rattoni F (2001) Spatial long-term memory is related to mossy fiber synaptogenesis. The Journal of neuroscience : the official journal of the Society for Neuroscience 21:7340-7348.

Ratnayaka A, Marra V, Branco T, Staras K (2011) Extrasynaptic vesicle recycling in mature hippocampal neurons. Nature communications 2:531.

Ricceri L, De Filippis B, Laviola G (2008) Mouse models of Rett syndrome: from behavioural phenotyping to preclinical evaluation of new therapeutic approaches. Behavioural pharmacology 19:501-517.

Ripley B, Otto S, Tiglio K, Williams ME, Ghosh A (2011) Regulation of synaptic stability by AMPA receptor reverse signaling. Proceedings of the National Academy of Sciences of the United States of America 108:367-372.

Rizzoli SO, Jahn R (2007) Kiss-and-run, collapse and 'readily retrievable' vesicles. Traffic 8:1137-1144.

Rodriguez LG, Wu X, Guan JL (2005) Wound-healing assay. Methods in molecular biology 294:23-29.

Royle SJ, Lagnado L (2003) Endocytosis at the synaptic terminal. The Journal of physiology 553:345-355.

Russell RA, Adams NM, Stephens DA, Batty E, Jensen K, Freemont PS (2009) Segmentation of fluorescence microscopy images for quantitative analysis of cell nuclear architecture. Biophysical journal 96:3379-3389.

Ryan TA, Smith SJ (1995) Vesicle pool mobilization during action potential firing at hippocampal synapses. Neuron 14:983-989.

Sabo SL, Gomes RA, McAllister AK (2006) Formation of presynaptic terminals at predefined sites along axons. The Journal of neuroscience : the official journal of the Society for Neuroscience 26:10813-10825.

Samoilova M, Li J, Pelletier MR, Wentlandt K, Adamchik Y, Naus CC, Carlen PL (2003) Epileptiform activity in hippocampal slice cultures exposed chronically to bicuculline: increased gap junctional function and expression. Journal of neurochemistry 86:687-699.

Santhakumar V, Aradi I, Soltesz I (2005) Role of mossy fiber sprouting and mossy cell loss in hyperexcitability: a network model of the dentate gyrus incorporating cell types and axonal topography. Journal of neurophysiology 93:437-453.

Sara Y, Mozhayeva MG, Liu X, Kavalali ET (2002) Fast vesicle recycling supports neurotransmission during sustained stimulation at hippocampal synapses. The Journal of neuroscience : the official journal of the Society for Neuroscience 22:1608-1617.

Scharfman HE, Sollas AL, Berger RE, Goodman JH (2003) Electrophysiological evidence of monosynaptic excitatory transmission between granule cells after seizure-induced mossy fiber sprouting. Journal of neurophysiology 90:2536-2547.

Schief WR, Howard J (2001) Conformational changes during kinesin motility. Current opinion in cell biology 13:19-28.

Schliwa M, Woehlke G (2003) Molecular motors. Nature 422:759-765.

Schluter OM, Basu J, Sudhof TC, Rosenmund C (2006) Rab3 superprimes synaptic vesicles for release: implications for short-term synaptic plasticity. The Journal of neuroscience : the official journal of the Society for Neuroscience 26:1239-1246.

Schluter OM, Schmitz F, Jahn R, Rosenmund C, Sudhof TC (2004) A complete genetic analysis of neuronal Rab3 function. The Journal of neuroscience : the official journal of the Society for Neuroscience 24:6629-6637.

Schoch S, Gundelfinger ED (2006) Molecular organization of the presynaptic active zone. Cell and tissue research 326:379-391.

Scholl M, Sprossler C, Denyer M, Krause M, Nakajima K, Maelicke A, Knoll W, Offenhausser A (2000) Ordered networks of rat hippocampal neurons attached to silicon oxide surfaces. Journal of neuroscience methods 104:65-75.

Shakiryanova D, Tully A, Levitan ES (2006) Activity-dependent synaptic capture of transiting peptidergic vesicles. Nature neuroscience 9:896-900.

Sharma AV, Nargang FE, Dickson CT (2012) Neurosilence: Profound Suppression of Neural Activity following Intracerebral Administration of the Protein Synthesis Inhibitor Anisomycin. The Journal of neuroscience : the official journal of the Society for Neuroscience 32:2377-2387.

Shimomura O, Johnson FH, Saiga Y (1962) Extraction, purification and properties of aequorin, a bioluminescent protein from the luminous hydromedusan, Aequorea. Journal of cellular and comparative physiology 59:223-239.

Shupliakov O, Haucke V, Pechstein A (2011) How synapsin I may cluster synaptic vesicles. Seminars in cell & developmental biology 22:393-399.

Siksou L, Varoqueaux F, Pascual O, Triller A, Brose N, Marty S (2009) A common molecular basis for membrane docking and functional priming of synaptic vesicles. The European journal of neuroscience 30:49-56.

Smetters D, Majewska A, Yuste R (1999) Detecting action potentials in neuronal populations with calcium imaging. Methods 18:215-221.

Smrt RD, Eaves-Egenes J, Barkho BZ, Santistevan NJ, Zhao C, Aimone JB, Gage FH, Zhao X (2007) Mecp2 deficiency leads to delayed maturation and altered gene expression in hippocampal neurons. Neurobiology of disease 27:77-89.

Sokal DM, Mason R, Parker TL (2000) Multi-neuronal recordings reveal a differential effect of thapsigargin on bicuculline- or gabazine-induced epileptiform excitability in rat hippocampal neuronal networks. Neuropharmacology 39:2408-2417.

Speese SD, Trotta N, Rodesch CK, Aravamudan B, Broadie K (2003) The ubiquitin proteasome system acutely regulates presynaptic protein turnover and synaptic efficacy. Current biology : CB 13:899-910.

Staras K, Branco T, Burden JJ, Pozo K, Darcy K, Marra V, Ratnayaka A, Goda Y (2010) A vesicle superpool spans multiple presynaptic terminals in hippocampal neurons. Neuron 66:37-44.

Stenmark H, Olkkonen VM (2001) The Rab GTPase family. Genome biology 2:REVIEWS3007.

Stokin GB, Lillo C, Falzone TL, Brusch RG, Rockenstein E, Mount SL, Raman R, Davies P, Masliah E, Williams DS, Goldstein LS (2005) Axonopathy and transport deficits early in the pathogenesis of Alzheimer's disease. Science 307:1282-1288.

Stone MC, Roegiers F, Rolls MM (2008) Microtubules have opposite orientation in axons and dendrites of Drosophila neurons. Molecular biology of the cell 19:4122-4129.

Stoppini L, Buchs PA, Muller D (1991) A simple method for organotypic cultures of nervous tissue. Journal of neuroscience methods 37:173-182.

Su D, Cha YM, West AE (2012) Mutation of MeCP2 alters transcriptional regulation of select immediate-early genes. Epigenetics : official journal of the DNA Methylation Society 7:146-154.

Sudhof TC (2004) The synaptic vesicle cycle. Annual review of neuroscience 27:509-547.

Sudhof TC (2012) The presynaptic active zone. Neuron 75:11-25.

Sutula T, He XX, Cavazos J, Scott G (1988) Synaptic reorganization in the hippocampus induced by abnormal functional activity. Science 239:1147-1150.

Sutula T, Zhang P, Lynch M, Sayin U, Golarai G, Rod R (1998) Synaptic and axonal remodeling of mossy fibers in the hilus and supragranular region of the dentate gyrus in kainate-treated rats. The Journal of comparative neurology 390:578-594.

Takamori S et al. (2006) Molecular anatomy of a trafficking organelle. Cell 127:831-846.

Tarsa L, Goda Y (2002) Synaptophysin regulates activity-dependent synapse formation in cultured hippocampal neurons. Proceedings of the National Academy of Sciences of the United States of America 99:1012-1016.

Taubenblatt P, Dedieu JC, Gulik-Krzywicki T, Morel N (1999) VAMP (synaptobrevin) is present in the plasma membrane of nerve terminals. Journal of cell science 112 (Pt 20):3559-3567.

Taylor AM, Dieterich DC, Ito HT, Kim SA, Schuman EM (2010) Microfluidic local perfusion chambers for the visualization and manipulation of synapses. Neuron 66:57-68.

Taylor AM, Blurton-Jones M, Rhee SW, Cribbs DH, Cotman CW, Jeon NL (2005) A microfluidic culture platform for CNS axonal injury, regeneration and transport. Nature methods 2:599-605.

Teschemacher AG, Paton JF, Kasparov S (2005) Imaging living central neurones using viral gene transfer. Advanced drug delivery reviews 57:79-93.

Tokioka R, Matsuo A, Kiyosue K, Kasai M, Taguchi T (1993) Synapse formation in dissociated cell cultures of embryonic chick cerebral neurons. Brain research Developmental brain research 74:146-150.

Tooker A, Meng E, Erickson J, Tai YC, Pine J (2004) Development of biocompatible parylene neurocages. Conference proceedings : Annual International Conference of the IEEE Engineering in Medicine and Biology Society IEEE Engineering in Medicine and Biology Society Conference 4:2542-2545.

Toth K, Suares G, Lawrence JJ, Philips-Tansey E, McBain CJ (2000) Differential mechanisms of transmission at three types of mossy fiber synapse. The Journal of neuroscience : the official journal of the Society for Neuroscience 20:8279-8289.

Trachtenberg JT, Chen BE, Knott GW, Feng G, Sanes JR, Welker E, Svoboda K (2002) Long-term in vivo imaging of experience-dependent synaptic plasticity in adult cortex. Nature 420:788-794.

Tsukita S, Ishikawa H (1980) The movement of membranous organelles in axons. Electron microscopic identification of anterogradely and retrogradely transported organelles. The Journal of cell biology 84:513-530.

Tu JC, Xiao B, Naisbitt S, Yuan JP, Petralia RS, Brakeman P, Doan A, Aakalu VK, Lanahan AA, Sheng M, Worley PF (1999) Coupling of mGluR/Homer and PSD-95 complexes by the Shank family of postsynaptic density proteins. Neuron 23:583-592.

Ungermann C, von Mollard GF, Jensen ON, Margolis N, Stevens TH, Wickner W (1999) Three v-SNAREs and two t-SNAREs, present in a pentameric cis-SNARE complex on isolated vacuoles, are essential for homotypic fusion. The Journal of cell biology 145:1435-1442.

Upreti C, Otero R, Partida C, Skinner F, Thakker R, Pacheco LF, Zhou ZY, Maglakelidze G, Veliskova J, Velisek L, Romanovicz D, Jones T, Stanton PK, Garrido-Sanabria ER (2012) Altered neurotransmitter release, vesicle recycling and presynaptic structure in the pilocarpine model of temporal lobe epilepsy. Brain : a journal of neurology 135:869-885.

Uva L, Librizzi L, Wendling F, de Curtis M (2005) Propagation dynamics of epileptiform activity acutely induced by bicuculline in the hippocampal-parahippocampal region of the isolated Guinea pig brain. Epilepsia 46:1914-1925.

van Spronsen FJ (2010) Phenylketonuria: a 21st century perspective. Nature reviews Endocrinology 6:509-514.

van Strien NM, Cappaert NL, Witter MP (2009) The anatomy of memory: an interactive overview of the parahippocampal-hippocampal network. Nature reviews Neuroscience 10:272-282.

Wadiche JI, Jahr CE (2001) Multivesicular release at climbing fiber-Purkinje cell synapses. Neuron 32:301-313.

Wallace RH, Wang DW, Singh R, Scheffer IE, George AL, Jr., Phillips HA, Saar K, Reis A, Johnson EW, Sutherland GR, Berkovic SF, Mulley JC (1998) Febrile seizures and generalized epilepsy associated with a mutation in the Na+-channel beta1 subunit gene SCN1B. Nature genetics 19:366-370.

Wang H, Chan SA, Ogier M, Hellard D, Wang Q, Smith C, Katz DM (2006) Dysregulation of brain-derived neurotrophic factor expression and neurosecretory function in Mecp2 null mice. The Journal of neuroscience : the official journal of the Society for Neuroscience 26:10911-10915.

Watson AH, Bazzaz AA (2001) GABA and glycine-like immunoreactivity at axoaxonic synapses on 1a muscle afferent terminals in the spinal cord of the rat. The Journal of comparative neurology 433:335-348.

Weckhuysen S et al. (2012) KCNQ2 encephalopathy: emerging phenotype of a neonatal epileptic encephalopathy. Annals of neurology 71:15-25.

Weng SM, McLeod F, Bailey ME, Cobb SR (2011) Synaptic plasticity deficits in an experimental model of rett syndrome: long-term potentiation saturation and its pharmacological reversal. Neuroscience 180:314-321.

Wennerberg K, Rossman KL, Der CJ (2005) The Ras superfamily at a glance. Journal of cell science 118:843-846.

Wienisch M, Klingauf J (2006) Vesicular proteins exocytosed and subsequently retrieved by compensatory endocytosis are nonidentical. Nature neuroscience 9:1019-1027.

Witter MP (2007) Intrinsic and extrinsic wiring of CA3: indications for connectional heterogeneity. Learning & memory 14:705-713.

Witter MP, Griffioen AW, Jorritsma-Byham B, Krijnen JL (1988) Entorhinal projections to the hippocampal CA1 region in the rat: an underestimated pathway. Neuroscience letters 85:193-198.

Witter MP, Wouterlood FG, Naber PA, Van Haeften T (2000) Anatomical organization of the parahippocampal-hippocampal network. Annals of the New York Academy of Sciences 911:1-24.

Yasaka T, Tiong SY, Hughes DI, Riddell JS, Todd AJ (2010) Populations of inhibitory and excitatory interneurons in lamina II of the adult rat spinal dorsal horn revealed by a combined electrophysiological and anatomical approach. Pain 151:475-488.

Yonekawa Y, Harada A, Okada Y, Funakoshi T, Kanai Y, Takei Y, Terada S, Noda T, Hirokawa N (1998) Defect in synaptic vesicle precursor transport and neuronal cell death in KIF1A motor protein-deficient mice. The Journal of cell biology 141:431-441.

Yoshihara M, Littleton JT (2002) Synaptotagmin I functions as a calcium sensor to synchronize neurotransmitter release. Neuron 36:897-908.

Yuste R, Bonhoeffer T (2001) Morphological changes in dendritic spines associated with long-term synaptic plasticity. Annual review of neuroscience 24:1071-1089.

Zha XM, Green SH, Dailey ME (2005) Regulation of hippocampal synapse remodeling by epileptiform activity. Molecular and cellular neurosciences 29:494-506.

Zhang G, Raol YS, Hsu FC, Brooks-Kayal AR (2004) Long-term alterations in glutamate receptor and transporter expression following early-life seizures are associated with increased seizure susceptibility. Journal of neurochemistry 88:91-101.

Zhou Z, Misler S (1995) Action potential-induced quantal secretion of catecholamines from rat adrenal chromaffin cells. The Journal of biological chemistry 270:3498-3505.

Zhu Y, Xu J, Heinemann SF (2009) Two pathways of synaptic vesicle retrieval revealed by single-vesicle imaging. Neuron 61:397-411.

Ziv NE, Smith SJ (1996) Evidence for a role of dendritic filopodia in synaptogenesis and spine formation. Neuron 17:91-102.